Fully Developed Forced Convection Heat Transfer and Pressure Drop in a Smooth Tube in the Transitional Flow Regime

by

Nicola Mary van der Merwe

Submitted in fulfilment of the requirements for the degree
Master in Engineering (Mechanical Engineering)
in the Faculty of Engineering, Built Environment and Information Technology,
University of Pretoria

July 2017

UNIVERSITEIT VAN PRETORIA
UNIVERSITY OF PRETORIA
YUNIBESITHI YA PRETORIA

Abstract

Title:	Fully developed forced convection heat transfer and pressure drop in a smooth tube in the transitional flow regime
Keywords:	Convection, forced convection, heat transfer, pressure drop, transition, transitional, laminar, turbulent, smooth tube, horizontal, constant heat flux, water, square-edge inlet
Name:	Nicola Mary van der Merwe
Supervisor:	Prof JP Meyer
Department:	Mechanical and Aeronautical Engineering
Degree:	Master in Engineering (Mechanical), MEng(Mech)
Submission date:	July 2017
Acceptance date:	August 2017

Extensive work has been done on characterising convective heat transfer and pressure drop in smooth tubes in the laminar and turbulent flow regimes. However, little work was completed in the transitional flow regime. In all previous transitional studies, experiments that were conducted between the laminar and turbulent flow regimes were with mixed convection in the laminar flow regime and not in the forced convection flow regime. The secondary flow that occurs during mixed convection should most probably influence the characteristics in the transitional flow regime. It can therefore be expected that the transitional flow characteristics of forced convection and mixed convection will be different. However, the transitional characteristics of forced convection flow have not yet been determined. The purpose of this study was therefore to determine the heat transfer and pressure drop transitional characteristics specifically in the forced convection flow regime. Furthermore, to focus on determining these factors for a circular, horizontal smooth tube for fully developed flow. The characteristics were determined in an experimental set-up through which flow occurred through a test section consisting of a horizontal and circular smooth tube. The test-section inside diameter was 4.04 mm, and the tube length was 8.4 m. Water was used as the test fluid and was circulated through the test section which was heated at a constant heat flux. A calming section with a square edge inlet was upstream of the test section. Temperatures at the tube inlet, outlet and outer surface of the test section were measured with a total of 58 thermocouples. Two pressure taps was also installed on the test section and was connected to a pressure transducer for pressure drop measurements. Experiments were conducted mainly on the last part of the test section where fully developed flow occurred. Experiments were conducted between Reynolds numbers of 1 000 to 10 000, Prandtl numbers of 3 to 8, and Rayleigh numbers of 330 and 11 000 (heat fluxes of 0.89 kW/m^2 to 3.26 kW/m^2). It was found that the heat transfer transitional range coincided with the friction factor transition range with a Reynolds number range of 2 484 to 2 849. Forced convection results in the laminar regime was achieved and compared well to literature. The results were mapped on published flow regime maps. This was inconclusive as the published flow regime maps have been specifically developed for fixed parameters that did not match the parameters of this study.

Acknowledgements

This project would not have been possible without the assistance of Maksal Copper Tubing who provided the special order tubes for this project.

I would like to thank the following institutions for their financial support: NRF, TESP, University of Pretoria, SANERI/SANEDI, CSIR, EEDSM Hub, and the NAC.

I would also like to thank the following personnel at the University of Pretoria for their assistance in this study:

- Prof Josua Meyer, my supervisor, for your invaluable knowledge and assistance.
- Charles Moon, Koos Mthombeni, Wim Murray and Peet Kruger for their assistance during the build and testing phase of the study.
- Danie Gouws for always providing helpful insight during the build and testing.
- Tersia Evans, Elzabe Pieterse and Barbara Huyssen for your support.

Finally, importantly, my family:

- Jennifer and Michaël van der Merwe, for never allowing me to give up, no matter what. Thank you for picking me up every time I fell.
- My children, Ann, Joshua and Christopher for your hugs and kisses.
- My husband Shane Kotzé, for helping me through every step of this process. Thank you for being my rock, for appearing in the lab when you knew I needed that extra bit of support.

Table of contents

Table of figures

List of tables

Nomenclature

Symbols

A	Area	[m^2]
C_p	Specific heat at constant pressure	[J/kg.K]
D	Diameter	[m]
E_P	Electrical input power	[W]
g	Gravity	[m/s^2]
h	Heat transfer coefficient	[$W/m^2.°C$]
I	Current	[A]
k	Thermal conductivity	[W/m.K]
L	Length	[m]
$\dot{m}$	Mass flow rate	[kg/s]
P	Pressure	[Pa]
$\dot{Q}$	Heat input	[W]
$\dot{q}$	Heat flux	[W/m^2]
r	Radius	[m]
P	Predicted result	[-]
R	Resistance	[Ω]
T	Temperature	[°C]
V	Velocity	[m/s]
V	Voltage	[V]
$\dot{V}$	Volumetric flow rate	[m^3/s]
X	Measured or calculated result	[-]
x	Distance from inlet of test section	[m]

Dimensionless parameters

a	Constant used in correlations
b	Constant used in correlations
c	Constant used in correlations
EB	Energy balance
f	Friction factor

Gr	Grashof number
Gz	Graetz number
j_H	Colburn j_H-factor
m	Constant used in correlations
Nu	Nusselt number
Pr	Prandtl number
Pw	Tube wall parameter
Ra	Raleigh number
Re	Reynolds number
St	Stanton number

Greek letters

β	Coefficient of expansion	[1/K]
ε	Internal surface roughness	[m]
μ	Dynamic viscosity	[kg/m.s]
v	Kinematic viscosity	[m^2/s]
ρ	Density	[kg/m^3]

Subscripts

a	Ambient
A – S	Thermocouple station designation on test section
avg	Average
B	Bulk
bottom	Bottom of test section
c	Cross sectional
cr	Critical
cs	Calming section
diabatic	Diabatic condition
elec	With reference to the heat input by electrical power
end	End of range
e	exit
film	Fluid film temperature

h	Heated
hw	Heating wire
hydro	Hydrodynamic
i	Inside, inner, inlet
insul	Insulation
isothermal	Isothermal condition
left	Left hand side of test section
lam	Laminar
low	Lower band
lre	Low-Reynolds-number-end
m	Mean
o	Outside, outer
PD	Pressure differential
right	Right hand side of test section
s	Surface
start	Start of range
top	Top of test section
therm	Thermal
trans	Transitional
ts	Test section
turb	Turbulent
up	Upper band
w	Water
water	With reference to the heat transferred into the water/taken up by the water

Abbreviations

BV	Bleed valve
EDSU	Engineering Sciences Data Unit
OAR	Open air ratio
PD1	Pressure tap in point 1
PD2	Pressure tap in point 2
RTD	Resistance temperature detectors

1 Introduction

1.1 Background

The generation of energy in a world where population growth and industrialization is continuous is presently considered to be a grand challenge by the US National Academy of Engineering [1]. In general, some of the world's electrical energy generation is produced by various methods such as hydroelectric means, wind turbines, photovoltaic cells, fuel cells etc. However most of the energy generation is currently being produced by making use of thermal heat in coal fired power stations, nuclear power stations and recently concentrated solar power stations. Heat exchangers in which boiling and condensation occurs, are essential components that form part of the thermodynamic cycles used at all these types of power stations.

Heat exchangers also influence many other areas in industry where energy is not generated but consumed. Examples include the petrochemical industry where crude oil or coal is refined to produce products such as petroleum, diesel and aviation fuel [2]. There are many different areas at a refinery wherein heat exchangers are necessary such as heat recovery from crude oil distillation units [3]. Gold mining forms a large part of South Africa's economy where gold can be extracted at depths of 3 800 m [4]. In this instance, rock temperatures can reach as high at 90 °C necessitating the need for cooled ventilation air, made possible using heat exchangers [4]. The use of nanofluids in automotive cooling systems have become important in the automotive industry, where the drive to improve radiator efficiencies and thus engine efficiencies is ever more prevalent [5]. In the food industry, scraped surface heat exchangers are extensively used for cooling or heating of high viscosity food products to ensure uniform heating or cooling is achieved [6]. Ultra-high temperature heat exchangers are used in the dairy industry for pasteurisation purposes [7].

On a smaller scale than that of the power generation industry, industrial applications, agriculture and domestic applications, heat exchangers are required to cool densely populated electrical and electronic enclosures [8]. Complications arise where the electronic components are not only more densely packed but are also becoming smaller and smaller. When considering electronic chips for automotive applications, the average heat flux of a typical chip has increased from 75 W/cm^2 in 2 000 to an expected heat flux of 240 W/cm^2 in 2016 [8]. Dispersing the waste heat from these applications becomes more difficult and has become a major challenge. Small heat exchangers known as heat sinks are used to convey heat from the electronic components by convection into a cooler air stream.

The heat exchanger applications that were highlighted in the previous three paragraphs transfer thermal heat from one stream to another, from a higher temperature to a lower temperature. The heat transfer modes may be one or more of the following, namely conduction, convection and radiation. In the majority of heat exchangers radiation heat transfer and conduction heat transfer are negligible. As a result, it is expected that most heat transfer in heat exchangers is typically convective heat transfer.

The flow field in convective heat transfer applications can be laminar, turbulent or transitional and has a significant influence on the heat transfer rate that occurs in convective heat transfer. Heat transfer and pressure drop is very well understood in laminar and turbulent flow. However, according to Meyer [9] and Tam and Ghajar [10], smooth tube heat exchangers may operate in, or close to the transitional flow regime. Previously, designers were encouraged to avoid operating in the transitional flow regime as the underlying physics and implications was not fully understood [9].

However, it has become more important that this flow regime is not to be avoided. Meyer [11] has found that:

a. It is an attractive flow regime when considering a compromise between heat transfer and pressure drop. In the laminar flow regime, the expected pressure drop is low but the heat transfer is also low which is not desirable. In the turbulent flow regime, the heat transfer is high but unfortunately the pressure drop is at least an order of magnitude higher than in the laminar flow regime. In many cases, the transitional flow regime may provide an optimal compromise with reference to high heat transfer rates and low pressure drops.
b. The transitional flow regime has become more important with the introduction of enhanced heat transfer tubes [12] in industry. The significant increase in surface area has resulted in an associated higher pressure drop. Therefore, many heat exchanger passages/tubes operate at lower Reynolds numbers as compared to their smooth tube equivalent tubes, and/or closer to the transition flow regime. Also, over time, scaling or changes in operating conditions occur in many industry applications. This can result in tubes operating in or closer to the transitional flow regime.
c. Previous work has indicated that the heat transfer and pressure drop results in the transitional flow regime are not discontinuous but smooth in nature between laminar and turbulent flow [13] and can be predicted if the inlet geometry of the tube is known [14, 15].

1.2 State of the art of tube flow in the transitional flow regime

The state of the art in transitional flow limited to flow through tubes is presented in three parts. The first part is a summary of a keynote paper delivered by Meyer at the 15th International Heat Transfer Conference in 2014. A significant part of the paper reviewed all the literature in the transitional flow regime. The second part is based on more recent work that was published after the review paper of Meyer. The third part is work that is highlighted which is closely related to this study.

1.2.1 Summary of the paper of Meyer

Meyer at the University of Pretoria, South Africa, completed an extensive review [11] of the available literature on transitional flow in tubes. He reviewed the conventional convective heat transfer and pressure drop literature in smooth tubes, work carried out by Ghajar and co-workers [14-22], Meyer and co-workers [9, 12, 23-28] and other related work.

He has found that a large body of work exists in forced and mixed convection heat transfer in horizontal tubes. This work has also been reviewed by many other researchers. However, a number of researchers pointed out that inlet effects such as the type of inlet have not yet been investigated previously.

Ghajar and co-workers [10, 14-22] were the first to investigate the effect of the type of inlet on heat transfer in horizontal tubes. They have found that the sharper the inlet type, the quicker transition would take place, conversely, the more rounded the entrance type, the more transition would be delayed. When considering heat transfer, the diabatic friction factors in laminar and transition and the start and end of transition differed significantly. However, turbulent results remained the same. This was attributed to mixed convection and secondary flow effects in the laminar flow regime.

Meyer also considered the characteristics of transitional flow in smooth [13, 28] and enhanced horizontal tubes [12, 29]. With his PhD student, Olivier, they focused on a constant wall temperature condition with varying inlets. In a similar fashion to Ghajar's results, the smooth tube study showed that the sharper inlets produced an earlier transition as compared to the smoother inlets which were delayed. Heat transfer results revealed that secondary flow was present as the Nusselt numbers were higher than expected.

Other work [26, 30] of less importance to this study in transition has been done in annular tubes, narrow rectangular passages, with nanofluids and microtubes. The low-Reynolds-number end is another area of interest. There are inadequacies with the discontinuities at transition using well established correlations. These correlations tend to over predict the Nusselt numbers from the start of transition as a Reynolds number of 2 300 up to a Reynolds number of 10 000.

Meyer [11] concluded his review paper by suggesting future work that should be conducted in order to gain a better understanding of heat transfer and pressure drop of tubes in the transitional flow regime. He identified 13 topics that must be considered. With specific reference to this study, he pointed out that most of the work thus far, specifically for tube flow in the transitional flow regime, investigated transitional flow characteristics with the laminar flow regime in the mixed convection flow regime and not in the forced convection flow regime. He suggested that work be conducted to also investigate the transitional flow characteristics with the flow regime in the forced convection flow regime. This recommendation is of specific relevance to this study as emphasised in Sections 1.3 and 1.4.

1.2.2 More recent literature

Five additional papers were published describing work in the transitional flow regime after the review by Meyer [11]. These five papers reported results on constant surface temperatures, surface roughness, inlet effects of micro-channels, annular passages, and developing flow, and each is summarised.

Meyer and Olivier considered flow through horizontal smooth tubes for varying types of inlet geometries [9]. A constant surface temperature (and not constant heat flux as in all other studies) was maintained during testing and four types of inlets were tested. It was found that during isothermal friction factor testing, transition was highly dependent on the inlet geometry. The smoother the inlet geometry, the more transition was delayed. Diabatic friction factor results were found to be independent of the inlet geometry and similar factors were obtained for all inlet geometries. However, laminar friction factors were higher than predicted in this instance. When considering diabatic results, laminar Nusselt numbers were much higher than predicted, therefore indicating that mixed convection occurred.

Everts *et al.* [24] considered the influence of surface roughness on heat transfer in the transitional flow regime. Smooth horizontal tubes and roughened horizontal tubes were heated at a constant heat flux. Diabatic results showed that while transition was delayed for increasing heat fluxes, transition occurred earlier in the roughened tubes as compared to the smooth tube. A mixed convection heat transfer mode was observed in laminar flow as Nusselt numbers of 10 and more was measured.

The inlet effects in micro-channels in the laminar and transitional regimes was investigated by Dirker *et al.* [23]. Three inlet geometries were tested and it was found that the inlet geometry had an effect on the transition characteristics. Diabatic results showed that transition was delayed as compared to isothermal results. Laminar Nusselt numbers were found to be in agreement with thermal entry length Nusselt number models for macro-channels. Conversely to tube flow, it was found that the smoother the inlet geometry, the quicker transition occurred in micro-channels.

Ndenguma *et al.* [27] considered transitional flow in a horizontal annular passage, with heating and cooling. The flow was considered to be not fully developed. A constant surface temperature was induced during testing. It was found that the measured heat transfer and friction factors were different to those in round circular tubes. The transition from laminar to turbulent flow when considering the Nusselt numbers was found to occur earlier than when considering the friction factors.

The heat transfer characteristics of developing flow at constant heat flux in the transitional flow regime was investigated by Everts and Meyer [25]. The transition region was shorter the further the measurements were taken from the entrance of the test section, thus indicating that the characteristics for developing flow in the transitional flow regime is different to that of fully developed flow. It was also found that the measured laminar Nusselt numbers were much higher than the predicted 4.36, even at the furthest point from the entrance of the test section, thus indicating that mixed convection was in play.

1.2.3 Other relevant literature

Yang and Lin [31] conducted an experimental investigation using stainless steel micro-tubes with an inner diameter ranging from of 0.123 mm to 0.962 mm. Each tube was of a different length and the purpose of the study was to determine forced convection heat transfer

performance. Flow in the test section was thermally developing. Non-contacted liquid crystal thermography was used for temperature measurement purposes with an uncertainty of 0.4°C. The Nusselt number uncertainties ranged between 2 and 53%, dependant on the Graetz number. Yang and Lin did not report any transitional heat transfer or friction factor results, nor did they report on the Colburn-j_H factor. They concluded that their results agreed well with literature for thermally developing heat transfer. Furthermore, as the inner diameter of gets smaller, the discrepancy in the developing Nusselt number results gets bigger.

Ghajar and Tam [16] developed a flow regime map for horizontal tubes using the ground work of Metais and Eckert [32] (who developed a flow regime map for a uniform wall temperature condition). Utilising the results from various experiments they had conducted on heat transfer with different inlet geometries, Ghajar and Tam created a map specifically for a uniform wall heat flux condition at an x/D_i of 3 and 192. The map defines the forced laminar regime, the mixed laminar regime, forced transition regime, mixed transition regime and forced turbulent regime, where the boundaries of the regimes are a function of the inlet geometry.

It is stated that they could not achieve Nusselt number results of 4.36 in laminar flow due to secondary flow effects. In order to determine where the forced laminar regime boundary would lie, they considered the local peripheral heat transfer coefficient. They concluded where the ratio of the top of tube heat transfer coefficient (h_{top}) to the bottom of tube heat transfer coefficient (h_{bottom}) is close to unity, forced convection would dominate. In the cases where it was less that unity ($h_{top}/h_{bottom} < 0.8$) mixed convection would dominate. They used this condition to develop the boundary.

Tam *et al.* [18] considered the effect of inlet geometries and heating on entrance and fully developed friction factors in laminar and transition regimes of a horizontal tube. During the introduction of the study, they concluded that the heat transfer correlations that were available to date accurately determine heat transfer in the entrance and fully developed regions for different geometries. They also concluded that the heat transfer correlation of Tam and Ghajar [22] best described heat transfer through all three flow regimes for varying inlet geometries for developing and developed flow. During a review of the recent cited literature, forced convection laminar Nusselt numbers of 4.36 were not obtained before transition and this was reflected on numerous occasions in the form of the Colburn *j*-factor versus Reynolds numbers graphs [10, 14, 16] in their works. It must also be noted that the correlations had specific ranges wherein they were valid, such as a maximum x/D_i ratio of 385.

During their experimental investigation of entrance and fully developed friction factors, Tam and Ghajar [22] isothermal friction factor results compared very well with literature. With heating, an increase in heat flux was found to delay the friction factor transition. Their diabatic friction factor results did not agree well with previously published correlations and it was concluded a correction factor regarding viscosity ratios should be applied to previously published literature. Tam and Ghajar [22] did not report laminar flow Nusselt number results of 4.36, indicating that there was mixed convection during heating in the laminar flow regime before entering into the transitional flow regime. Finally, they concluded that transitions for

heat transfer was different for friction factors and that the heat transfer transition range was much wider than that for friction.

1.3 Problem statement

All of the previous work that was conducted, as described in Section 1.2, has a common thread, namely, transition was investigated by assessing the heat transfer and pressure drop measurements of the flow through horizontal smooth tubes. Furthermore, the measurements of the flow were from laminar flow, through transition, and into the turbulent flow regime. Hysteresis effects of transition, whereby the mass flow rate is lowered from the turbulent flow regime, through the transitional flow regime, to the laminar flow regime was investigated by Meyer and Olivier [29] and found to be negligible.

However, to date, all the laminar flow work in smooth tubes was conducted in the ***mixed flow regime*** and not in the ***forced flow regime***. Therefore there is a gap in the literature (which was also identified by Meyer [9]) when considering transition characteristics if the laminar flow regime is in the forced convection flow regime before transition starts. The gap in literature is shown schematically in Fig. 1-1.

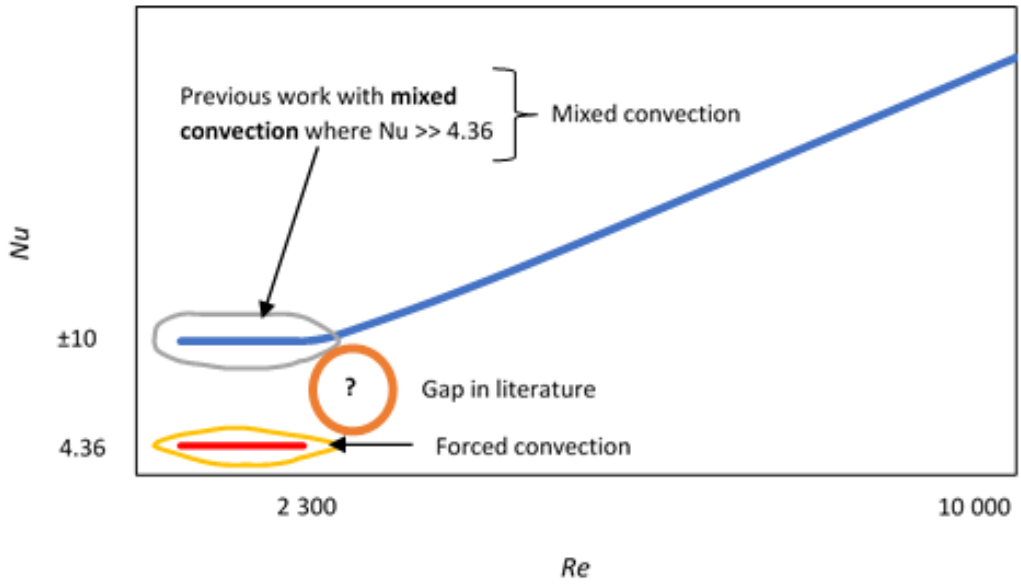

Fig. 1-1 - Schematic of the Nusselt number characteristics as a function of Reynolds number for a constant Prandtl number of 4 in a circular smooth tube heated with a constant heat flux and a squared-edge inlet. The question mark ("?") indicates the gap in literature

During mixed convection, secondary flow occurs. As this enhances the heat transfer, the secondary flow is an additional complicating factor when transition is studied. However, it is a practical challenge to operate heat transfer experiments in tubes with forced convection only and, in most experiments, mixed convection occurs. If the flow is fully developed forced convection, the Nusselt number is expected to be 4.36 for a constant surface heat flux condition [33].

During the works of Ghajar and co-workers [10] and Meyer and co-workers [9, 24] at constant heat flux in circular tubes, Nusselt numbers varying from approximately 10 to 20 were reported. These high Nusselt numbers are indicative of mixed flow in which secondary flow occurs. In these studies the inlet geometry of the test section also influenced the transitional characteristics. Sharper inlets, such as a re-entrant inlet, showed results where transition started earlier than expected, while as smooth inlets, such as a bell mouth showed a delayed start to transition.

Therefore, the problem statement of this study is that no transitional heat transfer and pressure drop work together, were done on horizontal smooth tubes, where the flow regime before transition was in the forced convection regime only.

1.4 Aim of this study

The purpose of this study was to investigate the heat transfer and pressure drop characterises in the transitional flow regime of fully developed forced convection in a horizontal smooth tube.

1.5 Objectives of the study

The objectives of the study to achieve the aim of the study were:

a) To develop and build an experimental set-up with a horizontal, smooth tube test section. Heat transfer and pressure drop measurements must be conducted on the test section. The flow regimes in the test section should be from the laminar flow regime just before transition, through the transitional flow regime and into the turbulent flow regime. The experimental set-up should be able to operate in the laminar forced flow regime before transition occurs.
b) To determine and quantify the inaccuracies of all instrumentation and to determine the uncertainties of all variables required.
c) To validate the experimental pressure drop and heat transfer measurements, and data reduction methodology, with literature by operating the experimental set-up in the same regimes as in previous studies.
d) To operate the test-section in the forced convection flow regime (fully developed) and measure the pressure drops and heat transfers together, close to and through the transitional flow regime.
e) To present the heat transfer and pressure drop results in an appropriate format.

1.6 Scope of work

As this project was for a one-year research masters, the work was limited to one circular smooth tube test section. Only one tube was used as the manufacture and build of the mixing wells, calming section and test section were time consuming and expensive. A circular tube was selected as most of the body of work in the transitional flow regime was for circular round tubes. The test section was heated using a constant surface heat flux as the selected method

had the advantage that the average fluid temperature along the tube length could be determined without additional/complicated measurements.

Only one sharp geometry inlet, namely the square edge inlet, was tested due to time constraints. This was the easiest of the sharp entrances to be manufactured and typical of most types of inlet (such as in for example) shell and tube heat exchangers. A smooth bell-mouth inlet could not be used as previous work reported that transition flow started at a Reynolds number of at least 3 500 [33] and could possibly be delayed to as much as 10 500 for fully developed flow [13]. This meant that the required test-section length would be too long (approximately 56 m to 168 m) and could not fit into the heat transfer laboratory available for this project. The test fluid was water (with Prandtl numbers from 3 to 8) as expensive equipment is needed if other fluids with higher Prandtl numbers are tested.

The experiments were mainly conducted in the fully developed flow regime only. This ensured that the velocity and temperature profiles in the tube were fully developed and theoretically known before transition occurred. The fact that the experiments were also conducted in the forced convection flow regimes ensured that the complications of developing and secondary flow on transition were eliminated. This is a much simpler and more appropriate approach than previous studies to investigate transition which is a very complicated phenomenon. However, the previous work in which mixed convection occurred is much more relevant to industry applications.

1.7 Original outcomes

The outcomes produced were for fully developed transitional flow in a smooth horizontal, circular tube with different constant heat fluxes and one inlet geometry. The following original contributions were made specifically in the forced convection and transitional flow regime:

a) Diabatic friction factors as a function of Reynolds numbers.
b) Nusselt numbers as a function of Reynolds numbers.
c) The Colburn j_H-factors as a function of Reynolds numbers.

1.8 Overview of dissertation

In Chapter 2, a literature survey is presented discussing the fundamental concepts in forced convection heat transfer related to the laminar, turbulent and specifically transitional flow regimes. In Chapter 3, the experimental set-up, calming section and test sections are described as well as the operating procedure that was followed during experimentation. The data reduction is presented in Chapter 4 and the results of an uncertainty analysis are also given. The results of the measurements are data reduction methodologies are validated in Chapter 4. Chapters 5 and 6 cover the pressure drop and heat transfer results. Chapter 7, summarises and concludes the study and provides recommendations for further work.

Appendix A contains the results of the internal surface roughness experiments of the test section. Appendix B describes the thermocouple calibration while Appendix C describes the pressure transducer calibration. Finally, an uncertainty analysis is presented in Appendix D.

2 Literature study

2.1 Introduction

The purpose of this chapter is to provide a framework of the theoretical phenomenon that supports this study. An overview is given of the various fundamental variables of fluid flow, heat transfer and pressure drop. The three different types of flow regimes are discussed and published correlations associated to these flow regimes is listed. Flow regime maps are also discussed in order to identify where boundaries between forced convection and mixed convection lie. The definition of developing and fully developed flow as well as the influences is described. Finally the work of Ghajar and Meyer is summarised.

2.2 Fundamental variables of fluid flow, heat transfer and pressure drop

A number of dimensionless numbers and correlations exist that can be used to quantify fluid flow, heat transfer and pressure drop which are applicable to this study are discussed in this section.

2.2.1 Reynolds number

During the 1880's, Osborne Reynolds established that transition from laminar flow to turbulent flow in a tube is a function of a number of variables, such as the geometry of the tube, the surface roughness, the average flow velocity, the surface temperature and fluid type to name a few. After extensive testing, Reynolds found that the ratio of inertial forces to viscous forces was the predominant factor in the determination of the flow regime which was named the Reynolds Number (*Re*). At high Reynolds numbers, the inertial forces are high, which produce chaotic eddies, vortices and flow instabilities. At low Reynolds numbers, the viscous forces are dominant and are able to suppress the instabilities in the flow. [34]

$$Re = \frac{inertial\ forces}{viscous\ forces} = \frac{\rho V_{avg} D_i}{\mu} \tag{2-1}$$

The convection heat transfer coefficient is a strong function of the Reynolds number in forced convection [35].

2.2.2 Prandtl number

The Prandtl number (*Pr*), was named after Ludwig Prandtl who discovered the concept of the boundary layer in 1904. It is used to describe the relative thickness of the velocity boundary layer as compared to the thermal boundary layer. In liquid metals, where the Prandtl number is much less than one, heat diffuses very quickly due to the relatively high conductivity of the product, therefore the thermal boundary layer is much thicker relative to the velocity boundary layer. In gases, the Prandtl number is approximately one. This means that the dissipation rate through the thermal boundary layer and velocity boundary layer is approximately the same [35].

$$Pr = \frac{molecular\ diffusivity\ of\ momentum}{molecular\ diffusivity\ of\ heat} = \frac{C_p \mu}{k} \quad (2\text{-}2)$$

The fluid of interest in this study is water and has a Prandtl number of 7 at 20°C [35]. As the Prandtl number is larger than one, the thermal boundary layer is thinner that the velocity boundary layer. The molecular diffusivity of momentum is thus quicker than the molecular diffusivity of heat.

2.2.3 Grashof number

Natural convection effects are described by the Grashof number (*Gr*) which is defined as the ratio of the buoyancy force to viscous force that is acting on a fluid [35] [36].

$$Gr = \frac{buoyancy\ force\ acting\ on\ fluid}{viscous\ force\ acting\ on\ fluid} = \frac{g\beta(T_s - T_B)D_i^3}{\nu^2} \quad (2\text{-}3)$$

Although it is recognized that natural convection always accompanies forced convection, it is considered negligible at high Reynolds numbers. This is because the heat transfer coefficients are typically much higher in forced convection than natural convection due to the associated higher fluid velocities in forced convection. However, as the fluid velocities lower, it becomes important to assess the relative magnitude of natural convection present in the fluid as this will affect the heat transfer coefficients [35].

2.2.4 Rayleigh number

The Rayleigh number (*Ra*), which is the product of the Grashof and Prandtl numbers, describes the relationship between buoyancy forces within a fluid in which temperature gradients, viscosity forces and diffusivities are accounted for [34].

$$Ra = \frac{buoancy\ forces\ within\ a\ fluid}{product\ of\ thermal\ and\ momentum\ diffusitivities} = GrPr \quad (2\text{-}4)$$

It can be also be defined as the ratio of buoyancy forces and (the products of) thermal and momentum diffusivities. Depending on the flow geometry and heating conditions, the Rayleigh number can be used to determine whether the dominant mode of heat transfer is considered to be forced convection or mixed convection. This is based on flow regime maps (discussed in section 2.3.5) that have been developed experimentally for different geometries and heating (or cooling) conditions.

2.2.5 Nusselt number

In 1915, Wilhelm Nusselt, who made significant contributions to the study of convective heat transfer, proposed the concept of dimensionless groups which led to the concept of the similarity theory of heat transfer. Consequently, the dimensionless number used to describe the ratio of convective to conductive heat transfer at a boundary was named the Nusselt

number (*Nu*). It signifies the improvement of heat transfer through a fluid layer as a result of convection as opposed to conduction through that same fluid layer [35].

$$Nu = \frac{convective\ heat\ transfer}{conductive\ heat\ transfer} = \frac{hD_i}{k} \tag{2-5}$$

Heat transfer is by convection at a wall, when there is motion next to the wall, while conduction will be present when the fluid is motionless. Therefore, where the Nusselt number is unity, heat transfer is considered to be by pure conduction across that fluid layer, whereas, the larger the Nusselt number, the more effective the convection heat transfer.

2.2.6 Graetz number

In 1885, Leo Graetz solved the problem for developing temperature profiles in a tube for Poiseuille flow [37]. Consequently, the Graetz number (*Gz*) was named after him. It can be used as an indication as to whether or not flow in a tube is thermally fully developed.

$$Gz = \left(\frac{D_i}{x}\right) RePr \tag{2-6}$$

According to Cengel and Ghajar [33], when the inverse of the Graetz number is greater than 0.05, fully developed conditions has been reached for heating in a tube for both conditions of heating at a constant heat flux or with a constant wall temperature. ESDU [30] states a value of 0.043 which is not much different from the value of 0.05.

2.2.7 Stanton number

The Stanton number (*St*) expresses the ratio of heat transferred into the fluid to the thermal capacity of the fluid [35].

$$St = \frac{h}{\rho C_p V_{avg}} = \frac{Nu}{Re\ Pr} \tag{2-7}$$

2.2.8 Colburn j_H-factor

The Colburn j_H-factor is named after Colburn [35]. It makes use of the analogy between the basic mechanisms and mathematics of heat, mass, and momentum transport are essentially the same.

$$j_H = StPr^{2/3} \tag{2-8}$$

It is also considered to be an alternative expression of a dimensionless heat transfer coefficient. The other dimensionless number is the Nusselt number which is normally influenced strongly by the fluid Prandtl number whereas the Colburn j_H-factor takes into

account the variation in the fluid Prandtl number. This is convenient when used in heat transfer experiments when it is normally extremely challenging to conduct heat transfer experiments while maintaining a constant Prandtl number of the convective fluid. The effect of varying property variations in the Prandtl numbers on Nusselt number can thus be eliminated by rather expressing the results in terms of the Colburn j_H-factor.

2.2.9 Pressure drop, friction factor and the Moody chart

This section will be presented in two parts. In the first part, section 2.2.9.1, the relationship between pressure drop and friction factor without heat transfer is discussed. In section 2.2.9.2 the relationship between pressure drop and friction factor with heat transfer is discussed.

2.2.9.1 Isothermal friction pressure drop

The pressure drop (ΔP) for isothermal flow can be written as [34]:

$$\Delta P = f \frac{L_{PD}}{D_i} \frac{\rho V_{avg}^2}{2} \tag{2-9}$$

The friction factor (f), has been determined analytically in the laminar flow regime and experimentally in the turbulent flow regime. In the laminar flow regime it has been found to be only dependant on the Reynolds number, and has been determined analytically for a circular tube by Poiseuille [33, 38]:

$$f = \frac{64}{Re} \tag{2-10}$$

For turbulent flow, it has been found that the friction factor is a function of both the Reynolds number and tube relative roughness (ε/D_i). This friction factor can be obtained from a Moody chart, or from empirical equations.

This chart was developed in 1944 by Moody to provide engineers with a graphical plot to determine the friction factors in both smooth and roughened tubes [39] in the laminar and turbulent flow regimes as a function of the tube's relative roughness and the Reynolds number. Moody used the implicit Colebrook equation, developed by Colebrook in 1939, to develop a chart that is ±15% accurate for friction factors in the turbulent flow regime [38].

The chart is divided into four regions namely laminar, critical, transitional and turbulent regimes. For smooth tubes, the critical zone of the chart lies between 2 000 and 4 000 Reynolds, where there is a strong discontinuity that lies between at a Reynolds number of 2 000 and 3 000. The lack of data in this area makes it challenging to use when operating in the transitional flow regime.

There are many empirical equations that exist that may be used to estimate the friction factor as discussed in a review paper by Fang *et al.* [40]. These equations can be solved either

explicitly or implicitly with varying degrees of accuracy. In this study a circular smooth tube is considered and therefore the relative roughness effect is negligible. The simplest equation with an acceptable error of less than 2.6%, for Re < 2 x 10^6, for a smooth, circular tube is the isothermal Blasius equation: [33, 38].

$$f = 0.316\, Re^{-0.25} \tag{2-11}$$

When determining the friction factors from Eq. 2-10 and 2-11, the density and viscosities terms in the Reynolds number (Eq. 2-1) are determined at the bulk temperature (T_b). This is taken as the average between the inlet and outlet temperature:

$$T_B = \frac{T_i + T_e}{2} \tag{2-12}$$

At this bulk temperature the fluid properties are referred to as the bulk properties.

For flow cases in a tube without heat transfer (isothermal conditions) the fluid inlet and outlet temperatures remains constant. The flow is therefore isothermal. As a result, all the other fluid properties that are temperature dependant, such as density, viscosity, Prandtl number, specific heat, thermal conductivity and thermal expansion coefficient would also remain constant.

2.2.9.2 Diabatic pressure drop

When considering flow through a tube in which heat transfer occurs, the inlet and outlet temperatures in Eq. 2-12, will differ. Although the bulk temperature might be the same as for isothermal flow discussed in 2.2.9.1, the pressure drop and thus friction factor will change. The reason is that the heat transfer changes the fluid viscosities on the wall. The viscous force on the tube wall is the product of the local fluid viscosity and velocity gradient on the tube wall.

In forced convection flow, a radial viscous force gradient occurs between the viscous forces on the tube wall and the fluid viscous forces on the tube centre line. This changes the pressure drop of the flow and the associated friction factor. Furthermore, the temperature difference between the fluid on the tube wall and the fluid on the centre, might also induce natural convection in the form of secondary flow. This will also influence the pressure drop and friction factor.

The combination of viscosity differences and temperature differences in the radial direction influences the velocity and viscosity force distributions in the same direction. The flow condition in laminar flow can be forced convection or mixed convection and is discussed in more detail in section 2.3. Although viscous force gradients exist during laminar diabatic flow conditions, it does not occur during turbulent flow conditions.

During turbulent conditions the inertial forces are so high that the effect of the viscous forces is negligible. As a result, it is generally found that the friction factors between isothermal and diabatic conditions differ, but not in turbulent flow.

Tam and Ghajar [22] showed that for a constant heat flux, in the laminar flow regime, an increase in the friction factor as compared to the Poiseuille relation was found. Conversely, Tam *et al.* [18] reported a diabatic friction factor that is slightly lower that the Poiseuille relation when considering a constant surface heat flux condition in the laminar flow regime. In both instances, this is attributed to secondary flow and should not be present in dominant forced convection flow [18]. Meyer and Olivier [9], who ran experiments using a constant surface temperature condition, reported that their laminar diabatic friction factors of approximately 35% higher than the predicted Poiseuille relation.

Furthermore, as discussed, when the flow regime is turbulent, both Tam and Ghajar [22] and Tam *et al.* [18] showed diabatic friction results are in agreement with the isothermal Blasius equation for isothermal flow.

To accommodate diabatic conditions the isothermal friction factors are normally corrected by including a viscosity ratio as shown in Eq. 2-13.

$$f_{diabatic} = f_{isothermal}\left(\frac{\mu_B}{\mu_s}\right)^m \tag{2-13}$$

where the exponent m varies dependent on the flow regime and inlet geometry.

This correction is based on previous experimental work for both the laminar flow regime [18, 22] and the turbulent flow regime [41].

2.3 Flow regimes

Traditionally, literature defines the flow regimes of fluid flow in three distinct regimes, namely laminar flow, transitional flow and turbulent flow. The Reynolds number, which is defined in paragraph 2.2.1, is used as a qualitative measure to identify the flow regime under consideration. The critical Reynolds (Re_{cr}) number is normally used to approximate if a flow regime is laminar or turbulent. The critical Reynolds number is dependent on surface geometry, surface roughness, upstream velocity, inlet geometry, and surface temperature [11].

As an example, the critical Reynolds number for flow over a flat plate is approximately 10^5 to 3×10^6, while the critical Reynolds number for flow through a circular tube is at a critical Reynolds number of approximately 2 300. The difference in critical number is thus one to two orders of magnitude. As this study addresses a smooth tube, only the transitional characteristics of a smooth tube is considered.

In most of the literature, fluid flow in a smooth pipe is considered to be laminar up to a Reynolds number of approximately 2 300 and fully turbulent at Reynolds numbers higher than approximately 10 000 [13, 17, 18, 23, 42, 43]. Transition is said to occur between Reynolds numbers of 2 300 to 10 000. However, literature also shows that fully laminar flow could be obtained at Reynolds numbers higher than 10 000, depending on the inlet geometry of the tube [13, 18]. In some instances, the flow shows fully turbulent friction characteristics at Reynolds numbers as low as 3000 to 4000 [15, 25, 28]

The three flow regimes are discussed in sections 2.3.1 (laminar), 2.3.2 (turbulent) and 2.3.3 (transitional flow regime).

2.3.1 Laminar flow

Laminar flow is described as where the flow is considered to be steady and smooth. In fully developed laminar flow in a smooth tube, it is expected that the fluid particles move in a constant axial velocity and that the velocity profile of the fluid stream remains unchanged in the axial direction of the fluid flow direction [34].

When heating a tube [33], it is possible to induce two different types of laminar flows, namely forced convection laminar flow and mixed convection laminar flow. For a constant heat flux with laminar forced flow the Nusselt number is 4.36. For a constant wall temperature, the Nusselt number is 3.66. Therefore, the temperature distribution on the wall in the flow direction will influence the heat transfer characteristics. It is therefore important to distinguish which mode of heat transfer occurs as each has different heat transfer characteristics [16].

Forced convection is where the fluid flow is initiated by an external source, such as a pump, where the fluid is pumped through the tube [35]. It is expected that during pure forced convection through a smooth tube, the fluid velocity is able to subdue any buoyancy forces present in the tube. Thus the expectation for forced convection would be that the ratio of the local peripheral heat transfer coefficient at the top and bottom of the tube be as close to unity as possible [16] i.e. where $h_{top}/h_{bottom} \approx 1$, $h_{left}/h_{bottom} \approx 1$ and $h_{right}/h_{bottom} \approx 1$. It is also assumed that the temperature profile of the tube is constant as shown in Fig. 2-1, where in the instance where the tube is being heated, the temperature of the fluid decreases towards the centre of the tube.

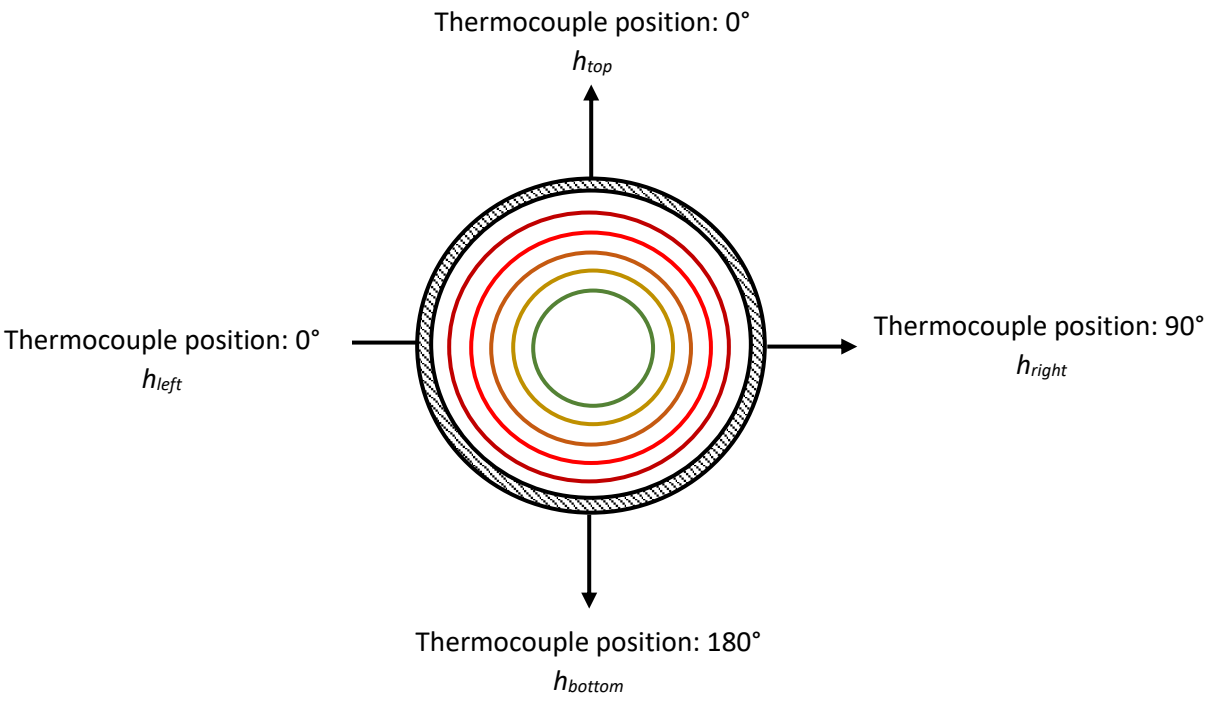

Fig. 2-1 - Constant cross-section temperature "rings" due to forced convection in a heated tube. The red colours indicate high temperatures and the green colours low temperatures

Mixed convection is considered to be a combination of natural convection and forced convection. In natural convection, any fluid motion is purely due to natural means. In the instance of tube flow heating, the buoyancy forces are induced due to the fluid temperature close to the tube wall being higher than the fluid at the center of the tube. This means that the density of the fluid is lower at the tube wall and higher at the center, causing the fluid to circulate naturally in a counter rotating motion [14].

This motion is shown schematically in Fig. 2-2. In principle, the same effects would occur if the tube were to be cooled. In this instance, the temperature of the wall would be lower than the temperature in the center of the tube and the flow direction will be opposite as indicated in Fig. 2-2.

Where mixed convection is dominant, it is expected that the heat transfer coefficient at the bottom of the pipe, h_{bottom}, will be higher than the heat transfer coefficient at the top of the pipe, h_{top}. The heat transfer coefficients are found by determining the heat flux input, the surface temperature (at the 180° and 0° positions respectively) and the bulk mean temperature. Tam and Ghajar [10] state that where $h_{top}/h_{bottom} < 0.8$, mixed convection is dominant.

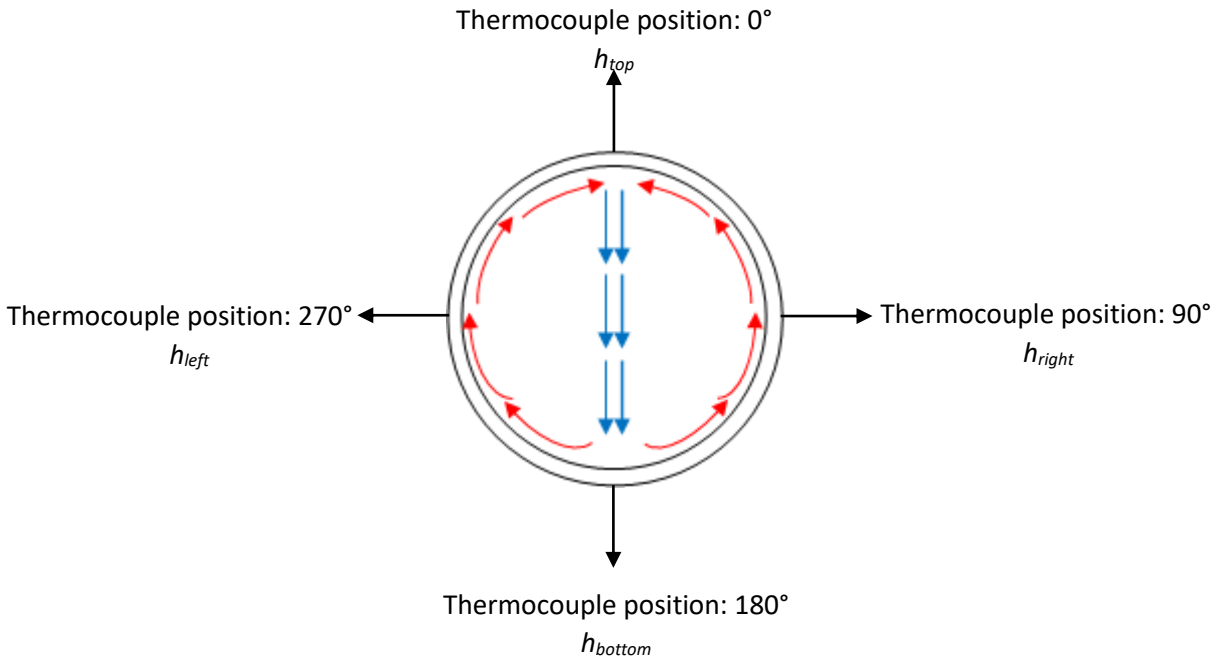

Fig. 2-2 - Fluid circulation in a heated tube due to natural convection (direction of flow out of the page). Red indicates a higher fluid temperature and blue a lower fluid temperature.

As discussed in section 1.2.1, Meyer [11] reported during his review of literature that in the instance where mixed convection was present during fully developed laminar flow in a constant heat flux condition, the heat transfer was increased significantly. The obtained Nusselt numbers were approximately 10 to 20 which are much higher than the accepted 4.36.

2.3.2 Turbulent flow

Fully developed turbulent flow is described as the flow regime where the flow becomes fluctuating and agitated [38]. Due to the highly disorganised nature of the flow, higher heat transfer coefficients are expected thus making this flow regime the most commonly utilised flow regime in practise [33]. However, with higher heat transfer coefficients comes higher pressure drops and thus a need for an increase in pumping power [11].

Turbulent flow is dominated by forced convection as the fluid motion is able to supress any buoyancy forces within the tube.

2.3.3 Transitional flow

In order for flow to be accelerated from laminar flow to turbulent flow, it is necessary for transitional flow to first occur. Transitional flow does not occur at a specific Reynolds number, but rather, over a region and is characterised by intermittent bursts of turbulence within the flow [38]. It is expected that at the start of the region, the flow is fully laminar and by the end of the region, the flow is fully turbulent.

The inlet geometry of the tube has a marked influence on when transitional flow starts and ends. The smoother the entrance (i.e. a rounded bell mouth type shape entrance) the longer it will take for transition to occur. The sharper the entrance (i.e. re-entrant type entrance, where the tube protrudes into the inlet section) will see transition occurring much quicker [33].

During her Masters research Everts [44] defined new nomenclature shown in Fig. 2-3 on a graph of Nusselt number as a function of Reynolds number to better distinguish the boundaries between transitional and turbulent flow. These definitions were used to define the transition characteristics, as there was no clear distinction in the literature between transitional and low-Reynolds-number-end regimes.

Everts defines the critical Reynolds number (Re_{cr}) as the point when transitional flow starts. The end of transition (Re_{lre}) is defined at the point where the gradient of the Nusselt number as a function of Reynolds number decrease. The flow then enters a regime known as the low-Reynolds number end, which is between Re_{lre} and Re_{turb}. In this regime the Nusselt and friction factors were fluctuating but did not have the characteristics of fully turbulent flow as yet. The turbulent flow regime in the figure was identified in Fig. 2-3 as Re_{turb}. For all Reynolds number larger than than Re_{turb}, the flow was fully turbulent.

Although the different flow regimes identified were described on a graph of Nusselt number as a function of Reynolds number, as shown in Fig. 2-3, Everts saw the same results when presenting her results as friction factor (as shown in Fig. 2-4) or j_H-factor as a function of Reynolds number.

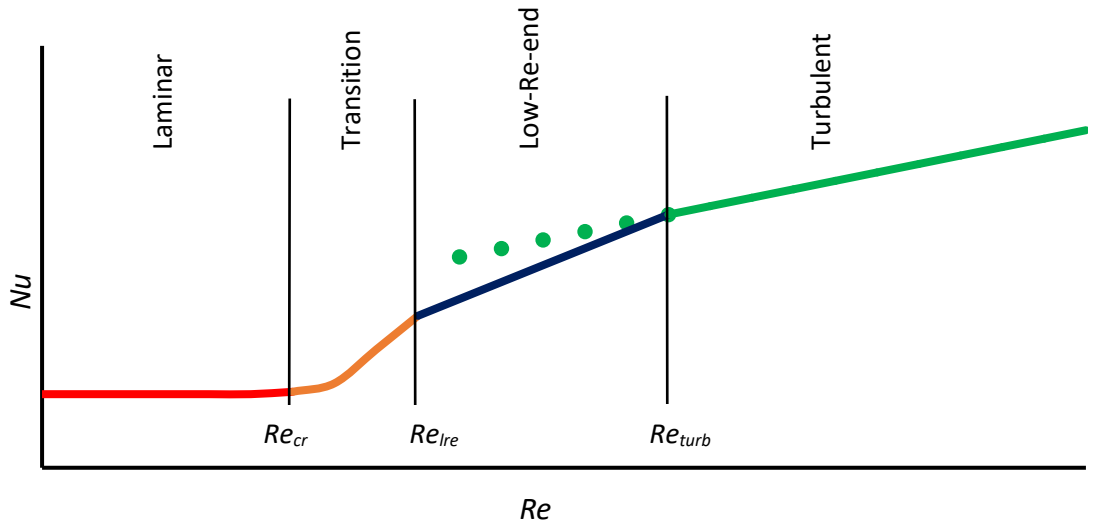

Fig. 2-3 - Representation of the boundaries between transition and turbulent flow for Nusselt numbers (adapted from Everts [44])

Consider Fig. 2-4. The start of transition (Re_{cr}) is defined at the point where the friction factors decrease to a point where there is a zero gradient. It is noted that the laminar friction results agree with fully developed laminar flow friction factor correlations. Once in transition, the friction factors increase up to a point where they once again reach a zero gradient, thus indicating the start of the low-Reynolds-number-end-region (Re_{lre}). Fully developed flow (Re_{turb}) is indicated where the friction factor results correspond to fully developed turbulent flow correlations.

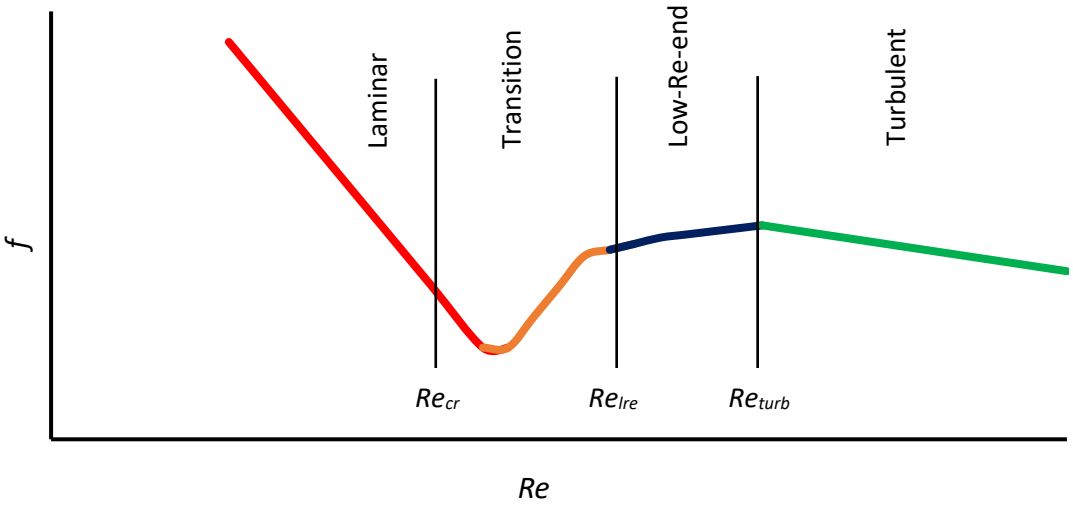

Fig. 2-4 - Representation of the boundaries between transition and turbulent flow for forced convection friction factor (adapted from Everts [44])

2.3.4 Correlations

Numerous heat transfer and pressure drop correlations exist for each of the flow regimes of laminar, turbulent and transitional flow as described in sections 2.3.1, 2.3.2 and 2.3.3. It is important to note that each of these correlations have specific ranges/parameters associated to them and should only be used where applicable to this specific study. All of these correlations are summarised in Table 2-1 to Table 2-6.

Table 2-1 is a summary of the Nusselt number correlations for laminar flow. It starts with the classical relationship that proved that for fully developed, forced flow, with constant heat flux (Eq. 2-15), the Nusselt number is 4.364. The state of art relation for mixed convection as described by Morcos and Bergles [45] is shown in Eq. 2-17. Correlations for constant surface temperature boundary conditions, entrance regions and developing flow are also listed.

In Table 2-2 correlations for friction factors in laminar flow is shown. The table begins with the classic relation of Poiseuille (equation 2-14) that gives the friction factor of isothermal, fully developed laminar flow with forced convection. Eq. 2-21 describes isothermal friction factors in the entrance region and fully developed region for forced convection while Eq. 2-22 describes diabatic friction factors in the entrance region and fully developed region for mixed convection. Fully developed diabatic friction factors for a square edge inlet and re-entrant inlet in mixed convection is described by Eq. 2-23.

Table 2-1 - Nusselt number correlations for laminar flow in a smooth tube

Investigator	Correlation		Parameters	Flow Condition
Classic relation [33]	$Nu = 4.364$	(2-15)	-	Laminar flow Fully developed Forced convection Constant surface heat flux
Sieder and Tate [33]	$Nu = 1.86(Re\ Pr)^{1/3}(x/D_i)^{1/3}(\mu_B/\mu_s)^{0.14}$	(2-16)	$0.6 \leq Pr \leq 5$ $0.0044 \leq (\mu_b/\mu_s) \leq 9.75$ All properties to be evaluated at T_b except μ_s, which is evaluated at the surface temperature	Laminar flow Entrance and fully developed Forced convection Constant surface temperature
Morcos and Bergles [45]	$Nu = \left[(4.36)^2 + \left\{0.055\left(\frac{Gr_{film}Pr_{film}^{1.35}}{Pw^{0.25}}\right)^{0.4}\right\}^2\right]^{1/2}$	(2-17)	$4 \leq Pr \leq 175$ $3 \times 10^4 \leq Ra \leq 10^6$ $2 \leq Pw \leq 66$	Laminar flow Fully developed Mixed convection Constant surface heat flux
Ghajar and Tam [14]	$Nu_l = 1.24[(Re\,\mathrm{Pr}\,D_i/x) + 0.025(GrPr)^{0.75}]^{1/3}\left(\frac{\mu_B}{\mu_s}\right)^{0.14}$	(2-18)	$40 \leq Pr \leq 160$ $1.2 \leq (\mu_b/\mu_s) \leq 3.8$ $3 \leq x/D_i \leq 192$ $280 \leq Re \leq 3800$ $1000 \leq Gr \leq 2.8 \times 10^8$	Laminar flow Entrance and fully developed Forced and mixed convection Constant surface heat flux
Gnielinski [46]	$Nu = (Nu_1^3 + 0.6^3 + (Nu_2 - 0.6)^3 + Nu_3^3)^{1/3}$ $Nu_1 = 4.354$ $Nu_2 = 1.953\sqrt[3]{Re\,\mathrm{Pr}\,D_i/L}$ $Nu_2 = 0.924\sqrt[3]{Pr}\sqrt{Re\ D_i/L}$	(2-19)	$2300 \geq Re$	Laminar flow Forced convection

Table 2-2 - Friction factor correlations for laminar flow in a smooth flow

Investigator	Correlation		Parameters	Flow Condition
Classic relation of Poiseulle [47]	$f = {}^{64}/_{Re}$	(2-20)	$2100 \geq Re$	Laminar flow Fully developed Forced convection Isothermal
Tam *et al.* [18]	$f = \frac{1}{Re}\left(64 + \frac{0.00314}{0.00004836 + 0.0609 \times \zeta^{1.28}}\right)$ $\zeta = \frac{x/D_i}{Re}$	(2-21)	$799 \leq Re \leq 2240$ $3 \leq x/D_i \leq 200$	Laminar flow Entrance and fully developed Forced convection Isothermal
Tam *et al.* [18]	$f = \frac{4}{Re}\left(64 + \frac{0.00314}{0.00004836 + 0.0609 \times \zeta^{1.28}}\right) \times \left(\frac{\mu_B}{\mu_s}\right)^m$ $\zeta = \frac{x/D_i}{Re}$ $m = -5.06 + 0.84Pr^{0.23}Gr^{0.09}$	(2-22)	$39 \leq Pr \leq 47$ $1.27 \leq (\mu_b/\mu_s) \leq 1.56$ $897 \leq Re \leq 2189$ $7141 \leq Gr \leq 18224$	Laminar flow Entrance and fully developed Mixed convection Diabatic
Tam and Ghajar [22]	$f = \frac{64}{Re}\left(\frac{\mu_B}{\mu_s}\right)^m$ $m = 1.65 - 0.013Pr^{0.84}Gr^{0.17}$	(2-23)	$6 \leq Pr \leq 36$ $1.25 \leq (\mu_b/\mu_s) \leq 2.4$ $1100 \leq Re \leq 7400$ $17100 \leq Gr \leq 95600$	Laminar flow Fully developed Mixed convection Diabatic Re-entrant and square-edge

Turbulent flow correlations for Nusselt numbers are listed in Table 2-3. Fully developed flow is expected to occur within ten diameters. The inner diameter of the tube considered in this study is equal to 4.04 mm, which implies that fully developed flow will be achieved within 44 mm. As a result, only fully developed equations are considered in Table 2-3.

The first four equations in the table are the well-known classical equations of Colburn [48], Dittus-Boelter [49], Sieder and Tate [50], and Gnielinski [51]. In general, it was found that over time the accuracies of these equations improved, with the most accurate being that of Gnielinski (Eq. 2-30). When considering Eq. 2-27 to Eq. 2-30, the radial temperature differences are not high enough to impact the fluid properties in the radial direction. This is generally true for turbulent flow. However, in the case where a high heat flux is used, there are significant changes in fluid viscosities in the radial direction. As a result, a viscosity correction term is used as shown in Eq. 2-31 as suggested by Ghajar and Tam [14].

Three isothermal friction factor equations are listed in Table 2-4, namely Petukhov (Eq. 2-24), Blasius (Eq. 2- 25), and Allen and Eckert (Eq. 2-26) equations. As with the Nusselt number equations listed in Table 2-3, flow in the turbulent flow regime is fully developed within ten diameters, therefore all of the equations in Table 2-4 is for fully developed flow. The Blasius equation [52] accurately predicts friction factors to within 2.6% if the Reynolds number is less than 100 000. The expected error of the Petukhov equation [53] error is up to 17% at low Reynolds numbers (<10 000). Eq. 2-34 of Allen and Eckert [41] is to be used with high heat fluxes when a significant viscosity gradient exists in the radial direction.

When considering transitional flow with a uniform wall heat flux condition, it is important to differentiate the inlet geometry of the test section as this has an impact on the applicable correlation. In the case of this study, there is one Nusselt number correlation as shown in Table 2-5 that is applicable to this study. Eq. 2-35 was developed by Ghajar and Tam [14] and has been specifically derived for a square edge inlet with a uniform wall heat flux.

Isothermal and diabatic friction factors are shown in Table 2-6. These correlations are specific for a square edge inlet geometry, which is the geometry of interest in this study. Eq. 2-36 of Ghajar and Madon [15] and Eq. 2-38 of Tam *et al.* [18] describes isothermal friction factors. Tam and Ghajar [22] and Tam *et al.* [18] also derived diabatic friction factors for a square edge inlet geometry as shown in Eq. 2-37 and Eq. 2-39 respectively.

Table 2-3 - Nusselt number correlations for turbulent flow in smooth tubes

Investigator	Correlation		Parameters	Flow Condition
Colburn [48]	$Nu = 0.023Re^{0.8}Pr^{1/3}$	(2-27)	$0.7 \leq Pr \leq 160$ $Re > 10000$	Turbulent flow
Dittus-Boelter [49]	$Nu = 0.023Re^{0.8}Pr^{0.4}$	(2-28)	$0.7 \leq Pr \leq 160$ $Re > 10000$	Turbulent flow
Sieder and Tate [50]	$Nu = 0.027Re^{0.8}Pr^{1/3}\left(\frac{\mu_B}{\mu_s}\right)^{0.14}$	(2-29)	$0.7 \leq Pr \leq 16700$ $Re > 10000$	Turbulent flow
Gnielinski [51]	$Nu = \frac{(f/8)(Re-1000)Pr}{1+12.7(f/8)^{0.5}(Pr^{2/3}-1)}$	(2-30)	$0.5 \leq Pr \leq 2000$ $3 \times 10^3 < Re < 5 \times 10^6$	Turbulent flow
Ghajar and Tam [14]	$Nu_{tur} = 0.023Re^{0.8}Pr^{0.385}\left(\frac{x}{D_i}\right)^{-0.0054}\left(\frac{\mu_B}{\mu_s}\right)^{0.14}$	(2-31)	$4 \leq Pr \leq 34$ $1.1 \leq (\mu_b/\mu_s) \leq 1.7$ $7000 \leq Re \leq 49000$ $3 \leq x/D_i \leq 192$	Turbulent flow Wall heat flux is significant

Table 2-4 - Friction factor correlations for turbulent flow in a smooth tube

Investigator	Correlation		Parameters	Flow Condition
Petukhov [53]	$f = (0.790 ln Re - 1.64)^{-2}$	(2-32)	$3000 \leq Re \leq 5 \times 10^6$	Turbulent flow Fully developed Isothermal
Blasius [52]	$f = 0.316 Re^{-0.25}$	(2-33)	$3000 \leq Re \leq 5 \times 10^6$	Turbulent flow Isothermal
Allan and Eckert [41]	$f = 0.316 Re^{-0.25} \left(\frac{\mu_B}{\mu_s}\right)^{-0.25}$	(2-34)		Turbulent flow Fully developed Diabatic

Table 2-5 - Nusselt number correlations for transitional flow, square edge inlet

Investigator	Correlation		Parameters	Flow Condition
Ghajar and Tam [14]	$Nu_{trans} = Nu_l + \left\{\exp\left(\frac{a - Re}{b}\right) + Nu_{tur}^c\right\}^c$ $Nu_l = 1.24[(Re \Pr D_i/x) + 0.025(GrPr)^{0.75}]^{1/3} \left(\frac{\mu_B}{\mu_s}\right)^{0.14}$ $Nu_{tur} = 0.023 Re^{0.8} Pr^{0.385} \left(\frac{x}{D_i}\right)^{-0.0054} \left(\frac{\mu_B}{\mu_s}\right)^{0.14}$ $a = 2617; b = 207; c = -0.95$	(2-35)	$5 \leq Pr \leq 55$ $1.2 \leq (\mu_b/\mu_s) \leq 2.6$ $1600 \leq Re \leq 10700$ $4000 \leq Gr \leq 250000$ $3 \leq x/D_i \leq 192$	Transitional flow Entrance and fully developed Forced and mixed convection Constant surface heat flux

Table 2-6 - Friction factor correlations for transitional flow, square edge inlet

Investigator	Correlation		Parameters	Flow Condition
Ghajar and Madon [15]	$f = 4c_f = -2.56 \times 10^{-2} + 2.49 \times 10^{-5} Re - 4.25 \times 10^{-9} Re^2$	(2-36)	$2055 \leq Re \leq 3140$	Transitional flow Fully developed Isothermal
Tam and Ghajar [22]	$f = 4c_f = \left[1 + \left(\frac{Re}{a}\right)^b\right]^c \left(\frac{\mu_B}{\mu_s}\right)^m$ $a = 4230; b = -0.16; c = -6.57;$ $m = -1.13 - 0.396 Gr^{-0.16} Pr^{5.1}$	(2-37)	$12 \leq Pr \leq 29$ $1.11 \leq (\mu_b/\mu_s) \leq 1.89$ $3500 \leq Re \leq 6900$ $6800 \leq Gr \leq 104500$ $3 \leq x/D_i \leq 192$	Transitional flow Fully developed Diabatic
Tam *et al.* [18]	$f = \left(\frac{64}{Re}\right)\{[1 + (0.0049 Re^{0.75})^a]^{1/a} + b\}$ $a = 0.5; b = -4.0$	(2-38)	$2111 \leq Re \leq 4141$ $3 \leq x/D_i \leq 200$	Transitional flow Fully developed Isothermal
Tam *et al.* [18]	$f = \left(\frac{64}{Re}\right)\{[1 + (0.0049 Re^{0.75})^a]^{1/a} + b\}\left[1 + \left(\frac{c}{x/D_i}\right)\right]$ $a = 0.5; b = -4.0; c = 3.0$	(2-39)	$2109 \leq Re \leq 4184$ $3 \leq x/D_i \leq 200$	Transitional flow Fully developed Diabatic

2.3.5 Flow regime maps

As discussed in section 1.5, the objective of this study was to ensure that forced convection results were obtained in the laminar flow regime before the flow moves into the transitional flow regime. In order to establish where forced convection would take place in laminar flow, flow regime maps in literature were investigated.

In 1964, the work of Metais and Eckert [32] was published. They presented their experimental results in the form of flow regime maps for flow through both vertical and horizontal tubes. These maps showed boundaries as to where the different convective flow regimes could be expected as a function of the Reynolds number and the Rayleigh number. The flow regime map for flow through horizontal tubes is shown in Fig. 2-5.

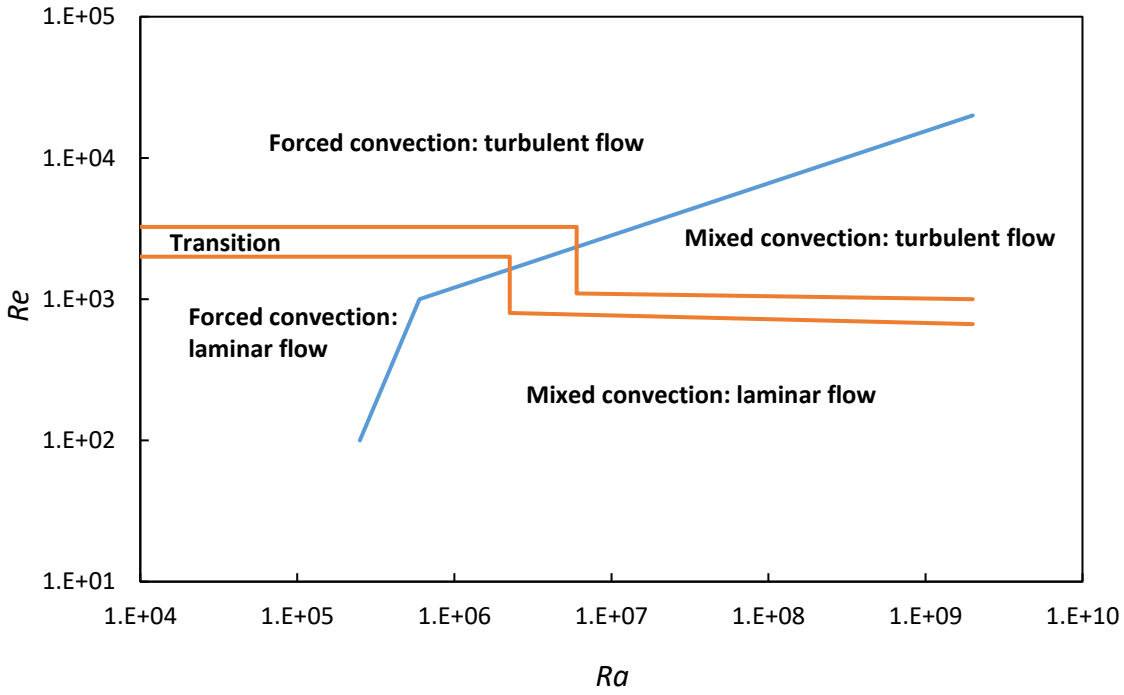

Fig. 2-5 - The flow regime map for constant wall temperature boundary conditions as developed by Metais and Eckert [32]

From Fig. 2-5, it follows that if the Reynolds number is kept between 10 and 2 200, with a Rayleigh number below approximately 100 000 to 150 000, forced convection could be expected. It is important to note that this flow regime map was developed for a constant wall temperature condition (and not for a constant heat flux as in this study) and the effect of using this map as a reference for a constant surface heat flux condition was not quantified in the publication.

In 1970, Petukhov and Polyakov [54] presented a flow regime map for flow through horizontal tubes where a constant heat flux condition was maintained. This is shown in Fig. 2-6. They observed mixed convection at Rayleigh numbers exceeding 2 000. At Rayleigh numbers below 2 000, with a Reynolds number range of between 40 and 2 000, the effect of free convection was not observed. Transition in their work occurred at an approximate Reynolds number range of between 2 000 and 9 000.

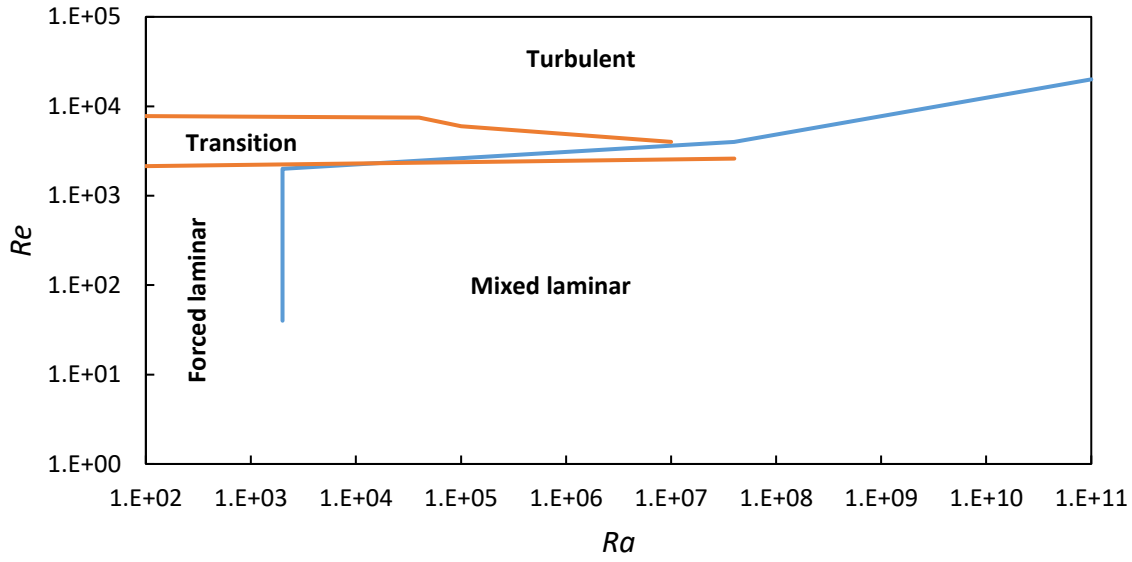

Fig. 2-6 - Flow regime map as developed by Petukhov and Polyakov [54] for a constant surface heat flux

More recently, Ghajar and Tam [16] developed a modified flow regime map for flow through a horizontal tube with a constant surface heat flux condition based on the work of Metais and Eckert [32]. Ghajar and Tam plotted their experimental results on Metais' map and found that while the forced turbulent convection data agreed well with the boundary set by the map, the experimental data did not agree with the forced convection, mixed laminar, mixed transition and forced transition regions. Ghajar and Tam concluded that the map of Metais and Eckert could not be used due to the influence of the boundary condition and the inlet geometry of the test section [16].

They developed a modified map, for three different inlet geometries whereby the lower and upper limits of transition are shown by lower and upper bounds at specific x/D_i locations. The map for a square edge inlet geometry is shown in Fig. 2-7. In order to determine the boundary of the forced convection region, Ghajar and Tam used the criterion where $h_{top}/h_{bottom} > 0.8$ which they indicate as indicative of forced convection. A total 51 data points for the three different inlet geometries was found to meet this criterion and used to plot the boundary. A least squares curve fitting program was used to create a smooth curve [16].

From Fig. 2-7, it follows that if the Reynolds number between 100 and 2 200, with a Rayleigh number below 320 000, forced convection could be expected.

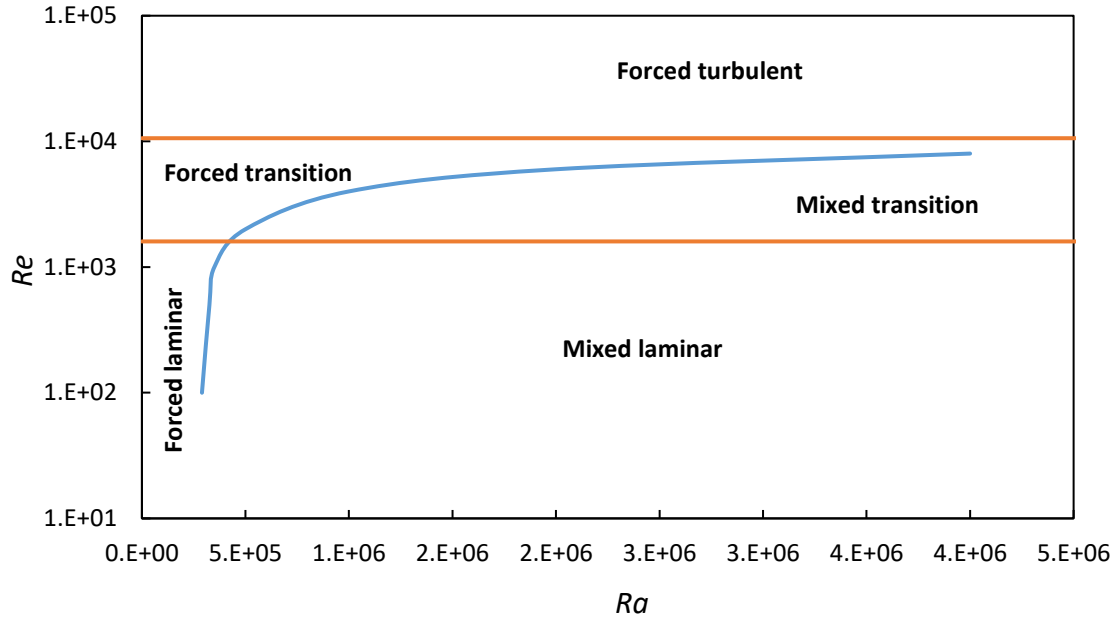

Fig. 2-7 - Flow regime map as developed by Ghajar and Tam [16] for a constant surface heat flux condition for a square edge inlet geometry; 280 < Re_B < 49 000; 4 < Pr_B < 185; 1 000 < Gr_B <250 000; 13 < Nu_B < 258; 4 < $\dot{q}$ < 670 [W/m²]; x/D_i = 3 lower bound; x/D_i = 192 upper bound

Each of the three maps of Metais and Eckert [32], Petukhov and Polyakov [54] and Ghajar and Tam [16] draw very different conclusions as to where forced convection can be expected. The parameters of the maps also tend to differ significantly from the expected operating parameters of this study.

The map of Metais and Eckert [32], shown in Fig. 2-5, was specifically derived for a constant surface temperature condition. It is expected that in turbulent flow, this should not present a problem. This was shown to be untrue in laminar flow. The experimental results of Ghajar and Tam [14] showed that the heating boundary condition influenced the expected ranges in which transition from laminar flow to transitional flow and similarly to turbulent flow for mixed and forced convection conditions.

However, when constructing their map, as shown in Fig. 2-7, Ghajar and Tam [14] were unable to define a clear boundary between forced laminar flow and mixed laminar flow as their Nusselt numbers results in the laminar flow regimes were above the accepted 4.364. Their assumption that the criterion where h_{top}/h_{bottom} > 0.8 was used to create this boundary. The accuracy of this assumption is still to be tested.

While the maps of Metais and Eckert and Ghajar and Tam show a similar Rayleigh number for the boundary between forced laminar and mixed laminar results (250 000 and 290 000 respectively) the work of Petukhov and Polyakov [54], as shown in Fig. 2-6, predict the boundary to occur at a Rayleigh number two orders of magnitude lower (2 000).

Due to the distinction differences in the maps, a strategy is needed in order to determine which of these maps most accurately describe the expected results of this study. It is possible to determine the transition range by monitoring the friction factors. Everts proved in her thesis that lower and upper bounds of the transition range for friction factors was the same for heat transfer [44]. If the Reynolds number is chosen in the laminar flow regime and is kept constant, the Rayleigh number can be slowly adjusted by applying different heat fluxes. By monitoring the Nusselt number, it will be possible to identify where the Rayleigh number moves between the boundary of forced laminar flow (where the Nusselt number is 4.364) and mixed convection laminar flow (where the Nusselt number is greater than 4.364). Once this point in the boundary has been identified, the Reynolds number can be adjusted, higher or lower, to determine how the boundary is shaped.

2.4 Developing and fully developed flow

One of the characteristics of the study was to consider fully developed flow. This is defined as the region in tube where two specific conditions are met. The first is that the velocity profile is fully developed and remains unchanged. This is known as the hydrodynamically fully developed region [33]. Fig. 2-8 schematically describes the development of the hydrodynamic boundary layer where the flow in the tube is laminar and isothermal. The velocity profile at the inlet is plug flow. Due to the wall shear forces, a parabolic velocity profile develops with time.

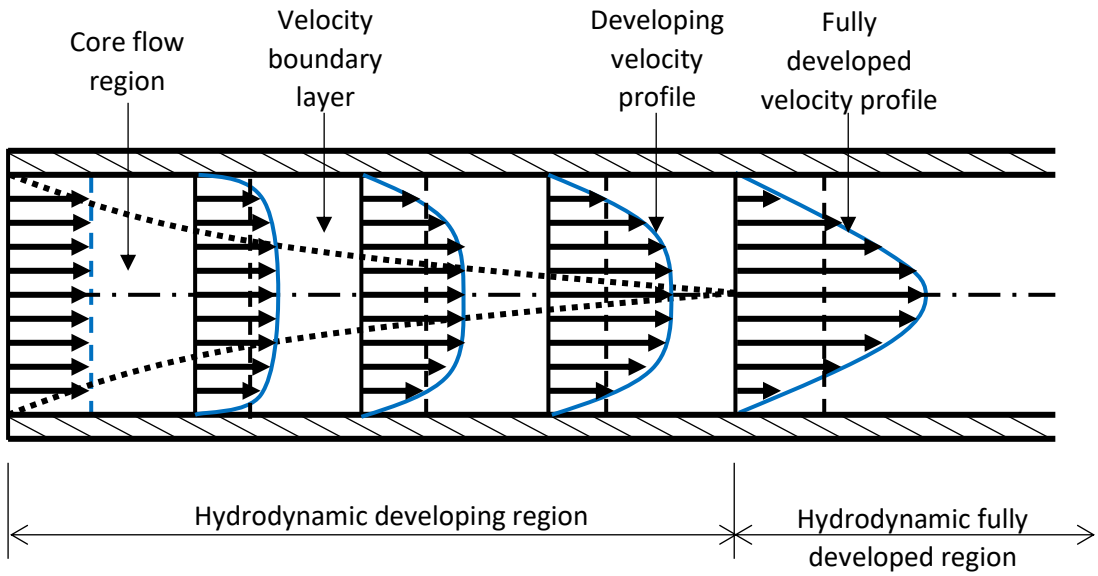

Fig. 2-8 - The development of the isothermal hydrodynamic boundary layer [33]

The second condition refers to the region in the tube where the thermal boundary layer reaches the centre of the tube. This is called the thermally fully developed region. Like the velocity profile, the temperature profile remains constant in the fully developed region of the tube for a constant surface heat flux [33]. It is noted that the magnitude of the temperature

in the profile changes, unlike the velocity profile which remains the same. Fig. 2-9 schematically describes where the thermal boundary layer is developed.

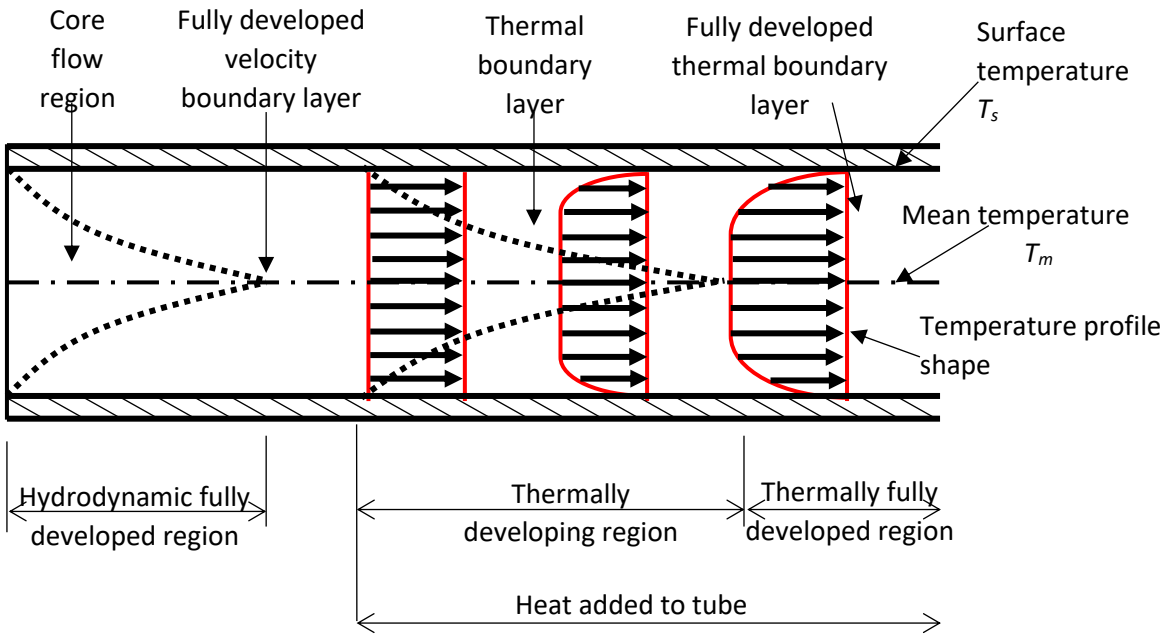

Fig. 2-9 - The development of the thermal boundary layer [33]

The dimensionless temperature profile in the fully developed region is expressed as $(T_s - T)/(T_s - T_m)$. If it remains unchanged in the flow direction, then the flow is considered to be thermally fully developed [33]. It is noted that although the temperature profile may vary with x, the dimensionless temperature profile remains constant in the fully developed region for a constant surface heat flux condition. Therefore, it follows that the derivative of $(T_s - T)/(T_s - T_m)$ with respect to r should also be independent of x [33].

This can be expressed mathematically as [33]:

$$\frac{\partial}{\partial r}\left(\frac{T_s - T}{T_s - T_m}\right)\Bigg|_{r=R} = \frac{-(\partial T/\partial r)\big|_{r=R}}{T_s - T_m} \neq f(x) \tag{2-40}$$

Consider a uniform wall surface heat flux condition, which is the heating condition of interest in this study. This is the product of the heat transfer coefficient and the difference between the surface temperature of the tube (T_s, equivalent to the temperature of the water in contact with the wall of the tube) and the mean temperature of the water in the tube (T_m) at a specific location x.

Therefore surface flux, with respect to r, can be expressed as:

$$\dot{q}_s = h_x(T_s - T_m) = k\frac{\partial T}{\partial r}\Bigg|_{r=R} \rightarrow h_x = \frac{k(\partial T/\partial r)\big|_{r=R}}{T_s - T_m} \tag{2-41}$$

Simultaneously developing flow, shown in Fig. 2-10, refers to the condition where the tube is heated from the tube inlet. In this instance, the hydrodynamic boundary layer and the thermal boundary layer develop at the same time. It is important to note that the heat transfer coefficient only becomes fully developed once the thermal boundary layer is fully developed. Similarly, the friction factor will be considered as fully developed once the hydrodynamic boundary layer is fully developed.

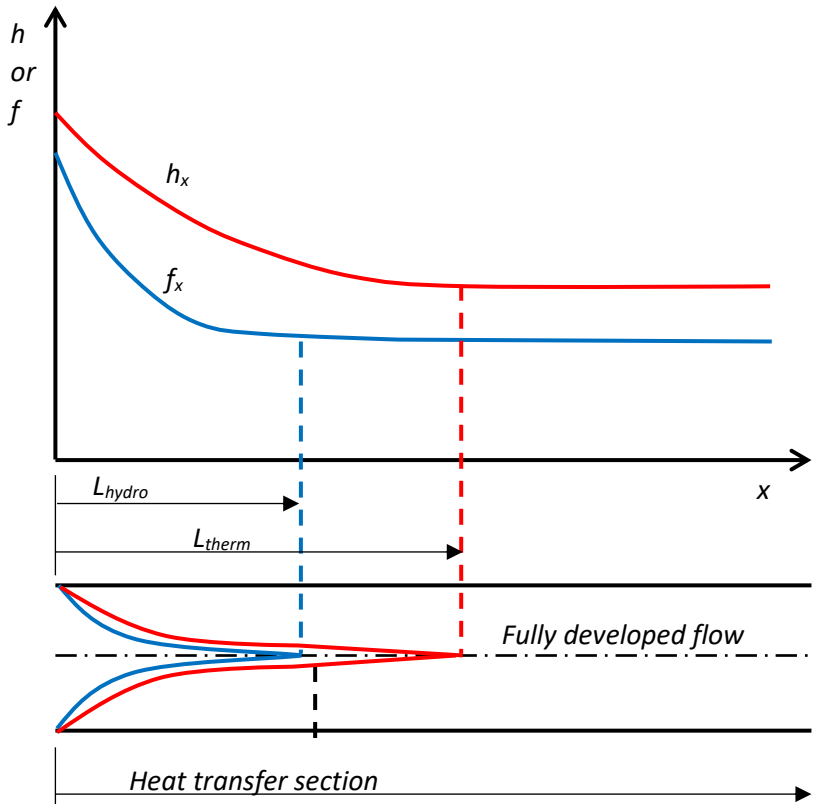

Fig. 2-10 - Schematic representation of simultaneously developing flow, where the variation of the friction factor and convection heat transfer coefficient is shown (Pr > 1) [33]

The hydrodynamic and thermal entrance lengths for laminar flow can be approximated as [33]:

$$L_{hydro,lam} \approx 0.05\, Re\, D_i \tag{2-42}$$

$$L_{therm,lam} \approx 0.05\, Re\, Pr\, D_i \tag{2-43}$$

As can be seen in Eq. 2-42, the hydrodynamic boundary layer develops independently of the Prandtl number in the laminar flow regime. However, in the case of the thermal boundary layer, the Prandtl number has a direct influence on the thermal entrance length, as shown in Eq. 2-43.

In laminar flow, the Prandtl number described the relative growth of the velocity and thermal boundary layers. Where the Prandtl number is approximately one, as is the case for most gases, the two boundary layers coincide with each other. Where the Prandtl number is less than one, the thermal boundary layer grows at a higher rate than the hydrodynamic boundary

layer, which will result in a thermal boundary layer that is shorter than the hydrodynamic boundary layer. Conversely, the opposite is true where the Prandtl number is greater than 1. In this instance the hydrodynamic boundary layer is shorter than the thermal boundary layer.

Water has a Prandtl number of 7.01 at 20°C [34]. In the case of this study, the temperature of water at the inlet of the test section was maintained as close to 20°C as possible. This inferred that the thermal boundary layer would always exceed the hydrodynamic boundary layer in the laminar flow regime.

The hydrodynamic and thermal entrance lengths for turbulent flow can be approximated as [33]:

$$L_{hydro,tur} \approx L_{thermal,tur} \approx 10\, D_i \tag{2-44}$$

As can be seen in Eq. 2-44, the hydrodynamic and thermal boundary layer develop at the same pace as a function of the inner diameter of the test section for turbulent flow. Fluid properties do not affect the entrance lengths.

2.5 Influences on transition

In his critical discussion of work completed in the transitional flow regime, Meyer [9] described a number of factors that can influence transition. These included the different types of inlet geometries, the effect of the re-entrant tube geometry, tube diameter layout and pitch, the effect of internal surface roughness of the tube, the effect of turbulence intensity at the test section inlet and so on.

To date, a fair amount of research has been concentrated on the different inlet geometries and the effect of internal surface roughness. Research has been conducted in micro tubes where in some cases, the effect of the internal roughness of the tube is quantified. These two areas are discussed in sections 2.5.1 and 2.5.2.

2.5.1 Inlet geometries

To date, four different types of inlet geometries, as shown in Fig. 2-11 have been researched when considering the effect of heat transfer and pressure drop in the transitional flow regime. Ghajar and co-workers [10, 14-16, 18, 21, 22] considered three types of inlets, namely the re-entrant, the square-edge and the bell mouth inlet. Meyer and co-workers [9, 12, 13, 24, 25, 29] also considered the previously mentioned inlet geometries as well as the hydrodynamically fully developed geometry. In all instances a calming section was used upstream of the inlet geometry. This is thought to replicate the header box of a heat exchanger.

The re-entrant geometry is one where the tube extrudes from the tube sheet by a certain length. Presently, the only re-entrant geometry that has been investigated is where a length of one diameter of the tube extrudes into a calming section. This is considered to be a “sharp” inlet geometry.

A square edge geometry is where the tube is flush with the tube sheet. This replicates a sudden contraction which is indicative of shell and tube heat exchangers where the flow enters the tube from a calming section. The value of the contraction ratio has not been quantified. This is also considered to be a “sharp” inlet geometry.

A bell mouth inlet is one where the contraction is smooth. This type of inlet is representative of the smooth rounded inlet types used in classical literature.

Finally, the hydrodynamically fully developed geometry allows for the flow to become hydrodynamically fully developed before entering the test section. Whereas the previous three inlet type have developing hydrodynamic flow, this inlet geometry ensures the velocity profile is fully developed before heating is started.

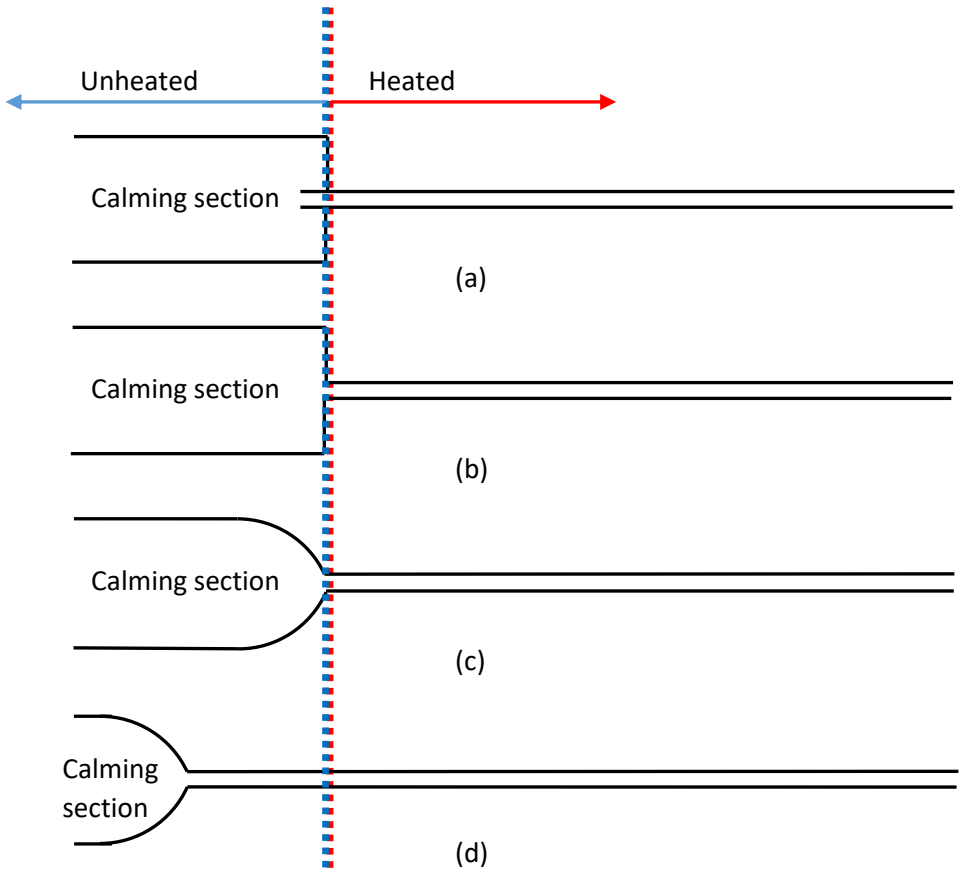

Fig. 2-11 - Inlet geometries where: (a) re-entrant, (b) square edge, (c) bell mouth and (d) hydrodynamically fully developed (as adapted from [11])

Research by Ghajar and co-workers and Meyer and co-workers has shown that the inlet geometry has an influence on when transition occurs for both heat transfer and pressure drop. The range of transition is also effected as the smoother the inlet geometry, the more delayed transition is and the wider the transition range while as the sharper inlet geometry types showed a much tighter transition range that occurs quicker.

In all instances of the work of Ghajar and co-workers, the transition range is based on a specific x/D_i parameter. The upper and lower limits of the heat transfer transition for the re-entrant,

square-edge and bell mouth inlet geometry for work of Ghajar and Tam is summarized in Table 2-7 [10] for $3 \leq x/D_i \leq 192$.

Table 2-7 - The lower Reynolds number (Re_{low}) and upper Reynolds number (Re_{up}) limits of heat transfer transition

Inlet geometry	Lower limit	Upper limit
Re-entrant	$Re_{low} = 2\,157 - 0.65\,[192 - (x/D_i)]$	$Re_{up} = 8\,475 - 9.28\,[192 - (x/D_i)]$
Square edge	$Re_{low} = 2\,524 - 0.82\,[192 - (x/D_i)]$	$Re_{up} = 8\,791 - 7.69\,[192 - (x/D_i)]$
Bell mouth	$Re_{low} = 3\,787 - 1.8\,[192 - (x/D_i)]$	$Re_{up} = 10\,481 - 5.47\,[192 - (x/D_i)]$

Tam *et al.* [18] revisited the work of Ghajar and Tam [14] by focusing on the expected friction factor results for a re-entrant and square-edge geometry. Their results for the heat transfer and friction factor transition range is summarized in Table 2-8 at a x/D_i of 200.

Table 2-8 – The start and end of transition of the fully developed heat transfer and friction factor at x/D_i of 200

Inlet geometry	Heat transfer Start of transition Re_{start}	End of transition Re_{end}	Friction factor Start of transition Re_{start}	End of transition Re_{end}
Re-entrant (isothermal)	-	-	2 032	3 031
Re-entrant (diabatic)	2 001	7 919	2 257	3 250
Square edge (isothermal)	-	-	2 222	3 588
Square edge (diabatic)	2 298	8 357	2 316	3 941

It can be concluded from the results in Table 2-8 that the friction factor transition range differs significantly from that of the heat transfer transition range, where the heat transfer range is much wider than that of the friction factor range [18].

However, the work of Everts [44] showed conflicting results to that of Tam *et al.* [18]. Her results showed that the friction factor transition range did not differ from the heat transfer range and were equally wide.

2.5.2 Micro tubes

Ghajar *et al.* [17] investigated the friction factor in the transition regime in mini and micro tubes. Twelve stainless steel tubes were studied, with an internal diameter ranging from 2.083 mm to 0.337 mm. It was found that the start and end of the friction factor transition range was influenced by the tube diameter. They concluded that as the tube diameter became smaller, the relative roughness of the tube become more significant, thus influencing the

friction factor. They also concluded that as the relative roughness became more significant, the onset of transition was accelerated. [17]

Morini *et al.* [42] considered micro convective heat transfer in the laminar and transitional regions. They completed their experiments using roughened stainless steel tubes with internal diameters ranging of 0.44 mm, 0.28 mm and 0.146 mm. The relative surface roughness (ε/D_i) of those tubes were 0.00682, 0.0107 and 0.041 respectively. It was found that where the relative roughness was considered to be insignificant (where the ratio of the internal surface roughness as compared to the inner diameter was below 4%), heat transfer was not affected in laminar flow regime. It was found that the onset of transition was dependent on many parameters such as the internal surface roughness, the heated length and the inlet geometry [42].

Yang and Lin [31] considered the heat transfer characteristics of water flow in micro tubes. Non-contacted liquid crystal thermography was used for temperature measurements. The flow was hydrodynamically fully developed before heating was induced and measurements taken. Tubes ranging from 0.962 mm to 0.123 mm in internal diameter were assessed. The internal surface roughness of the tubes was not quantified. It was found that the developing thermal entrance length for micro tubes is longer than that of conventional macro tubes. Yang and Lin concluded that the conventional heat transfer correlation for laminar and turbulent flow can be applied for predicting fully developed heat transfer performance in micro tubes. [31]

2.6 Effect of axial conduction

At lower Reynolds number, the effects of axial conductive heat transfer through the tube wall can become a competitive mechanism to the internal convective heat transfer [42].

Maranzana *et al.* [55] investigated this effect and found that if the inequality as shown in equation 2-45 is satisfied, the effect of axial conduction through the walls of the tubes can be neglected.

$$\mathrm{M} = \left(\frac{k_s}{k_B}\right)\left(\frac{D_o^2 - D_i^2}{D_i L_h}\right)\frac{1}{Re\ Pr} < 10^{-2} \tag{2-45}$$

2.7 Work of Ghajar

Ghajar from Oklahoma State University in the United States of America and his co-workers has completed extensive research with regards to the effect of inlet geometries on transitional flow with a constant surface flux condition. They have investigated the heat transfer and friction factor characteristics of horizontal macro tubes with varying inlets [10, 14, 15, 18, 21, 22] as well as friction factor characteristics in micro tubes [17]. They also developed a flow regime map, as discussed in section 2.3.5, where they investigated the boundary between forced and mixed convection [16].

As discussed in section 2.5.1, the types of inlets that were experimentally investigated were re-entrant, square-edge and bell mouth. In their early works, they used stainless steel tubes with a constant heat flux condition which was induced by passing current through the tube [14, 15].

They found, with isothermal friction results, that transition was affected by the type of inlet in use and that the sharper the inlet type, the quicker transition would take place, conversely, the more rounded the entrance type, the more transition would be delayed [15]. When considering the diabatic friction factors in laminar and transition and the start and end of transition differed significantly. However, turbulent results remained the same. This was attributed to mixed convection and secondary flow effects [22].

The heat transfer results revealed that mixed convection was a definite mode of heat transfer when plotting the Colburn j_H-factor as a function of Reynolds. The results did not follow the forced convection line of Nusselt number of 4.36 from laminar flow to transitional flow [10]. In fact, they experimentally found an average Nusselt number of 14.5 in laminar flow. This is indicative of the influence of natural convection on heat transfer [10]. As was the case with the friction factors, the inlet geometry had an effect on the start and end of transition with the turbulent results remaining constant [14].

When considering pressure drop in mini- and micro-tubes they found that while the friction factors were not influenced by the tube diameters of tubes larger than 1 372 µm, they did find that transition was affected by smaller tubes, from 838 µm to 337 µm. They attributed this to the ratio of the internal surface roughness to internal diameter, thus, in effect, indicating that the tube was no longer considered to be smooth [17].

Most recently, Ghajar's co-worker Tam [18], published a paper where he developed a single correlation for friction factors that was valid from laminar flow through transitional flow into turbulent flow. Experiments were completed using a copper tube and a direct current power supply using a square edge and re-entrant inlet geometry. It was found that the transition for heat transfer was much wider as compared to friction.

2.8 Work of Meyer

Meyer of the University of Pretoria in South Africa also spent a significant amount of time considering the characteristics of transitional flow. With his PhD student, Olivier [13], his first focus was on transitional flow in a smooth tube with a constant wall temperature, thus inducing cooling. He considered four different types of inlets and while it was found that it was challenging to maintain the constant surface temperature, it was also challenging to determine the average fluid temperatures [12, 29]. In a similar fashion to that of Ghajar and his co-workers, the experimental results showed that the sharper inlets produced an earlier transition as compared to the smoother inlets which was delayed. Heat transfer results revealed that secondary flow was present as the Nusselt numbers were higher than expected [13].

Meyer and Olivier [28] also considered enhanced tubes as these has a significant applications in the chiller industry. They found that the isothermal friction factor in enhanced tubes was higher as compared to smooth tubes. This was expected as the fins would increase flow resistance. They also found that the start and end of transition changed with varying inlet geometries, with the smoother inlet having the most delayed transition. The diabatic results differed significantly to the isothermal results. Diabatic laminar and transitional friction results increased when heat transfer occurred, while as turbulent friction results were similar. Secondary flow effects are thought to be the cause of this increase. The overall heat transfer was found to be slightly lower than in smooth tubes. Meyer attributed this to the negative effect the fins may have in restricting the flow path for secondary flow.

Nanofluids were also investigated by Meyer and his co-workers [26]. It was expected that the addition of carbon nanofluids would increase the heat transfer of the working fluid. Diabatic friction results revealed that the addition of nanofluids did not affect the turbulent friction factors significantly as compared to water. However, in the laminar and transitional regime, there was a significant difference. This is attributed to the change in viscosity of the water due to the addition of nanofluids. It was also found that the transition range was affected as the greater the concentration of nanofluids, the earlier transition occurs.

It was found that the addition of nanofluids showed an increase in Nusselt number with a decrease in heat transfer coefficients. This was due to the increase in the thermal conductivity of the base fluid. As the concentration of nanofluids increased, the transition of the Nusselt number as a function of Reynolds occurred earlier. When considering the heat transfer results as a function of velocity, the higher the concentration, the more transition was delayed. This showed that the changing viscosity of the fluid makes a comparison very difficult.

Dirker *et al.* [23] considered the inlet flow effects in micro-channels. The flow regimes that were considered were laminar and transitional flow while varying the inlet geometries (a sudden contraction (square edge), bellmouth and swirl geometry). It was found that the inlet geometry influenced the transitional behaviour of the heat transfer coefficients and friction factors. While isothermal friction factor results agreed well with literature, the diabatic results were lower than expected. The reason for this was assumed to be due to the change in the fluid viscosity on the wall and its effect on the flow field. The bellmouth inlet geometry displayed a smoother transition and thus a wider transition range than that of the sudden contraction. When considering the Nusselt numbers, good agreement was found in the laminar flow regime for the sudden contraction and bellmouth inlets. The swirl showed an improved heat transfer coefficient as compared to that of the sudden contraction and bellmouth. The reason for this is assumed to be due to the swirl inlet creating a condition where better fluid mixing can occur.

Everts and Meyer [25] considered heat transfer characteristics of developing flow in the transitional flow regime of a solar receiver tube. During this study, the Reynolds number was varied between 500 and 10 000. It was determined that the width of the transition region decreased as the flow became more fully developed. The heat transfer coefficients decreased as well as the flow reached a fully developed state.

2.9 Summary and conclusion

In order to gain significant insight into the study at hand, it was necessary to review the literature relevant to this study. Basic concepts associated to fluid flow, heat transfer and pressure drop was summarised. The three different flow regimes were described and nomenclature pertaining to the start and end of transitional flow, as defined by Meyer was given. While many correlations exist, and are accepted for heat transfer coefficients and friction factors in the laminar flow regime and turbulent flow regime, little information is available in the transitional flow regime.

Work in the transitional flow regime has predominantly been carried out by two groups, namely Ghajar and his co-workers and Meyer and his co-workers. While Ghajar has focused on high Prandlt number fluids with a constant heat flux boundary condition in stainless steel tubes, Meyer initially focussed on water based experiments with a constant surface temperature condition. Meyer has since shifted his research towards a constant heat flux boundary condition in copper tubes using water as the working fluid.

Both Ghajar and Meyer concluded that the inlet geometry of the test section had a definite influence on the flow characteristics in a tube. The smoother the inlet geometry, the more transition would be delayed. This was proven to be true for both heating boundary conditions. While Ghajar concluded that the transitional heat transfer range was wider than the transitional friction factor range for all inlet geometries, Meyer had conflicting results that stated that the ranges were approximately the same.

Flow regime maps form an important area within this study. While some maps do exist, their applicability to this study is uncertain. The development of these maps has been based on very specific experimental conditions with well-defined boundaries and ranges that will not necessarily be applicable to the study. There is no agreement between the maps when considering the boundary between laminar forced convection and laminar mixed convection. A strategy of maintaining a laminar Reynolds number, based on the friction factor result, will be used. The Rayleigh number will be adjusted whilst monitoring the Nusselt number. Once a point on the boundary between the two flows is identified, the Reynolds number will be increased and decreased thus identifying the boundary.

3 Experimental Set-up

3.1 Introduction

This chapter discusses the test section within the context of a general experimental infrastructure facility that was available in the Heat Transfer Laboratory of the University of Pretoria. The test section, calming section and mixing wells that were specifically developed and built for the set-up is discussed in detail. The instrumentation that formed part of the test section as well as the calibration of the instrumentation and experimental procedure is also discussed.

3.2 Testing facility

The testing facility is shown schematically in Fig. 3-1. It consists of the components 1 – 10, defined in the figure. It consisted of a system circulating water from a feed water reservoir (3) with a capacity of 1 000 l to a test section (8) where the water was heated and circulated back to the water reservoir (3). The feed water reservoir was connected to a 5 000 l storage tank (1). The storage tank was connected to a 30 kW chiller where a thermostat was used to control the temperature in the storage tank to 0.5 °C of a preselected temperature. The water was provided by the local utility. The results from previous work [44] indicated that no water treatment was required.

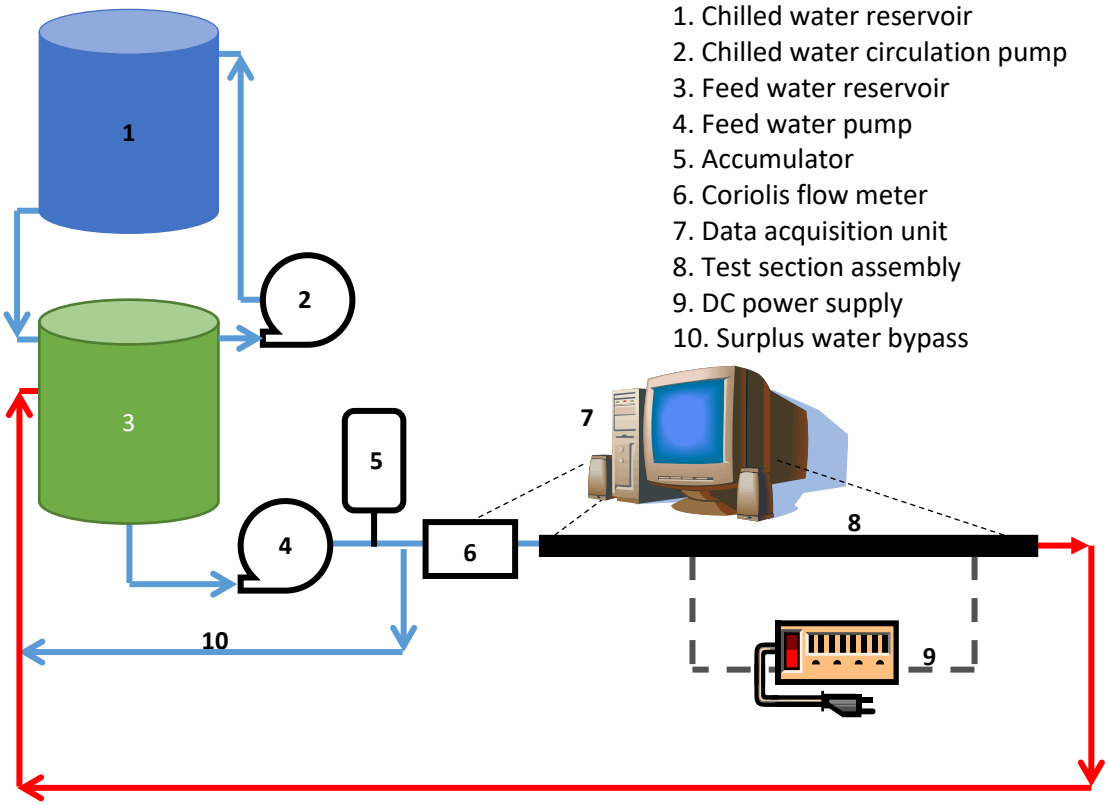

Fig. 3-1 - Schematic layout of test facility with test section

A positive displacement pump (4) was used to circulate the water through the test section. The pump had a maximum flow rate of 2 670 l/hr, which was much higher than the required flow rate in the test section, therefore surplus water was bypassed back into the reservoir via the surplus water bypass line (10). The pump was controlled via a variable speed drive thus allowed for accurate control of the mass flow rate through the test section.

In order to decrease pulsations in the flow, which is indicative of a positive displacement pump, a 4 l accumulator (5) was installed prior to the flow meter and test section. The accumulator contained a pressurized nitrogen gas bladder which was used to maintain the pressure in the system by dampening pulsations in the flow. The bladder was pressurized to 3 MPa.

The water then flowed through a Coriolis flow meter (6) that measured the mass flow rate through the test section (8) before returning it to the feedwater reservoir (3).

3.3 Test section assembly

The test section assembly consisted of an inlet mixer, a calming section, a test section and an outlet mixer as shown schematically in Fig. 3-2. The mixers are discussed in 3.3.1, the calming section in 3.3.2 and the test section in 3.3.3.

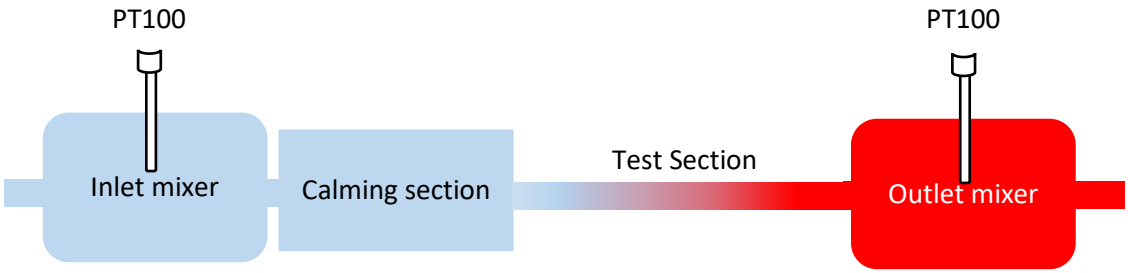

Fig. 3-2 - Schematic layout of the test section assembly

3.3.1 Mixers

Mixers were installed upstream of the calming section and downstream of the test section. This was to ensure that the inlet and outlet temperatures to the test section were measured accurately during laminar flow conditions when radial temperature stratifications occurred in the flow stream. The design of the mixers was based on the work of Szalai and Muzzio [56] that used flat plate mixer plates.

Each of the mixers was constructed from copper sheet which was cut into a strip, 5 mm wide and 20 mm long. The copper plate strip was then partitioned into five equal segments and then symmetrically, transversely cut on the boundary of each segment, leaving only a very small piece of copper intact along the center line of the copper strip. The strip was then placed on a lathe where it was twisted to create 120° tape elements as recommended in the study. As the copper strip was only partially cut, the mixer remained as a single assembly, with five

individual twisted elements pivoting on its centre line. After twisting, the diameter of the elements was reduced to 4 mm to allow for a sliding fit into the test section.

The L/D_i ratio impacts the performance of the mixer at high flow rates, where a ratio of 2 showed the best results as compared to the ratio of 1 and 1.5. Due to the physical constraints within the test section it was not possible to twist an element with a L/D_i ratio of 2 to 120°. As a result, a ratio of 3.75 was used.

The mixers were each fitted in an Acetal tube. This was done so as to prevent axial conduction from the calming section and test section as Acetal has a low thermal conductivity of 0.23 W/m°C. A calibrated PT100 (± 0.08°C at 60°C) was installed in each of the mixer assemblies, directly in the flow field just downstream of the mixer. This ensured that the mean inlet and exit temperatures were measured were well mixed.

3.3.2 Calming Section

Prior to the flow entering the test section, a calming section was used (Fig. 3-3) that ends in a squared edge inlet to the test section. The primary purpose of the calming section was to ensure a uniform velocity distribution at the inlet of the test section with low turbulence levels.

The design of the calming section was based on the work of Tam and Ghajar [22] where the spacing and design of the acrylic plates, steel mesh and the straws was replicated with reference to the inlet of the calming section. The internal diameter of the calming section was also the same as that of Tam *et al*. Where possible, the open air ratio (OAR) of the two test sections were matched as closely as possible, based on the available material.

While the length of the calming section used during the study was 1.062 m, Tam *et al.* used a calming section with a total length of 0.927 m. The contraction ratio was significantly different. Tam et al.'s calming section contraction ratio was approximately ten while as the contraction ratio for this study was 42.

The calming section was constructed from an acrylic tube with an acrylic socket flange. The tube had an outer diameter of 180 mm and a wall thickness of 5 mm. Acetyl flanges were bolted to the acrylic flanges with 3 mm plastic gaskets. Three perforated acrylic plates with an outer diameter of 170 mm were placed in series at the inlet to the calming section. Each plate was 10 mm thick with an OAR of 0.299 (73 holes per plate, 11 mm per hole).

Tightly packed soda straws approximately 102 mm long with an outer diameter of 5.3 mm were placed between two stainless steel wire meshes. The straws had an OAR of 0.855 while the mesh had an OAR of 0.577. A third stainless steel wire mesh with the same OAR of 0.577 was placed downstream of the straws. The water then flowed undisturbed through the remaining portion of the calming section (385 mm) before entering the test section.

Bleed valves were installed at the top of the calming section at several positions. This was to remove any air that may have entered the calming section. A removable T-type thermocouple (T_{CS}) was also placed in the centre of the calming section as a secondary inlet mean temperature measurement point (the PT100 was the primary measuring point). This thermocouple was removed from the centre line of the calming section during the transition experiments.

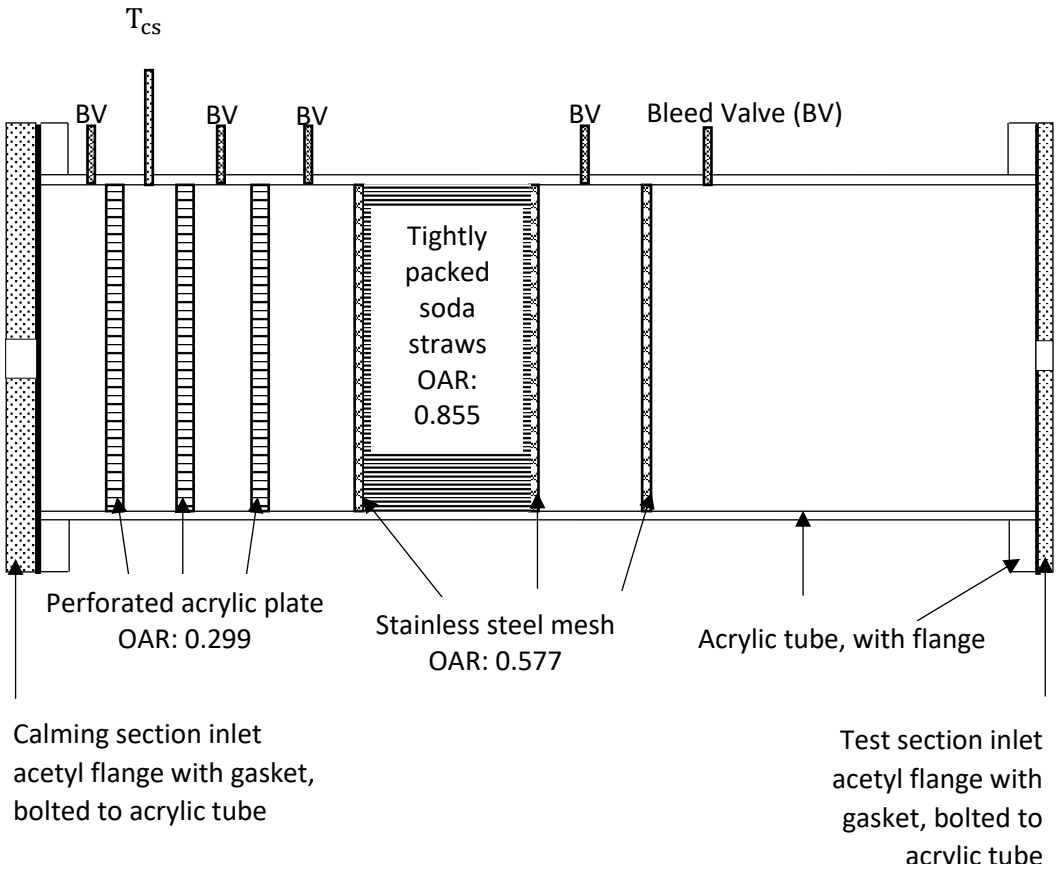

Fig. 3-3 - Schematic layout of the calming section

The purpose of the acetyl flanges was to prevent any axial and radial heat conduction from the calming section to the mixing well and test section. Insulation material with a thickness of 40 mm and a thermal conductivity of 0.04 W/m°C was also placed around the calming section to prevent heat losses to the environment.

A compression fitting, as shown in Fig. 3-4, was screwed into the outlet flange of the calming section allowed for the flexibility to align a square edge geometry. This was achieved by positioning the farrell of the compression fitting at the exact point that the tube would be flush with the acetyl flange. The compression fitting was machined to remove any rounded edges so that it was flush with the Acetyl flange.

During construction, care was taken to ensure that the test section tube inlet was flush with the outlet flange. This was to warrant that no disturbance to the inlet flow occurred due to the compression fitting.

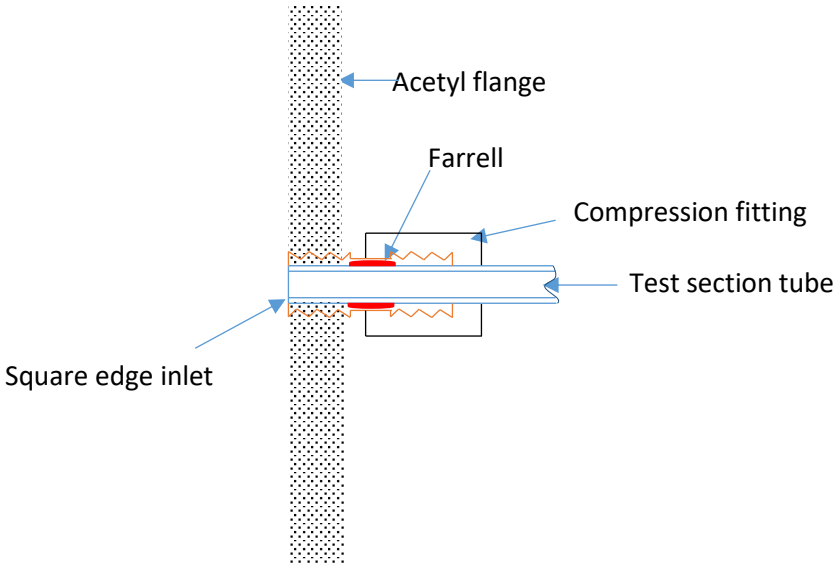

Fig. 3-4 - Schematic diagram of the square edge inlet geometry

3.3.3 Test Section

A tube with an inner diameter of 4.04 mm, an outer diameter of 5.04 mm, and length of 8.32 m was used for the test section. The test section was especially manufactured by a local South African manufacturer as one hard drawn length made from copper for the purpose of this study. This longer tube length was required in order to ensure that fully developed flow was achieved as previous work [14] showed that the flow might take up to approximately 4 m to become fully developed (based on equation 2-43) if the Prandtl number is eight.

Two methods (laboratory surface roughness measurement and profilometer measurement) were used to measure the relative surface roughness of the tube. This was found to be approximately 2.5×10^{-5} for the laboratory surface roughness measurement and 1.16×10^{-5} for the profilometer. It can therefore be assumed that the tube is smooth. Details regarding the internal surface roughness is detailed in Appendix A.

The longer length test section was selected to ensure that, conservatively, the flow was both hydrodynamically and thermally fully developed over the last two meters of the test section. As a result, heat transfer and pressure drop measurements were concentrated on the latter half of the test section. The tube diameter was also chosen to be small so as to meet the physical constraints of the laboratory. Lower heat fluxes were induced on the tube in order to ensure that forced convection in the laminar flow regime was achieved.

The test section was instrumented with a total of 64 thermocouples as shown in Fig. 3-5.

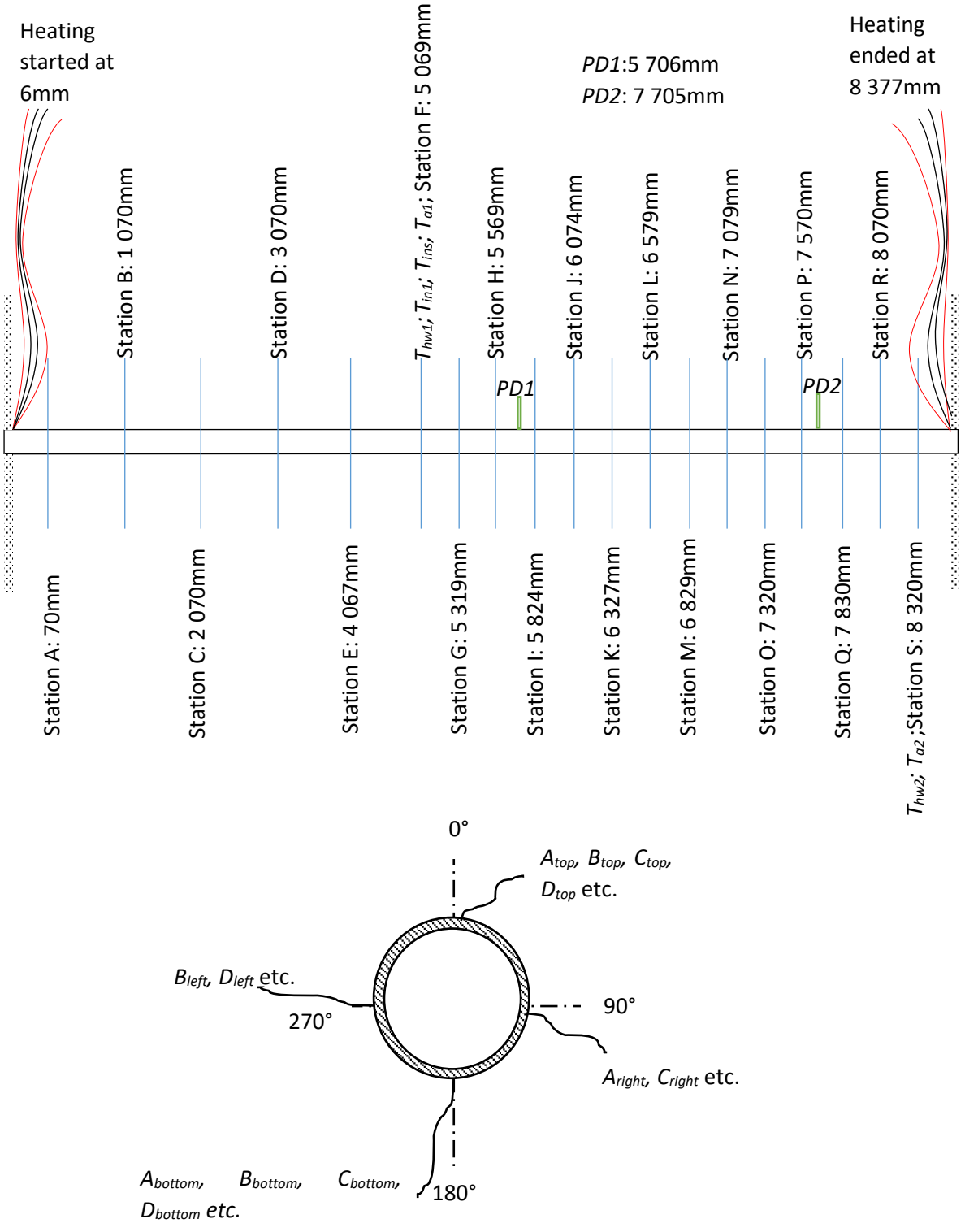

Fig. 3-5 - Thermocouple and pressure tap configuration

T-type thermocouples were used with a wire diameter of 0.254 mm. Of the 64 thermocouples, 57 were axially attached to the outside of the tube surface at 19 thermocouple stations. A shallow 1 mm hole was drilled at the three axial locations per station and widened with a 2 mm drill after which solder was melted into the hole. The thermocouples were then attached to the tube by soldering them onto the tube surface in the holes.

The first thermocouple station, station A, was placed 70 mm from the tube inlet. Five thermocouple station, each spaced 1 m apart follows station A up to station F. The remaining 14 stations are each spaced 250 mm apart, from station F to station S. The density of temperature measurements was concentrated to the back end of the test section where fully developed flow was expected.

At each thermocouple station, a total of three thermocouples were attached as shown in Fig. 3-5. It was too challenging to install four thermocouples at each thermocouple station because of the small tube diameter. In all instances, a thermocouple was placed at 0° (A_{top}, B_{top}, C_{top}, D_{top} etc.) and 180° (A_{bottom}, B_{bottom}, C_{bottom}, D_{bottom} etc.). The remaining thermocouple's position was alternated between 90° (A_{right}, C_{right} etc.) and 270° (B_{left}, D_{left} etc.) along the length of the tube.

The test section was covered with 130 mm of insulation material with a thermal conductivity of 0.04 W/m·K. One-dimensional heat transfer calculations were used to estimate the maximum losses at the worst-case conditions at a Reynolds number of 2 300 and a surface wall temperature of 86°C. It was found that the heat losses were approximated to be 1% of the heat transfer rate in the test section.

Seven remaining thermocouples were used to monitor other points of interest. These included the actual temperature of the heating wire which was monitored at two locations, namely in line with Station F, approximately midway of the test section(T_{hw1}) and the end of the tube (T_{hw2}) in line with Station S, where the highest heating wire temperature was expected. An internal insulation temperature (T_{insul1}) placed within the insulation at a radial thickness of 48.2 mm was monitored at Station F to check the temperature of the insulation material in a radial direction. The insulation skin temperature (T_{insul2}) was also monitored at this location for the same purpose. Finally, the laboratory ambient conditions (T_{a1} and T_{a2}) was monitored at Station F and Station S respectively.

As the focus of the study was on fully developed flow, pressure measurements were only taken over 2 m on the back end of the tube. The positions of the pressure taps are shown in Fig. 3-5. The first pressure tap (*PD1*) was positioned 5.7 m from the inlet of the tube with a 2 m gap to the second pressure tap (*PD2*). According to equation 2-43, fully developed flow should be achieved within 3.25 m of the tube inlet if transition occurs at the critical Reynolds number of 2 300 and a conservative Prandlt number of 7 is assumed. This additional tube length of 2.45 m allowed for some leeway should transition occur later. Additionally, the distance of 2 m between the pressure taps ensured the uncertainty of the friction factors were low (see Appendix D).

The second pressure tap (*PD2*) was installed approximately 160 diameters (645 mm) upstream of the test section outlet. This was done to ensure that the flow in the exit mixing well did not influence the pressure drop measurement. International instrumentation manufacturers and experts have found that a palpable pulsation in the flow may generate measurement inaccuracies at the instrument [57]. Singh *et al.* [58] considered the performance of orifice plate assemblies and suggested a minimum downstream length of 40 diameters to ensure proper specifications of the boundary conditions.

The pressure taps were installed by soldering a 3.5 mm capillary tube to the test section tube at 0° at the desired locations. Holes were then drilled through the copper tube using a 0.35 mm drill. The dimensions of the taps were based on the work of McKoen *et al.* [59] which suggests that the pressure tap dimensions be 10% or less than the tube inner. This ensured that the taps do not cause any flow obstructions within the tube which may lead to localised eddies.

After drilling the holes, any burs which may have formed were removed. A long thin and stiff wire was wrapped in material and installation tape. This wire was used to clean in inside of the tube. Lastly, a compression fitting with a quick coupler was inserted over the capillary tube. A 3 mm nylon tube was used to connect the pressure taps to the differential pressure transducer.

A constant surface heat flux condition was induced by heating the test section with heating wire. Constantan wire with a thickness of 0.38 mm, coated in a telfon sheath with a wall thickness of 0.2 mm was used as the heat source for the test section. The heating wires were spiralled tightly along the length of the tube to ensure a uniform heat flux was maintained. At each thermocouple station, the heating wire was manipulated around the thermocouple junctions so as to ensure that while the heating wire covered as much of the surface area of the test section, it did not come in contact with the junction. The reason for this was to ensure that the thermocouples accurately measured the surface temperature of the wall and not the heating wire temperature. This is shown schematically in Fig. 3-6.

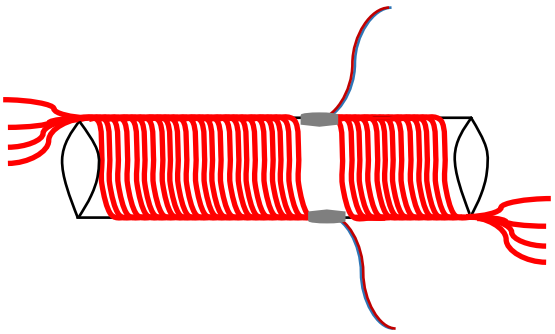

Fig. 3-6 - Schematic diagram of the heating wire wrapped around the test section

As the expected resistance of the wire was 3.61 Ω/m, due to the long length of the tube and the constraints in voltage supply, a total of four wires were needed to wrap the tube. These wires were connected in parallel to the direct current power supply. Two of the wires operated with a positive to negative charge from test section inlet to outlet while as the other

two wires operated with a negative to positive charge from test section inlet to outlet. This was put in place to try and balance any electromagnetic forces the spiralled wire might have had on the measurements.

3.4 Instruments

Over and above the thermocouples that were attached to the test section, various other instrumentation was used during the study. The accuracy of these instruments formed part of the uncertainty analysis as detailed in Appendix D.

3.4.1 Resistance temperature detector

Two resistance temperature detectors (RTD's) or PT100 probes were used to determine the mean inlet and outlet temperature of the test section. Ultra-precise probes were sourced from OMEGA Engineering with an instrumentation accuracy of ± 0.08 °C at 60 °C.

3.4.2 Coriolis flow meters

In order to determine the mass flow rate of the fluid in the test section, Coriolis flow meters were used. As the mass flow rate varied between 3 l/hr and 125 l/hr, it was necessary to make use of two flow meters. The smaller of the two had a maximum flow capacity of 108 l/hr and was used for the bulk of the tests. When higher flow rates were required, the larger flow meter, with a maximum flow capacity of 2 180 l/hr, was used.

The accuracy of each flow meter was 0.05% of its full scale value. Therefore, the expected resolution of the small flow meter was 0.054 l/hr while as the expected resolution of the large flow meter was 1.09 l/hr.

3.4.3 Pressure Drop

Two differential pressure transducers, each with a differential pressure diaphragms were utilized during testing. The accuracy of the pressure transducer with differential diaphragm was 0.25% of the full scale of the diaphragm.

The 14 kPa diaphragm, with an accuracy of 35 Pa, was sized to operate at Reynolds numbers between 0 and 5 000, with its greatest accuracy at a Reynolds number of 5 000. The 55 kPa diaphragm, with an accuracy of 137.5 Pa was able to operate in a Reynolds number range of 0 to 12 000. However, its predicted inaccuracy below 3 000 exceeded 10%. Therefore, in order to minimize the uncertainty of the results, measurements in overlapping ranges was obtained in to showcase congruency between the two diaphragms.

Each diaphragm was calibrated using a static water column and manometer.

3.4.4 Power supply

A direct current power supply with a maximum power rating of 1500 W was used to induce the constant heat flux condition. Constantan wires were connected in parallel to the positive and negative poles of the power supply. The use of constantan was calculated, as the metal has a constant electrical resistivity between 0°C and 100°C. This was within the boundaries of the study.

The power supply had a maximum current output of 15 A and a maximum voltage output of 360 V. The accuracy of the current and voltage was 0.2% of its maximum output (0.03 A and 0.072 V respectively).

3.4.5 Data acquisition unit

A National Instruments data acquisition unit with Labview software was used to log any data that was obtained during the experiments. Temperature measurements, flow meter measurements and pressure drop measurements were logged by the data acquisition unit (indicated as 7 in Fig. 3-1) during the experiments. The raw temperature data (in °C), flow meter data and pressure drop data (both in mA) was post processed in Matlab and Excel.

3.5 Experimental procedure

As discussed in section 3.2, an existing testing facility at the University of Pretoria was used to carry out the experiments. In order to manage the inlet temperature entering the test section, the temperature of the chilled water reservoir was set to be maintained at 20°C. The chilled water recirculation pump was switched on approximately one hour prior to the start of testing to allow the water in the feed water tank to be mixed and maintained at a constant temperature. This pump was kept on throughout the experiments to maintain the bulk temperature of the feed water tank.

After one hour, water was introduced to the test section. Air was bled out of the calming section and from the pressure taps to reduce measurement error.

Due to the length of the test section and the small inner diameter of the tube, very small volumes of water was circulated through the test section. In the laminar flow regime, flow rates as low as 0.01 m^3/hr was required. In this instance, steady state conditions were reached within four to five hours, dependent on the mass flow rate and the heat flux applied to the tube. Once a measurement was taken, the mass flow rate was reduced whilst keeping the heat flux constant. It took an additional two hours for steady state to be reached again before another measurement could be taken.

At higher mass flow rates, steady state conditions could be reached within 30 minutes, once again dependent on the heat flux applied to the tube and the mass flow rate. Multiple measurements could be taken in this instance, where approximately 30 minutes was required between measurements. As in the case of laminar flow measurements, a mass flow rate was reduced incrementally.

According to Meyer [11], the effect of hysteresis is negligible in the transitional flow regime. As a result, measurements were taken for decreasing Reynolds numbers. This was beneficial due to the time required for steady state conditions at lower mass flow rates.

Steady state conditions were met were there was no significant changes in the inlet and outlet temperatures, wall temperatures, mass flow rates and pressure drop measurements. This was monitored on a constant basis.

Experiments were carried out from bulk Reynolds numbers of 11 000 down to bulk Reynolds numbers of 1 000. Variable speed drives connected to the pump were used to decrease the mass flow rate. The pump speed was maintained between 1 000 and 1 500 rpm. As a result, in instances where the mass flow rate needed to be reduced, the valve at the inlet of the test section bypass was throttled. Due to the low mass flow rates, the accumulator on the pump was able to reduce flow pulsations. A total of 100 measuring points at a frequency of 10 Hz was captured and averaged to obtain one data point. Temperature (in °C), mass flow rate (in mA, converted to m^3/s) and pressure drop results (in mA, converted to Pa) were obtained simultaneously.

3.6 Conclusion

The experimental and test section configuration was described in detail in this chapter. A long smooth copper tube with a uniformly wound heating wire was used as the test section. The length of the copper tube was chosen to allow for fully developed flow. Thermocouples were attached to the test section at predetermined intervals to allow for accurate measurements of wall temperatures while PT100's were used to determine mean inlet and exit temperatures. A calming section was used to replicate the header box of a heat exchanger and allow for a square-edge inlet geometry. Pressure taps were installed on the test section at the latter end of the test section to ensure that fully developed friction factors could be measured.

4 Data reduction and validation

4.1 Introduction

The purpose of this chapter is to discuss the equations used to experimentally obtain friction factors and heat transfer coefficients and to provide validation of the experimental results using those published in literature. The data reduction of the measurements obtained during the experiments is given. Validation of isothermal friction factors and diabatic friction against those found in literature in all flow regime is shown. Heat transfer measurements are compared to literature in the laminar flow regime for forced and mixed convection as well as turbulent heat transfer measurements.

4.2 Data reduction

In order to calculate experimental friction factors and heat transfer results, it was necessary to determine both local and average results.

As a constant surface heat flux condition was applied, the mean temperature of the fluid will increase linearly along the length of the heated tube. As a result, the mean temperature, $T_{x,m}$ at axial position x of the test section was calculated using Eq. 4-1:

$$T_{x,m} = \left(\frac{T_e - T_i}{L_{ts}}\right) x + T_i \tag{4-1}$$

where T_i and T_e were the measured inlet and exit temperatures, L_{ts} is the length of the test section and x is the physical position of the measuring point on the tube.

The mean surface temperature, $\overline{T_{x,s}}$ at an axial position x at each thermocouple station was calculated by taking the average of the measured surface temperatures:

$$\overline{T_{x,s}} = \frac{T_{top} + T_{left/right} + T_{bottom}}{3} \tag{4-2}$$

where T_{top} is the surface temperature at the top of the tube (radial position 0°), $T_{left/right}$ is the surface temperature on either the left hand side or right hand side of the tube (radial position 270° or 90° respectively) dependant on the installation of the thermocouple and T_{bottom} is the surface temperature at the bottom of the tube (radial position 180°).

While the measured wall thickness of the tube was 0.5 mm, it was necessary to determine temperature difference between the outer wall of the tube and the inner wall. The thermal resistance, R_{ts} across the tube wall was calculated used Eq. 4-3:

$$R_{ts} = \frac{ln\left(\frac{D_o}{D_i}\right)}{2\pi L_{ts} k_{ts}} \tag{4-3}$$

where D_o and D_i is the measured outer and inner diameter of the test section and k_{ts} is the thermal conductivity of the test section. The thermal resistance across the tube was 1.048×10^{-5} °C/W.

The thermal resistance across the tube wall, calculated using Eq. 4-3 was used in Eq. 4-4 to determine the temperature difference, ΔT, between the inner wall and outer wall of the test section:

$$\Delta \mathrm{T} = E_p R_{ts} \tag{4-4}$$

where E_p is the electrical inout power to the test section.

A maximum temperature difference of 0.0052°C was calculated using the maximum electrical heat input of 500 W that was used in this study. This was considered negligible as the thermocouples could only be measured to 0.1°C accuracy. As a result, it was assumed that the surface temperature, as measured on the outer wall was equal to the surface temperature on the inner wall.

When considering local temperatures at each of the thermocouple stations, local thermophysical properties of the water dependent on temperature, namely the local density, $\rho_{x,w}$, local dynamic viscosity, $\mu_{x,w}$, local specific heat capacity, $C_{p,x,w}$, local thermal conductivity, $k_{x,w}$ and local Prandtl number, $Pr_{x,w}$, were calculated at the different station temperatures using the correlations derived by Popiel and Wojtkowiak [60].

The local Reynolds number, Re_x, at any point x in the axial tube direction was calculated using:

$$Re_x = \frac{\dot{m} D_i}{\mu_{x,w} A_c} \tag{4-5}$$

where $\dot{m}$ is the measured mass flow rate, and A_c is the cross-sectional area of the tube which was calculated as $A_c = D_i^2 \, \pi/4$.

In the instance where average results were calculated over the total test section length, the bulk temperature, T_B, was determined by:

$$T_B = \frac{T_i + T_e}{2} \tag{4-6}$$

The bulk Reynolds number, Re_B, was then calculated using:

$$Re_B = \frac{\dot{m} D_i}{\mu_{B,w} A_c} \tag{4-7}$$

where $\mu_{B,w}$ was calculated at the bulk temperature of the fluid.

The heat input into the water, $\dot{Q}_{water}$, was calculated as shown in Eq. 4.8 below:

$$\dot{Q}_{water} = \dot{m}C_{p,w}(T_e - T_i) \tag{4-8}$$

where $C_{p,B,w}$ is the specific heat of the water at the bulk temperature.

The electrical power input, E_p, into the test section was calculated by:

$$E_p = \mathrm{V} \times \mathrm{I} \tag{4-9}$$

where V is the measured input voltage and I is the measured input current from the DC power supply. This power input remained constant during each experiment thus imparting a uniform wall heat flux condition.

The heat flux, $\dot{q}$, was determined from the heat transfer rate described in Eq. 4-8 as shown in Eq. 4-10:

$$\dot{q} = \frac{\dot{Q}_{water}}{A_s} \tag{4-10}$$

where A_s was determined from $A_s = \pi D_i L_{heated}$ where L_{heated} is the measured heated length of the test section.

The heat transfer rate of the water was used in place of the electrical heat input as it was judged to be the more accurate of the two as there were some heat losses through the insulation to the environment.

An energy balance, EB, over the test section was calculated using Eq. 4-11 to determine how effectively the electrical heat transferred into the water:

$$EB = \left| \frac{E_p - \dot{Q}_{water}}{\dot{Q}_{water}} \right| \times 100 \tag{4-11}$$

At low Reynolds (<1 100) numbers and low electrical heat input (<100 W), the energy balance in the system was approximately 10%. This was due to the low mass flow rate and low heat input. However, at higher electrical heat inputs (>200 W), the energy balance was below approximately 5%.

The local heat transfer coefficient, h_x, was calculated as follows:

$$h_x = \frac{\dot{q}}{T_{x,s} - T_{x,m}} \tag{4-12}$$

The average heat transfer coefficient, $\bar{h}$, was calculated as follows:

$$\bar{h} = \frac{\sum_E^Q h(x)}{13} \tag{4-13}$$

where E refers to thermocouple station E and Q refers to thermocouple station Q. The numeral 13 refers to the number of thermocouple stations over which the heat transfer coefficient was averaged, where the physical spacing between the thermocouples was equal. This specific range of thermocouple stations ($E - Q$) was chosen as the purpose of the study was to consider fully developed flow (as shown in Fig. 3-5).

The local Nusselt number, Nu_x, was calculated as follows:

$$Nu_x = \frac{h_x D_i}{k_{x,w}} \tag{4-14}$$

The average Nusselt number, $\overline{Nu}$ was calculated from the average of the local Nusselt numbers between stations E and Q:

$$\overline{Nu} = \frac{\sum_E^Q Nu_x}{13} \tag{4-15}$$

Due to the change in temperature along the length of the test section, it was important to determine the effect in the variation in the Prandtl number. This was achieved by considering the Colburn j_H-factor.

The local Colburn *j*-factor, j_{Hx}, was calculated as:

$$j_{Hx} = \frac{Nu_x}{Re_x Pr_x^{1/3}} \tag{4-16}$$

The average Colburn *j*-factor, $\overline{j_H}$, was calculated as:

$$\overline{j_H} = \frac{\sum_E^Q j_{Hx}}{13} \tag{4-17}$$

In order to determine the fully developed friction factor, the measured pressure drop, ΔP between the two pressure taps in the fully developed length of the test section was used. The friction factor, f, was calculated using Eq. 4.18:

$$f = \frac{\pi^2 \Delta P {D_i}^5 \rho_w}{8\dot{m}^2 L_{PD}} \tag{4-18}$$

where L_{PD} is the measured length between the pressure taps (as shown in Fig. 3-5). The density of the fluid was evaluated at the bulk temperature of the fluid between the pressure taps.

The errors, $\%\ error$, in this study were determined as:

$$\%\ error = \frac{|X - P|}{X} \times 100 \tag{4-19}$$

where the general error of the measured or calculated result, X, was calculated by comparing the value with the predicted result, P, as published in literature. This was considered as the absolute error of the data points.

4.3 Validation: isothermal friction factors

In Fig. 4-1, a total of 87 measured friction factor results is given as a function of Reynolds number. The measurements for the pressure drops of the two types of pressure transducers are shown. The smaller 14 kPa pressure drop transducer was used in the Reynolds number range of 500 to 4 600. The larger 55 kPa pressure drop transducer was used in the Reynolds number range of 2 700 to 11 100. Thus, from a Reynolds number range of 2 700 to 4 600, both pressure drop transducers were used.

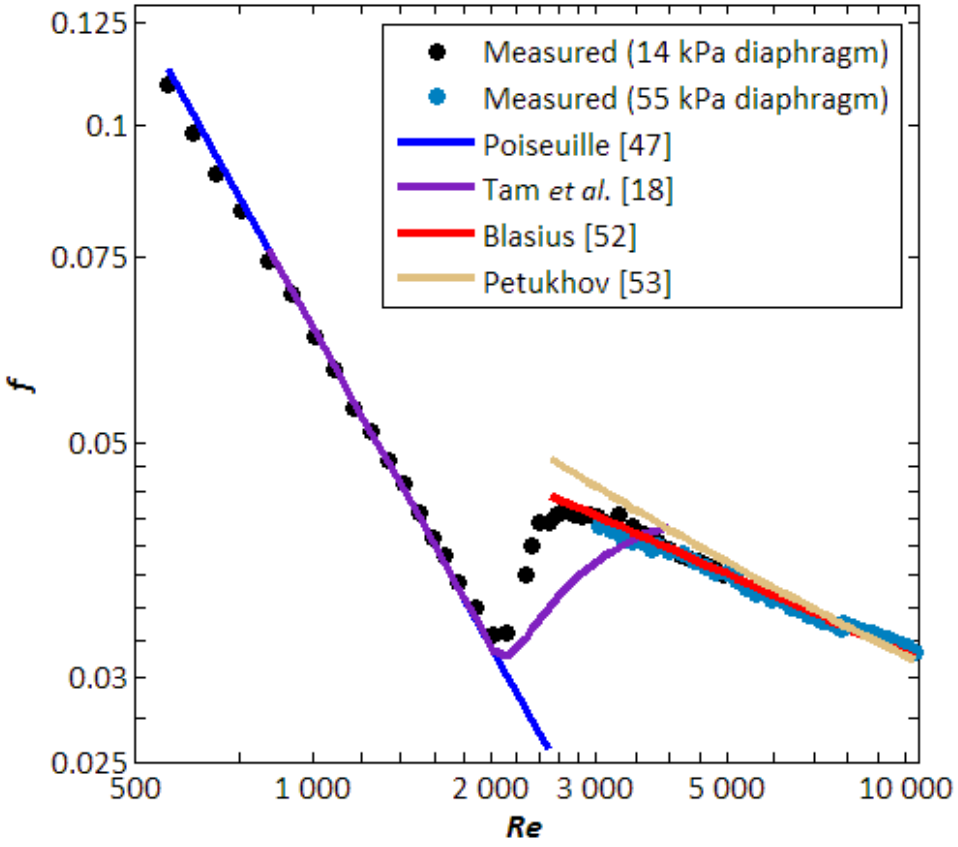

Fig. 4-1 – Isothermal friction factors as a function of the Reynolds number

The friction factors, which were calculated from the measured pressure drop are compared in the laminar flow regime to the Poiseuille [47] and Tam *et al.* [18] equations. When considering transitional flow, the fully developed measured results is compared to Tam *et al.* [18] while as in the turbulent flow regime, the measured results are compared to the Blasius equation [52] and the Petukhov equation [53].

In general, the agreements of the experimental results with the theoretical predicted values are very good and both fall within the uncertainty of the measurements which was 7.6% in the laminar flow regime and 4.4% in the turbulent flow regime. In the laminar flow regime the average error was 1.8% with a maximum error of 4% at a Reynolds number of 625. In the turbulent flow regime the average error is 1.3% and the maximum is 3.1%, which occurred at a Reynolds number of 4 600. In the overlapping region of the two pressure drop transducers the results also compare well and were within 2% of each other.

When considering the transitional flow regime, the experimental results show some agreement with the predicted results of Tam *et al.* [18]. The average error is 11.5% and a maximum error of 19.1%. Two observations are evident when considering the experimental results and predicted results. Transition occurs earlier and at a quicker rate when comparing the experimental results with the predicted results. While the transition range is between Reynolds numbers of 2 013 and 2 635 for the experimental results, it is between 2 122 and 3 628 for the predicted results.

Overall, it can be concluded that the agreement of the experimental results with theory is excellent. The agreement in the transitional flow regime, with the work of Tam *et al.* [18] is acceptable but not as good as what was observed in the laminar and turbulent flow regimes. A possible reason for this is that the equation derived by Tam *et al.* [18] has been developed for specific Reynolds number and x/D_i conditions. While the Reynolds number conditions are met when comparing the two sets of results, the x/D_i is not met. The experimental results ratio, x/D_i is 1 658 (where the median of the pressure taps is 6.7 m from the test section inlet) while the correlation of Tam is specifically for a x/D_i range of 3 to 200.

4.4 Validation: average and local Nusselt numbers

In Fig. 4-2, a total of 18 average Nusselt numbers and 18 local Nusselt numbers are given as a function of the Reynolds numbers. Each average Nusselt number consists of 12 measured local Nusselt numbers at a specific Reynolds number. The local Nusselt numbers represents one of the measured Nusselt numbers for each average Nusselt number. Varying heat fluxes, of 1.94 kW/m^2, 2.94 kW/m^2 and 3.26 kW/m^2 was applied to the tube in minimize the uncertainty of the results, where the measurement uncertainty is as low as 2.86% in the laminar flow regime but as high as 33.68% in the turbulent flow regime.

The measured results in the laminar flow regime, from a Reynolds number of 1 377 to 2 093, are compared to the Nusselt number of 4.364 which is expected for fully developed forced convection flow up to Reynolds numbers of 2300. The average error is 21% while the average uncertainty is 4.0%. This error is indicative there was secondary flow during testing. The

measured results were then compared to the equation of Morcos and Bergles [45] which was specifically derived for fully developed mixed convection. An average error of 16% is seen. The equation of Morcos and Bergles [45] has specifically been derived for a Rayleigh number of greater than 30 000. In the case of this study, the Rayleigh number is much lower, at an average of 5 072. As the Rayleigh number describes the strength of the buoyancy forces and hence secondary flow within the flow, it is expected that the Rayleigh number parameter for the Morcos and Bergles [45] equation plays an important role with regards to the accuracy of the equation.

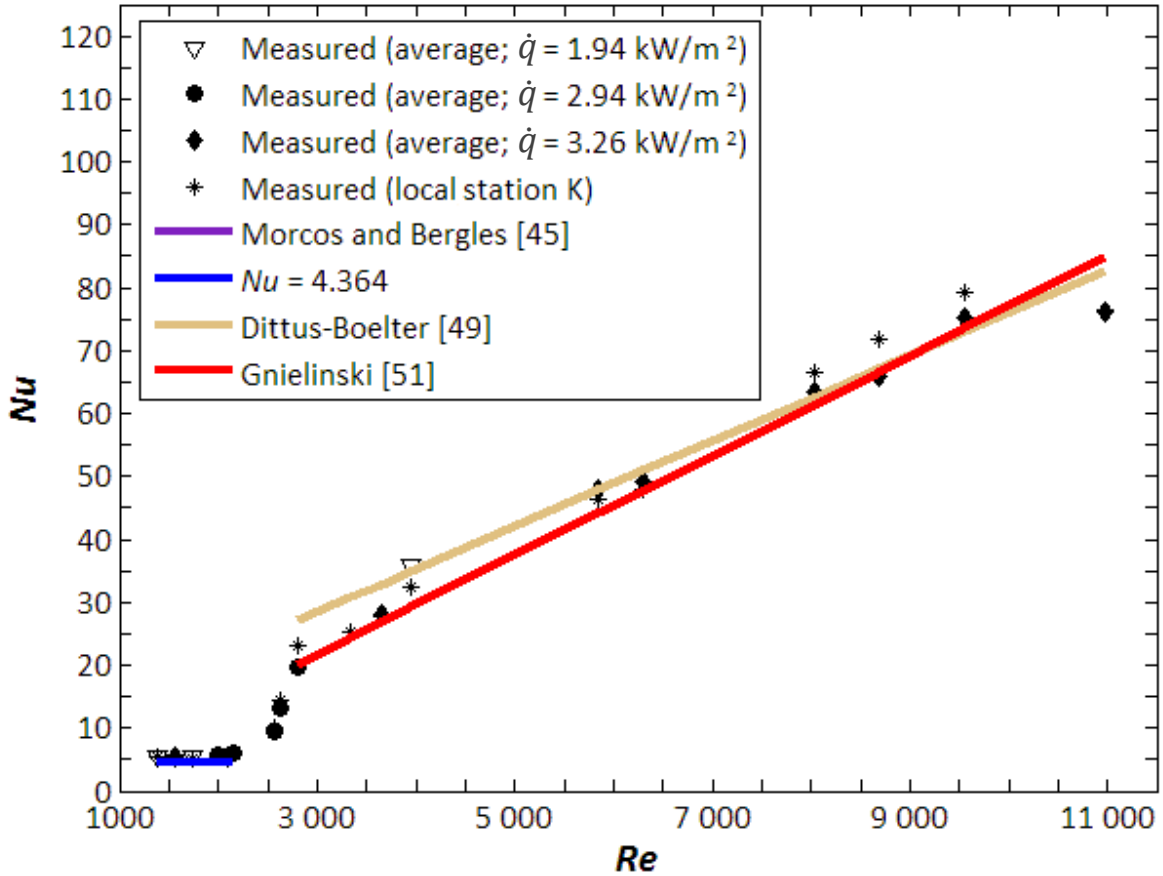

Fig. 4-2 - Average and local Nusselt numbers of a function of the Reynolds number

The equations of Gnielinski [51], which is valid from a Reynolds number greater than 3 000 and Dittus-Boelter [49], which is valid for Reynolds numbers greater than 10 000, is used for comparison purposes in the turbulent flow regime. An average uncertainty of 24% is calculated for this Reynold's number range. An average error of 5.8% in the turbulent flow regime is found when comparing the measured results with the predicted results of Gnielinski. The Reynolds number range is from 3 335 to 10 975. The average error is 3.1% for a Reynolds number range of 3 951 to 10 975 when considering the Dittus-Boelter equation. In both instances, the agreement with the experimental results is excellent and well within the uncertainty of the measurements.

An exploded view of the transition from laminar flow to turbulent as shown in Fig. 4-2 is shown in Fig. 4-3. The start of transition, Re_{cr}, was defined at a Reynolds number of 2 158, where the average Nusselt number results starts to rise sharply.

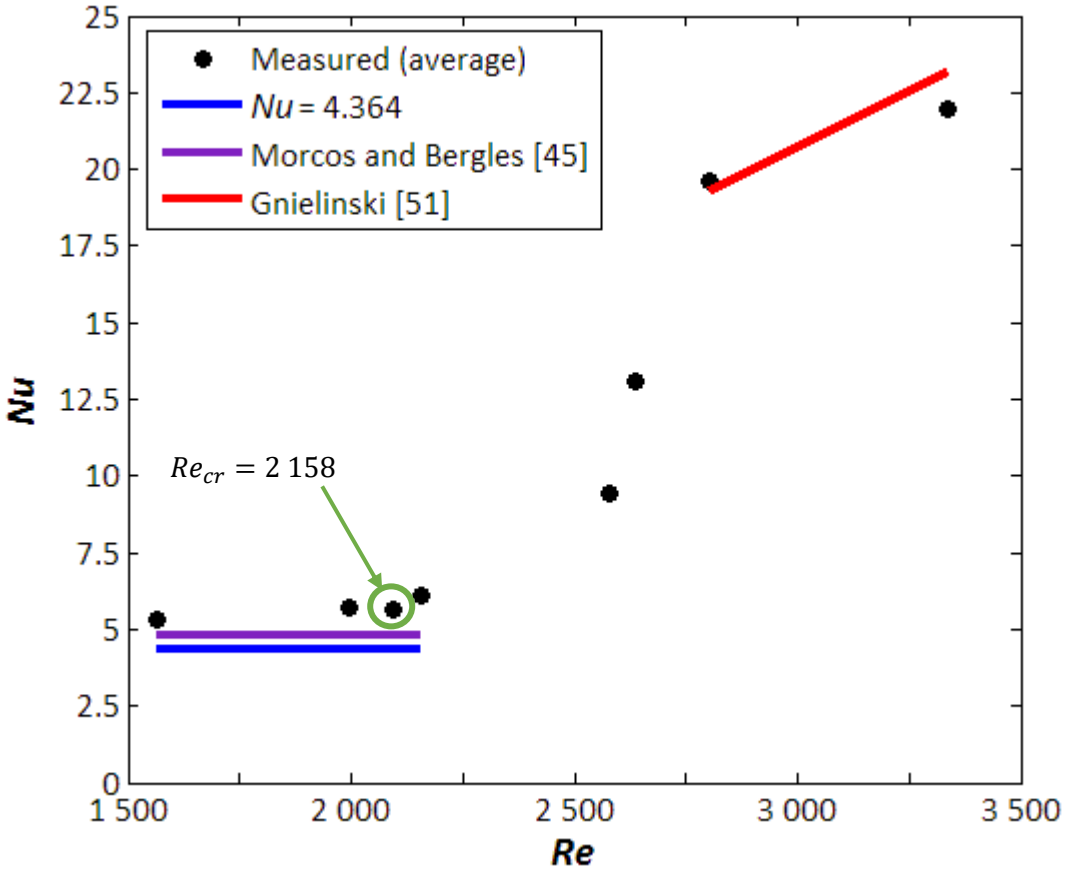

Fig. 4-3 - Exploded view of transition

4.5 Validation: diabatic friction factors

In Fig. 4-4, the fully developed measured friction factors for the average Nusselt numbers plotted in Fig. 4-2, are shown as a function of the local Reynolds numbers. A total of 18 measured points has been plotted.

In the laminar flow regime, the measured results have been compared to the classical correlation of Poiseuille [47] and the more recent correlations of Tam and Ghajar [22] and Tam *et al.* [18]. The average uncertainty is calculated to be 5.9%. When considering Reynolds numbers of 1 363 up to 2 127, the average error is 1.7% when comparing the measured results with Poiseuille. The error is slightly larger, at 8.2% and 12% when a comparison is made to Tam and Ghajar and Tam *et al.* respectively. In both instances, the Prandtl number and Grashof number of the measured results are out of the parameter range for the correlation which may explain the slightly higher error.

There is very good agreement between the measured results and the predicted results in the turbulent flow regime. The average error is 1.5% with a maximum error of 3.8%, when comparing the measured results with the predicted results of Allen and Eckert [41]. The measured results fall well within the average uncertainty of 4.6%.

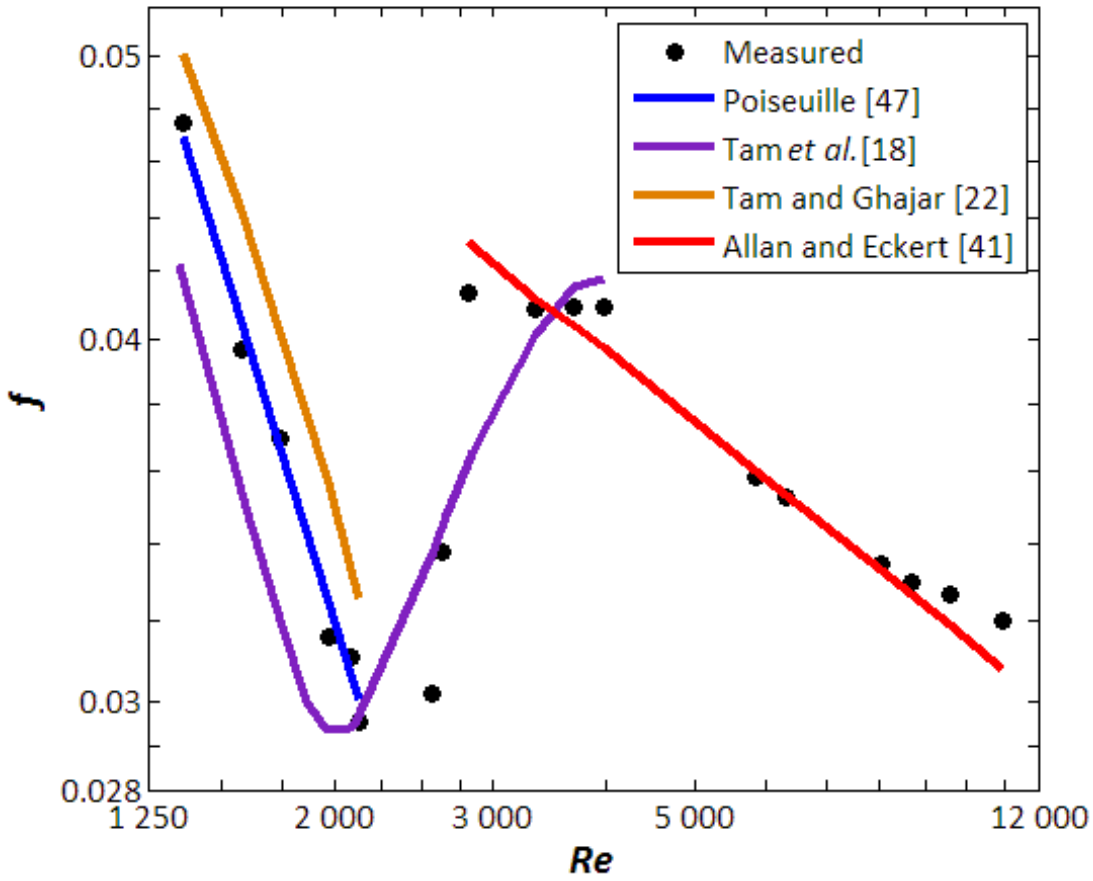

Fig. 4-4 - Diabatic friction factors as a function of the Reynolds number

An exploded view of transition is shown in Fig. 4-5. The measured results are compared to that of Tam et al. [18] where an average error of 7.6% is seen with an uncertainty is 4.9%. This shows that there is a good agreement between the measured and predicted results, where the error can be accounted for by considering that the x/D_i parameter is not met as with this study, the x/D_i parameter is 1 658 and should be between 3 and 200 for the correlation of Tam *et al.* [18].

Transition begins at a local Reynolds number of 2 127 where the friction factor abruptly begins to increase. Turbulent flow is indicated at 2 812, where the gradient of the friction factor once again changes. The Reynolds number transition range for the diabatic friction factors are in agreement with the range as described in section 4.4 for the Nusselt numbers. This is an expected phenomenon as pressure and temperature are directly proportional.

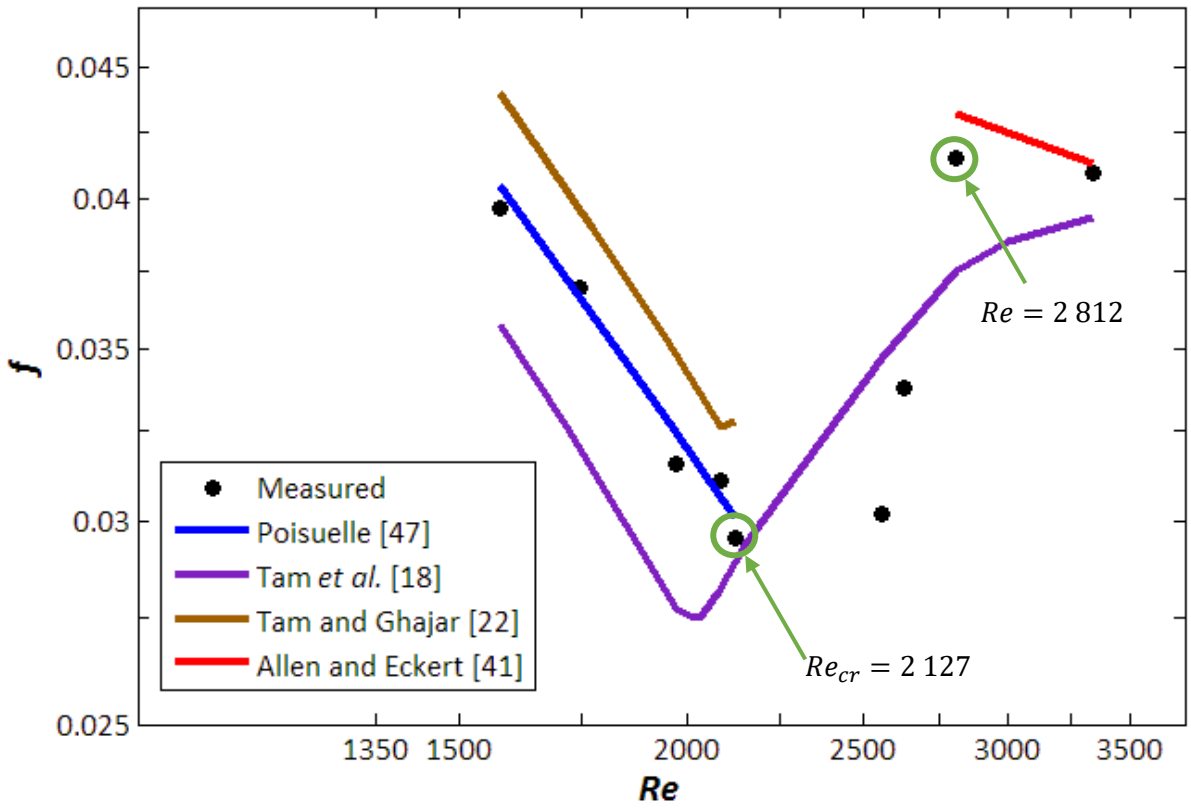

Fig. 4-5 - Exploded view of transition

4.6 Conclusion

The purpose of this chapter was to validate the experimental set-up, experimental procedure and data reduction method. The data reduction method was presented, where the reduction of experimental measurements was described. Following this, these results were validated against published literature where the average isothermal friction factor, average Nusselt number, local Nusselt number and average diabatic friction factor were presented.

Measured isothermal friction factors were compared in all three flow regimes. Whilst very good agreement was seen in the laminar and turbulent flow regime, the error in the transitional regime was higher. It was concluded that a possible reason for this was due to the parameters imposed on the equation of Tam *et al.* [18]. In the case of the measured results, the x/D_i ratio was 1 658 and this is significantly higher than the imposed range of 3 to 200. It is important to note that the pressure drop was measured in the fully developed region of the test section which attributed the good agreement between the measured results and predicted results.

The measured heat transfer was validated using both the average and local Nusselt numbers. Laminar results were predicted using the classical Nusselt number of 4.364 for forced convection and the equation of Morcos and Bergles [45] for mixed convection. The error was 21% when considering the classical Nusselt number of 4.364. This was indicative that some

secondary flow was present during testing. The predicted results of Morcos and Bergles [45] showed an error of 16%. A possible reason for this was the difference in the Rayleigh number parameter where the measured results showed an average Rayleigh number of 5 072 while the equation of Morcos and Bergles [45] is valid for Rayleigh numbers greater than 30 000.

Turbulent flow heat transfer results showed excellent agreement with predicted results, where an average error of 5.8% was seen when comparing the measured results with those predicted by Gnielinski [51].

Diabatic friction factors were considered and showed good agreement in all flow regimes. In the laminar flow regime, an average error of 1.7% is seen when comparing the results to that of Poiseuille. The error is slightly larger, at 8.2% and 12% when considering the equations of Tam *et al.* [18] and Tam and Ghajar [10] respectively. The increase in error is attributed to the x/D_i ratio. Agreement in the turbulent flow regime is excellent with an average error of 1.5% when a comparison is made to Allen and Eckert [41]. The transitional flow results also showed good agreement with an average error of 7.6% as compared to Tam *et al.* [18].

Isothermal friction factor results show transition occurring between Reynolds numbers of 2 013 and 2 635 while the diabatic friction factor transition occurs between 2 127 and 2 812. When considering the heat transfer results, transition is seen between Reynolds numbers of 2 158 and 2 804. While the isothermal transition range starts slightly earlier than that of the diabatic results, the magnitude of the range is similar. The transitional range for the heat transfer results and diabatic friction factor results is equivalent which is an expected result.

It is concluded that the friction factor results and the heat transfer results have good agreement with published literature. As a result, the experimental setup, as well as the experimental procedure and date reduction of the measurements is validated.

5 Results: Heat transfer and pressure drop in the transitional flow regime

5.1 Introduction

The heat transfer and pressure drop results under diabatic conditions are presented in this chapter. The focus of the results is on the fully developed forced convection results in the transitional flow regime. Both local and average Nusselt numbers are presented and the associated pressure drop for those results are given. The effect of secondary flow is discussed and the local heat transfer coefficients are presented in terms of the Colburn j_H-factor. The results are also compared with flow regime literature. A total of 42 data sets, each consisting of 6 200 data points before averaging was used.

5.2 Temperature profile and local Nusselt number of fully developed flow

The temperature profile and local Nusselt number for a heat input of 99 W (0.89 kW/m^2) for a bulk Reynold number of 1 081 is shown in Fig. 5-1 (a) and (b) respectively. At this specific laminar flow condition, with an inlet temperature of 19.62°C, fully developed flow was expected to occur within 1.4 m (x/D_i = 346) of the test section inlet.

As shown in Fig. 5-1 (a), when considering the fully developed portion of the test section, the equation of the linear curve fit for the surface temperature is $y = 0.83x + 21.1$ while the equation for the linear curve fit for the mean temperatures is $y = 0.85x + 19.62$. When comparing the slope of each line, a difference of 2.5% is seen. It can be concluded that fully developed flow occurred approximately at 1.2 m (where x/D_i is approximately 300) from the test section inlet, slightly earlier than the theoretically calculated entrance length of 1.4 m. The average temperature difference between the tube surface and the mean fluid is 1.4°C.

The local Nusselt number is plotted as a function of x/D_i is shown in Fig. 5-1 (b). The local heat transfer coefficients do not remain perfectly constant in the fully developed flow region. This slight fluctuation is attributed to the uncertainty of the heat transfer coefficient which is approximately 6.85% at low Reynolds numbers.

There is a significant increase in the heat transfer coefficient at the end of the test section, within 500 mm of the test section exit into the exit mixing well. This is indicative that the exit mixing well affected the hydrodynamic and thermal boundary layer. According to Singh *et al.* [58], upstream effects of the mixing well should have been limited to 40 diameters or 162 mm (see section 3.3.3).

Fully developed flow is shown to occur approximately 1.2 m from the test section inlet which is slightly earlier than the theoretically calculated entrance length of 1.4 m. In general, the local Nusselt numbers in the fully developed region are close to the expected value of 4.364 for forced convection.

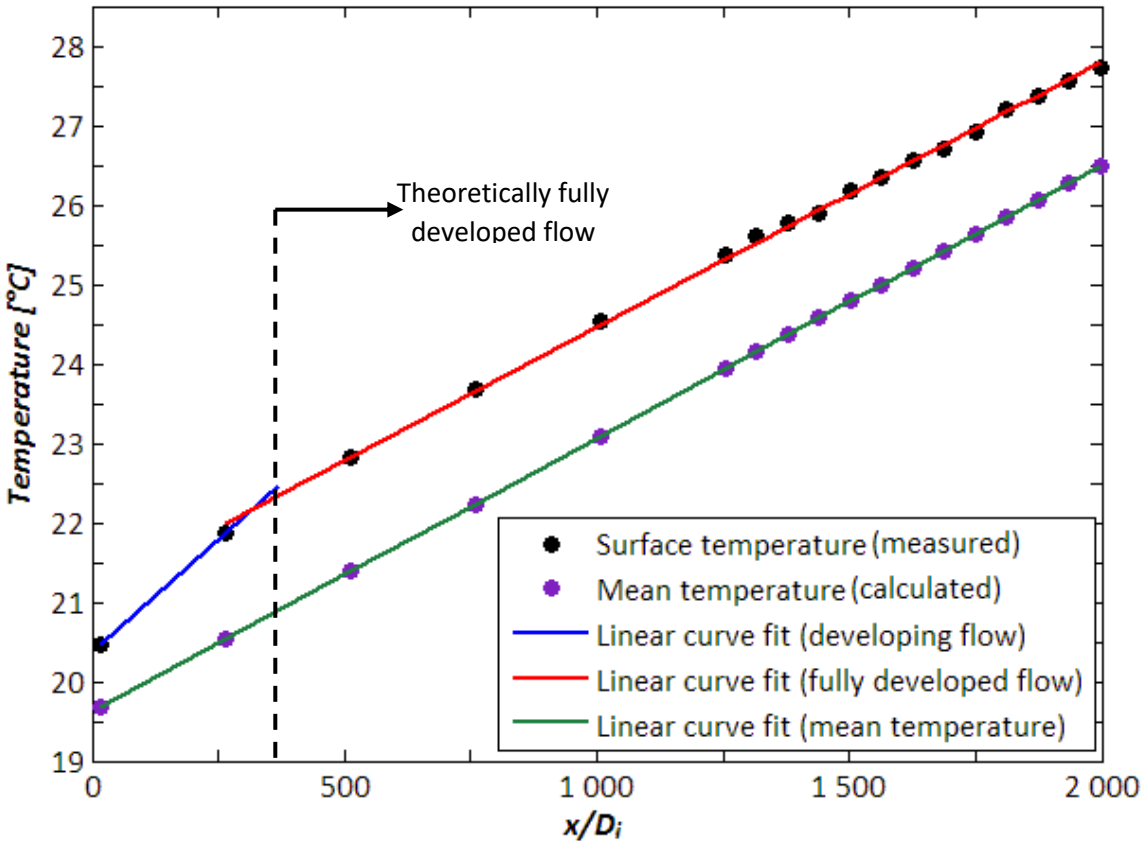

(a)

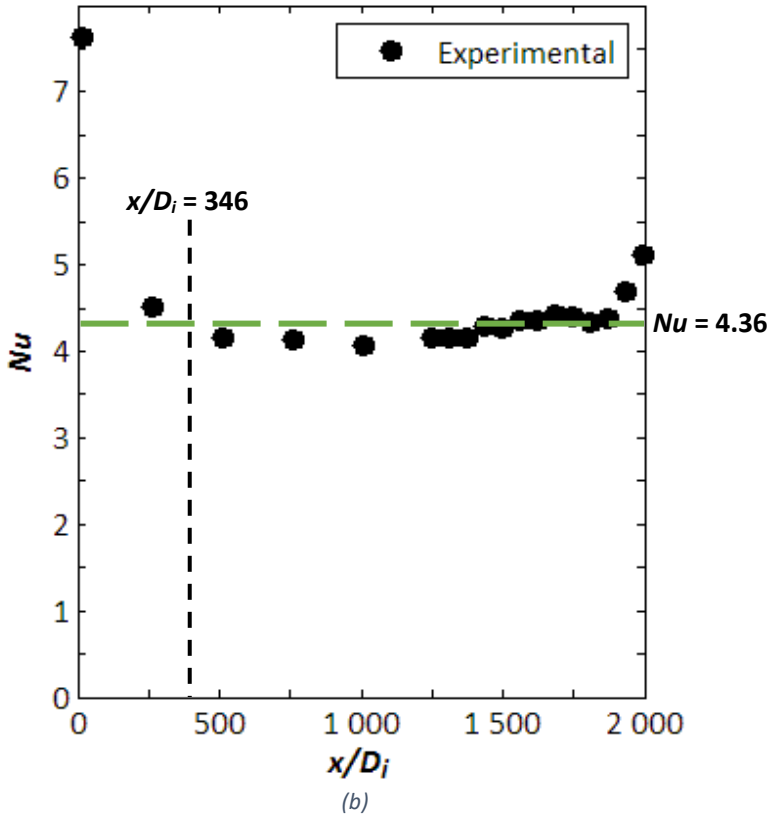

(b)

Fig. 5-1 - Temperature profile (a) and local heat transfer coefficient (b) for a diabatic test of 0.89 kW/m² (laminar flow with a bulk Reynolds number of 1 081)

A similar analysis is completed at a higher heat input of 342 W (3.23 kW/m^2) for a bulk Reynolds number of 1 349 (laminar flow), 10 055 (turbulent flow) and 2 674 (transitional flow).

When considering laminar flow in Fig. 5-2 (a), fully developed flow was expected to occur 1.8 m (where x/D_i is approximately 445) from the test section inlet (the inlet temperature into the test section was 22.4°C). In this instance, the equation of the linear curve fit (between $x = 1.07$ and $x = 8.07$) for the surface temperatures is $y = 2.83x + 25.99$ and the mean temperatures is $y = 2.85x + 22.37$. The difference in the slope of the lines is 0.7% thus confirming that fully developed flow occurred earlier than predicted, at 1.1 m from the test section inlet. The average temperature difference for this scenario was 3.5°C.

The local Nusselt number plotted as a function of x/D_i is shown in Fig. 5-2 (b). Similar observations as seen in Fig. 5-1 (b) can be seen in Fig. 5-2 (b). The local heat transfer coefficients do not remain perfectly constant in the fully developed flow region and there is a significant increase then decrease in the heat transfer coefficient at the end of the test section. Fully developed flow is shown to occur at approximately 1.4 m, slightly quickly than what theory dictates.

In general, the local Nusselt numbers in the fully developed region are approximately 5.3, which is higher than the expected value of 4.364 for forced convection. The reason for the higher Nusselt numbers is that mixed convection occurred.

Turbulent flow was analysed as shown in Fig. 5-3 (a) and (b). The temperature profile is shown in Fig. 5-3 (a). Fully developed flow was predicted to occur within 40 mm (where x/D_i is approximately 10) of the test section inlet before the first thermocouple station. The equation of the linear curve fit for the surface temperatures is $y = 0.32x + 21.53$ and the mean temperatures is $y = 0.33x + 21.16$ (between $x = 0.04$ and $x = 8.07$) with a 3% difference in the slopes of the lines. The average temperature difference between the surface of the tube and mean fluid temperature difference was 0.31°C. It was concluded that the flow was fully developed within the predicted 40 mm length of the test section.

The local Nusselt number plotted as a function of x/D_i is shown in Fig. 5-3 (b). Here, there is significant fluctuations in the local Nusselt number result. This is expected as the uncertainty of the heat transfer coefficients in highly turbulent flow is very high (39.4%) due to the small temperature difference between the wall of the tube and the centreline of the tube.

It is not possible to visually determine if fully developed flow occurred within 40 mm of the test section inlet due to the significant fluctuations in the local heat transfer coefficients.

As seen in Fig. 5-1 (b) and Fig. 5-3 (b), there is a variation in the Nusselt number within 500 mm of the test section exit. The upstream effect of the mixing well is seen to affect the boundary layer profile in thermocouple stations R and S negatively and as a result, the local results for these stations were ignored for the remainder of this study.

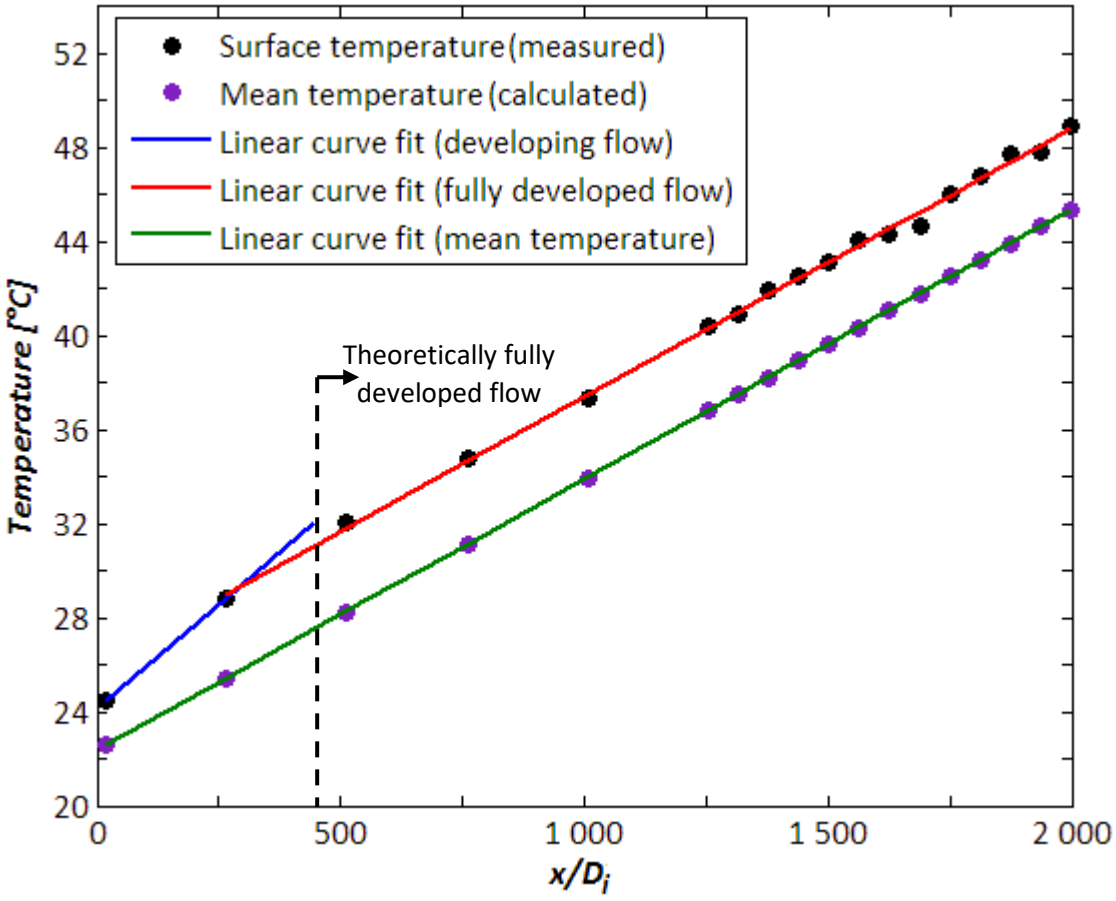

(a)

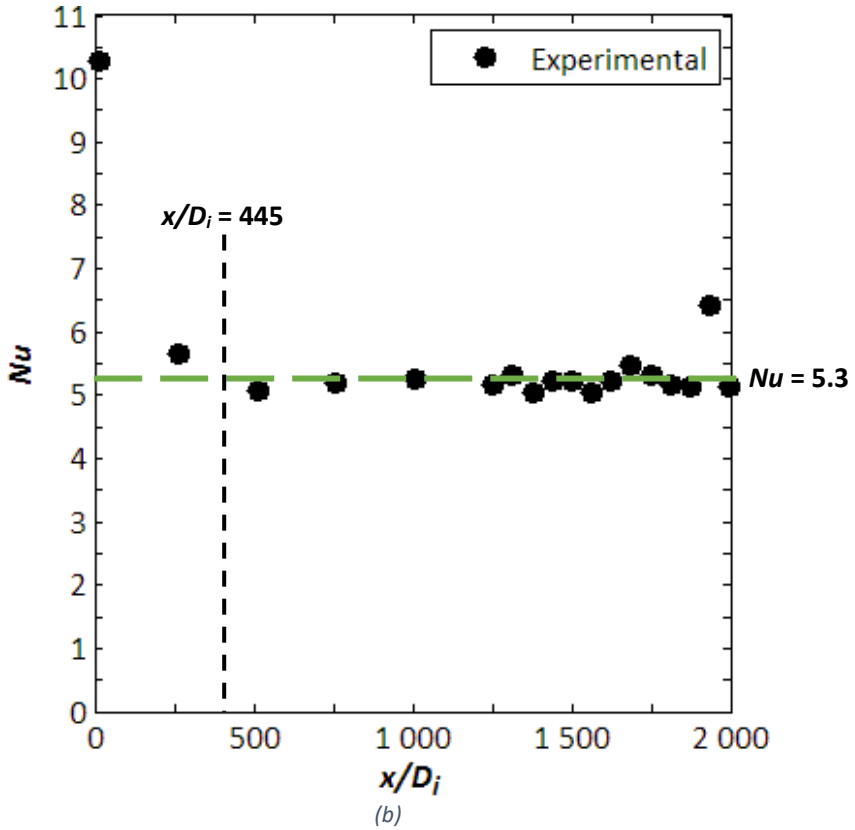

(b)

Fig. 5-2 - Temperature profile (a) and local heat transfer coefficient (b) for a diabatic test of 3.23 kW/m² (laminar flow with a bulk Reynolds number of 1 349)

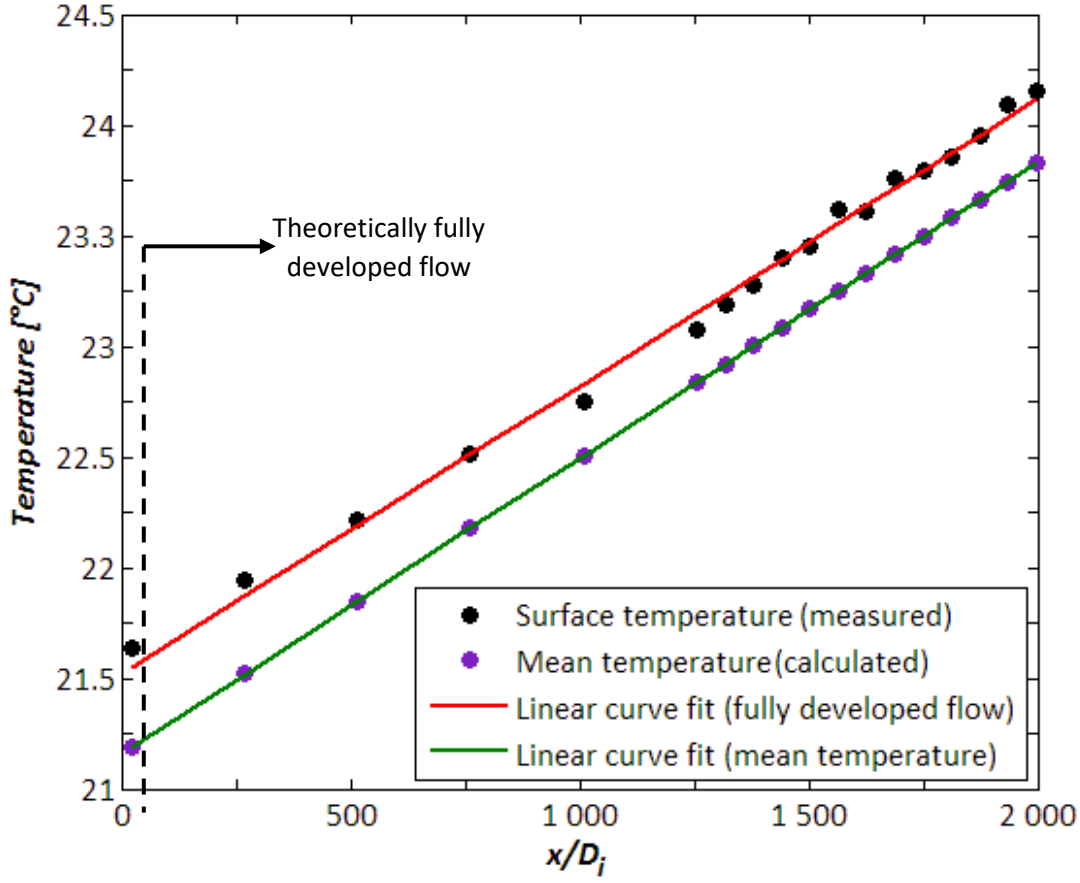

(a)

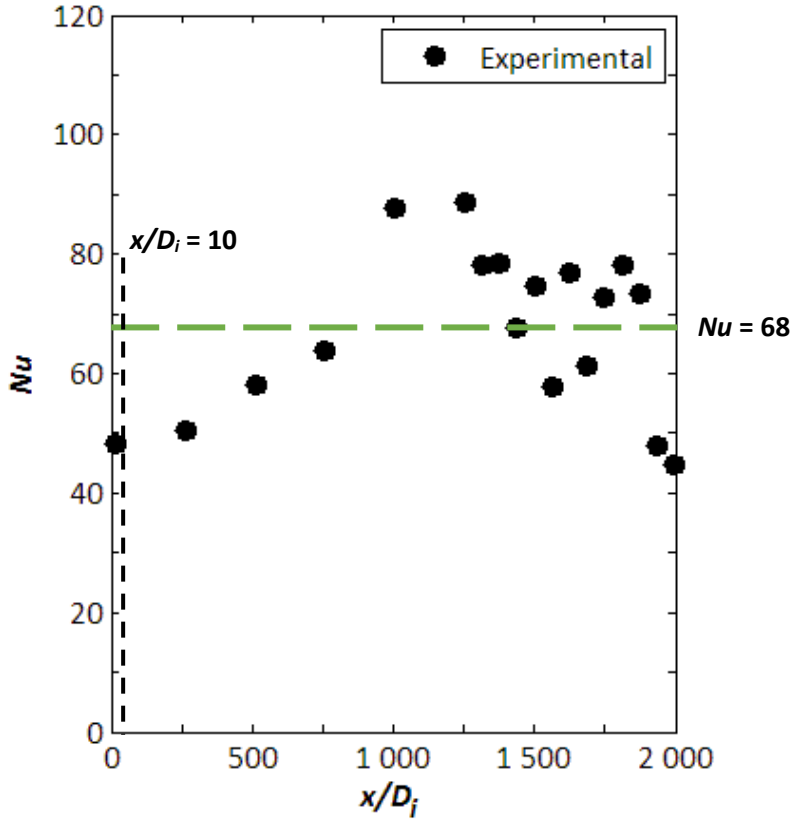

(b)

Fig. 5-3 - Temperature profile (a) and local heat transfer coefficient (b) for a diabatic test of 3.23 kW/m² (turbulent flow with a bulk Reynolds number of 10 055)

The temperature profile associated to transitional flow is considered Fig. 5-4 (a). The inlet temperature for this test was 21.7°C and the bulk Reynolds number was 2 647. The temperature profile of the surface temperatures is erratic and does not conform with predicted literature as shown in Fig. 5-1 (a).

It seems as through the flow developed quickly, within 2 m of the test section inlet, where a reasonably constant temperature gradient is seen. However, the flow temperature profile changes again at approximately 6.2 m from the test section inlet. The profile then becomes reasonably constant again from 6.8 m until the test section outlet, 8.377 m from the test section inlet.

Theoretically, for laminar flow conditions, fully developed flow is predicted to occur within 2.8 m of the test section inlet. Turbulent flow conditions dictate that fully developed flow occurs within 40 mm of the test section inlet. There was no known correlation at the time of this study that described the entrance length for fully developed flow in the transitional flow regime.

The equation of the linear curve fit line for the mean temperature is $y = 1.4529x + 21.66$. The equation of the line for the surface temperatures from 2 m to 6.2 m from the test section inlet is $y = 1.27x + 25.87$. There is a 12.8% difference in the slope in this instance. For the surface temperatures between 6.8 m and 8.377 m, the equation of the linear curve fit line is $y = 1.482x + 23.78$. There is a 2% difference in the slope in this instance. This shows reasonable agreement that the gradient was constant in these two cases.

The local Nusselt number is shown in Fig. 5-4 (b). As shown with the temperature measurements in Fig. 5-4 (a), the local heat transfer coefficients are reasonably constant before fluctuating towards the latter end of the test section. This fluctuation is seen approximately 2 m before the test section exit. This corresponds to the temperature profile gradient change. The significant fluctuations seen at the end of the test section corresponds to those seen in Fig. 5-1 (b), Fig. 5-2 (b) and Fig. 5-3 (b).

It is concluded that due to the erratic behaviour of transitional flow, where the flow profile fluctuates between laminar and turbulent flow, the surface temperatures as well as the local heat transfer coefficients fluctuates as well as shown in Fig. 5-4 (a) and (b).

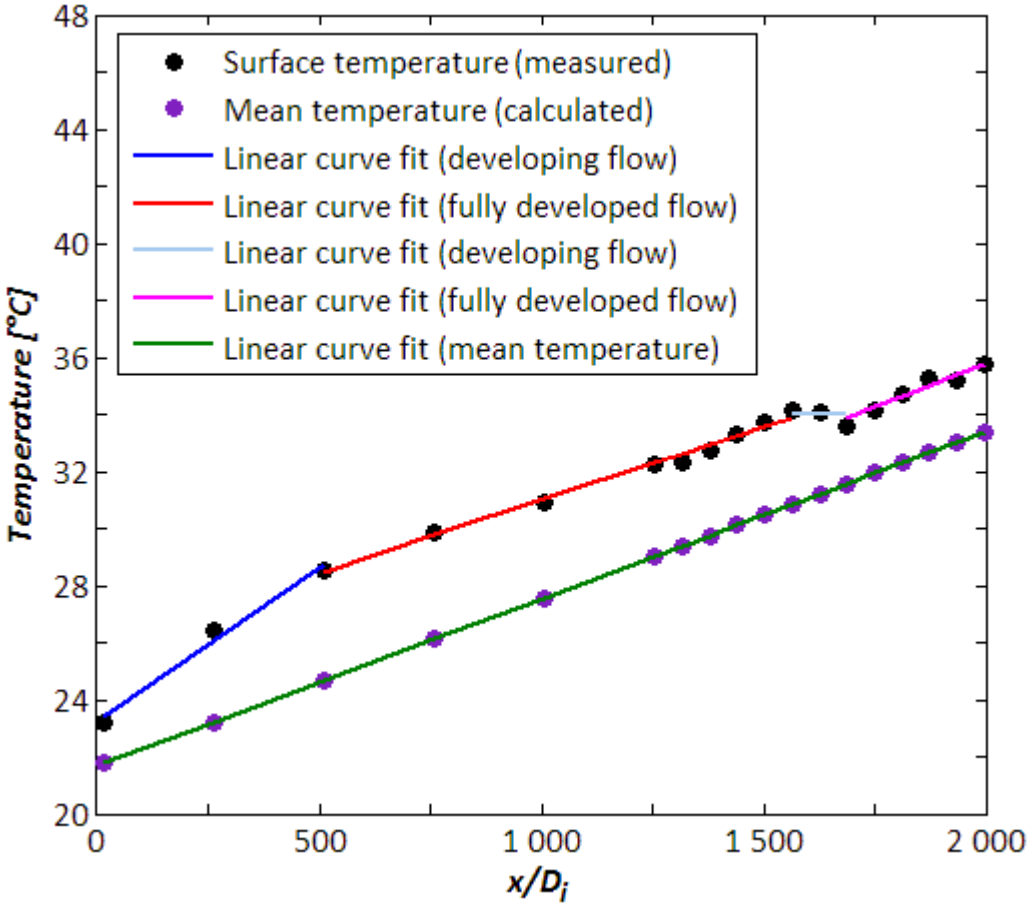

(a)

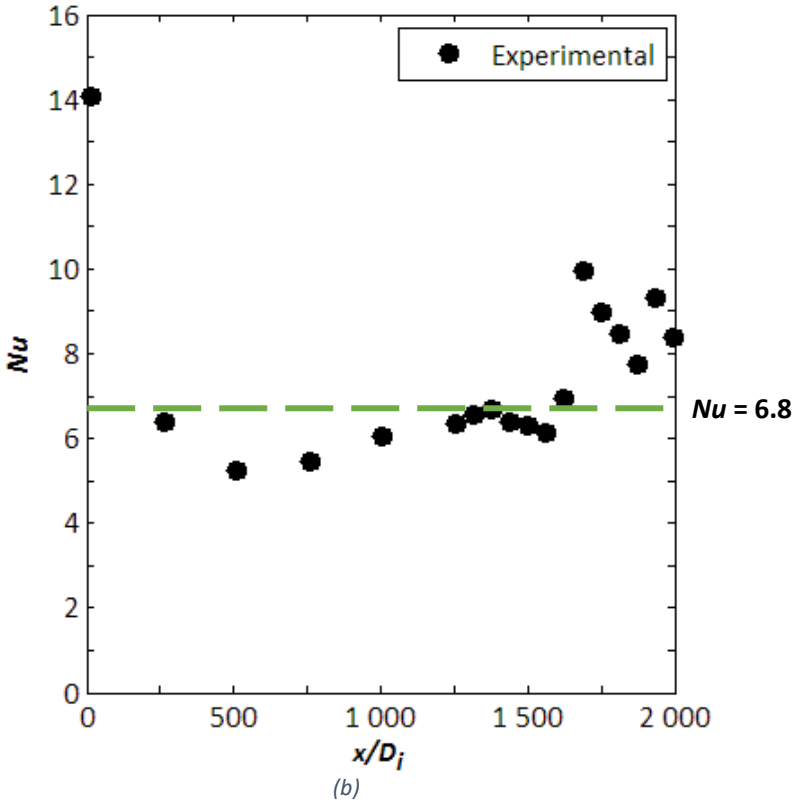

(b)

Fig. 5-4 - Temperature profile (a) and local heat transfer coefficient (b) for a diabatic test of 3.23 kW/m² (transitional flow with a bulk Reynolds number of 2 647)

5.3 Thermocouple station temperature profiles

It is expected with forced convection that the temperatures on the circumference of the tube are equal. That is to say that at each thermocouple station, the standard deviation of the temperatures at that station should not exceed 0.2°C as the accuracy of the temperature measurements is ±0.1°C.

Four scenarios were considered, namely at a laminar Reynolds number and low heat input, a laminar Reynolds number and high heat input, a transitional Reynolds number and high heat input and a turbulent Reynolds number and high heat input.

Consider the temperature measurements for each thermocouple station for a Reynolds number of 1 081, 1 349, 10 055 and 2 647 as shown in Fig. 5-5. For a Reynolds number of 1 081, a heat flux of 0.81 kW/m^2 was applied to the test section. As expected, the fluctuation in temperature per thermocouple station is negligible, with an average standard deviation of 0.027°C across the data set. A maximum deviation of 0.093°C was seen with a minimum of 0.0037°C.

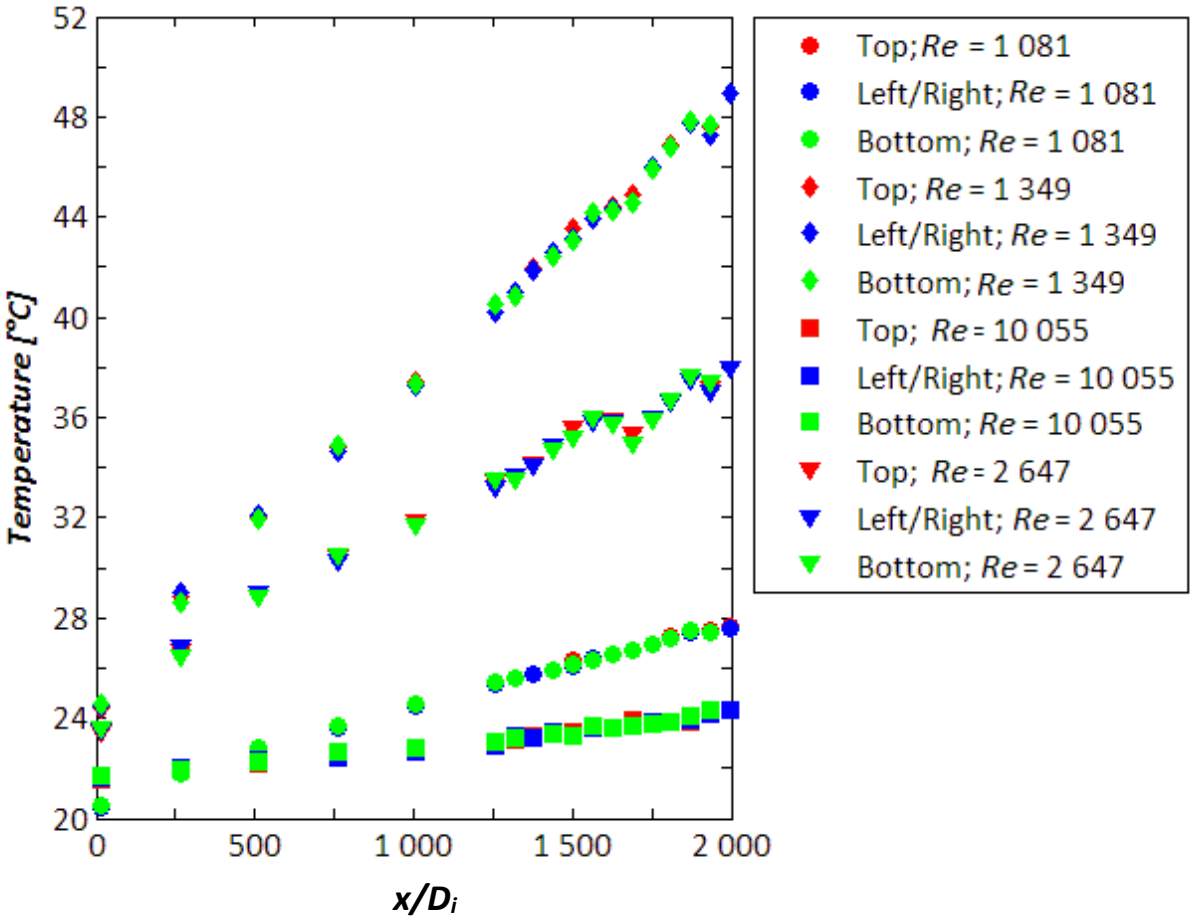

Fig. 5-5 - Temperature measurements per thermocouple station for Reynolds numbers of 1 081, 1 349, 10 055 and 2 647 at a heat flux of between 0.81 kW/m^2 and 3.23 kW/m^2

It is concluded that this data set, which represents the lowest mass flow rate and heat input for the study is representative of forced convection. This is indicative that a Nusselt number result of 4.346 should be achieved for this data set.

The remaining data sets seen in Fig. 5-5 were obtained where a heat flux of 3.23 kW/m^2 was applied to the test section.

Consider the data set with a Reynolds number of 1 349. Temperature fluctuations per thermocouple station is minimal, with an average standard deviation of 0.089°C. A maximum deviation of 0.21°C is seen in this data set with a minimum deviation of 0.031°C. This is once again indicative that the data set is representative of forced convection.

The results of temperature measurements in fully turbulent flow is reflected by a Reynolds number of 10 055. In this instance, a standard deviation of 0.057°C with a maximum and minimum deviation of 0.117°C and 0.017°C respectively is seen. This is expected as turbulent flow is always considered to be in forced convection.

Transitional results are shown where the Reynolds number was 2 647. An average standard deviation of 0.091°C with a maximum and minimum deviation of 0.189°C and 0.027°C respectively is seen.

In conclusion, analysis of the temperature profiles show that the heat transfer results should be in forced convection for both the lowest heat input of 99W (heat flux of 0.891 kW/m^2) and the highest heat input of 342 W (heat flux of 3.26 kW/m^2) in the laminar flow regime.

5.4 Ratio of heat transfer coefficients

Ghajar and Tam [14] and Tam and Ghajar [10] discuss the effect of secondary flow or mixed convection by considering the ratio of the heat transfer coefficient at the top of the tube to the heat transfer coefficient at the bottom of the tube (h_{top}/h_{bottom}) along the length of the tube. It was concluded that where the ratio was close to unity, namely between 0.8 and 1.2, forced convection was the dominant mode of heat transfer.

In the instances where the ratio exceeded 1.2 or was less than 0.8, mixed convection was the dominant mode of heat transfer. This is considered accurate for ethylene glycol and is not necessarily appropriate for water.

Consider where the ratio of the heat transfer coefficients is plotted as a function of the length of the tube for Reynolds numbers from 1 081 to 2 157 (laminar flow) as shown in Fig. 5-6.

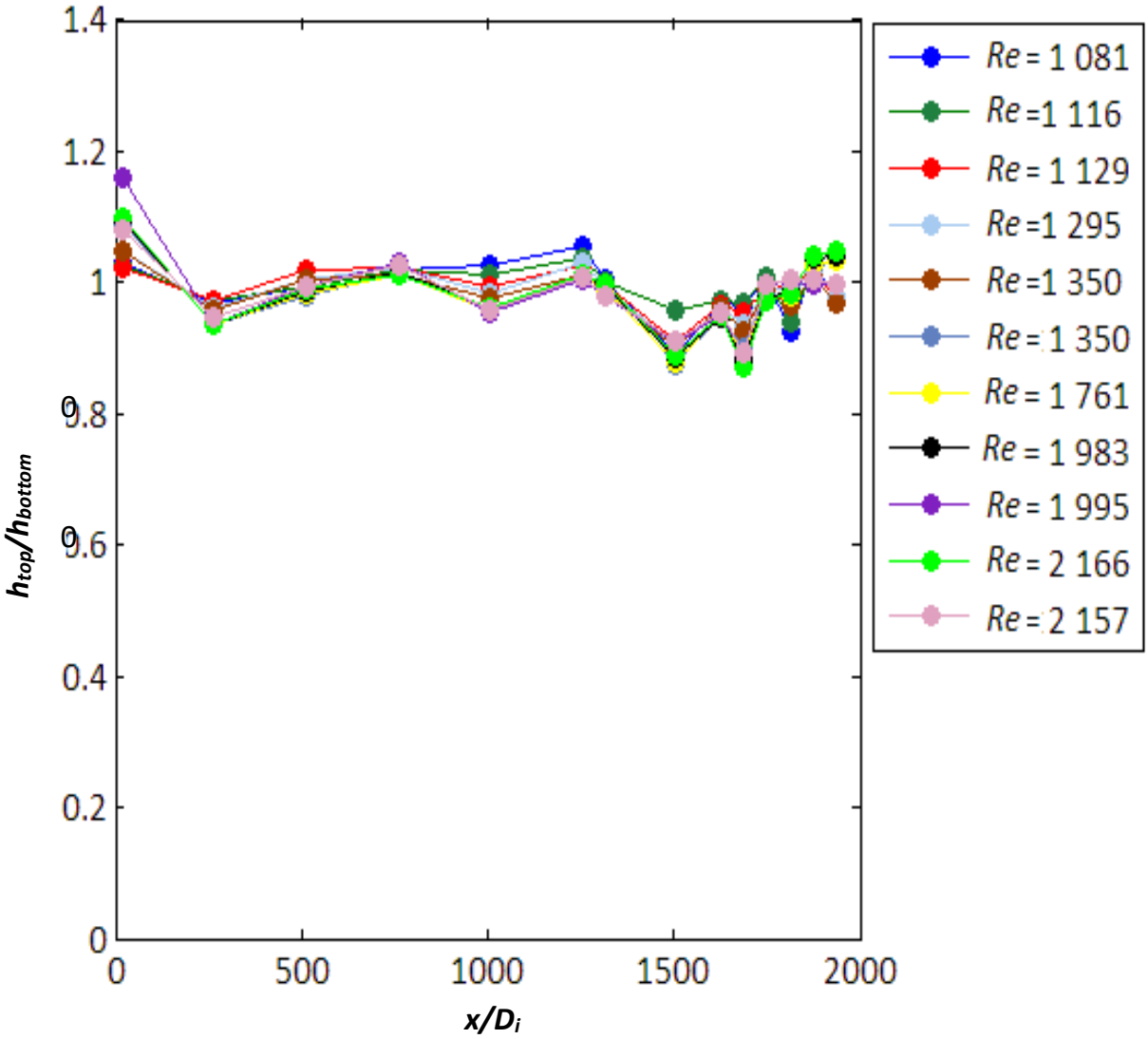

Fig. 5-6 - Ratio of heat transfer coefficients over the length of the test section for Reynolds numbers between 1 081 and 2 157 in the laminar flow regime with a heat flux of between 0.81 kW/m² and 3.23 kW/m²

In this instance, the ratio remains within the criterion of forced convection as set out by Ghajar and Tam [14] and Tam and Ghajar [10] where all data points stay above 0.87 and below 1.16. The heat flux applied to the test section varied from between 0.81 kW/m^2 (where the Reynolds number was 1 081) and 3.23 kW/m^2 (where the Reynolds number was higher than 1 081).

The data points shown in Fig. 5-7 range between 0.824 and 1.17. This is for transitional flow for a Reynolds number range of 2 411 to 2849. As with the results shown for laminar flow in Fig. 5-6, the ratio remains close to unity, which is indicative of forced convection.

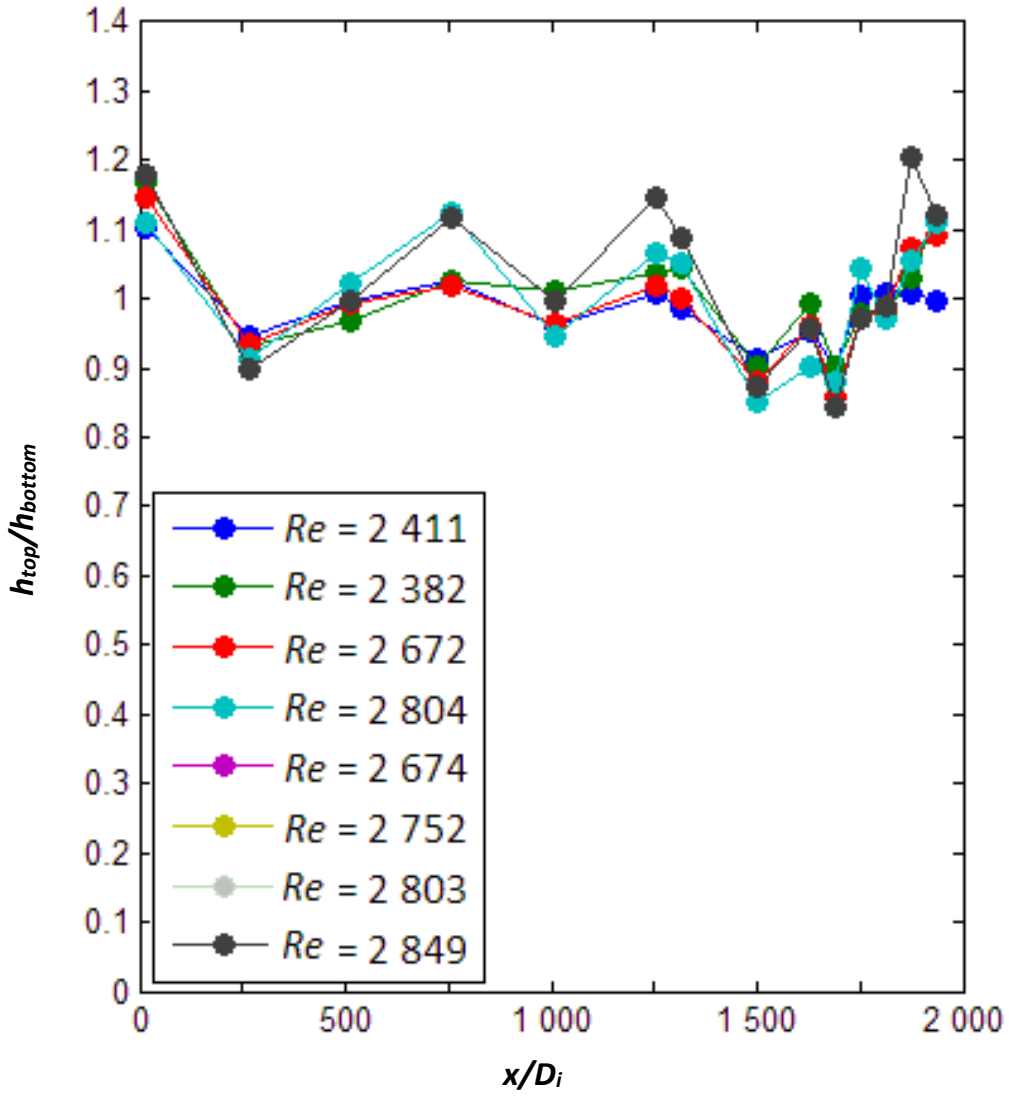

Fig. 5-7 - Ratio of heat transfer coefficients over the length of the test section for Reynolds numbers between 2 411 and 2 849 in the transitional flow regime with a heat flux of 3.23 kW/m²

The calculated uncertainty for low Reynolds numbers of approximately 1 000 and heat input of 99 W is 6.7% for the heat transfer coefficient. As the Reynolds numbers increase to above 10 000, the uncertainty of the heat transfer coefficient is in excess of 39% due to the small temperature difference between the wall of the tube and the centre of the tube. This is reflected in Fig. 5-8 where the Reynolds number range is between 3 123 and 5 834.

In Fig. 5-8, the ratio ranges between 0.758 and 1.395. This does not compare very well with theory as fully turbulent flow is in forced convection, thus the ratio should range between 0.8 and 1.2. However, in this instance, as the Reynolds number increases, the uncertainty of the heat transfer coefficients increases as well to as high as 39%.

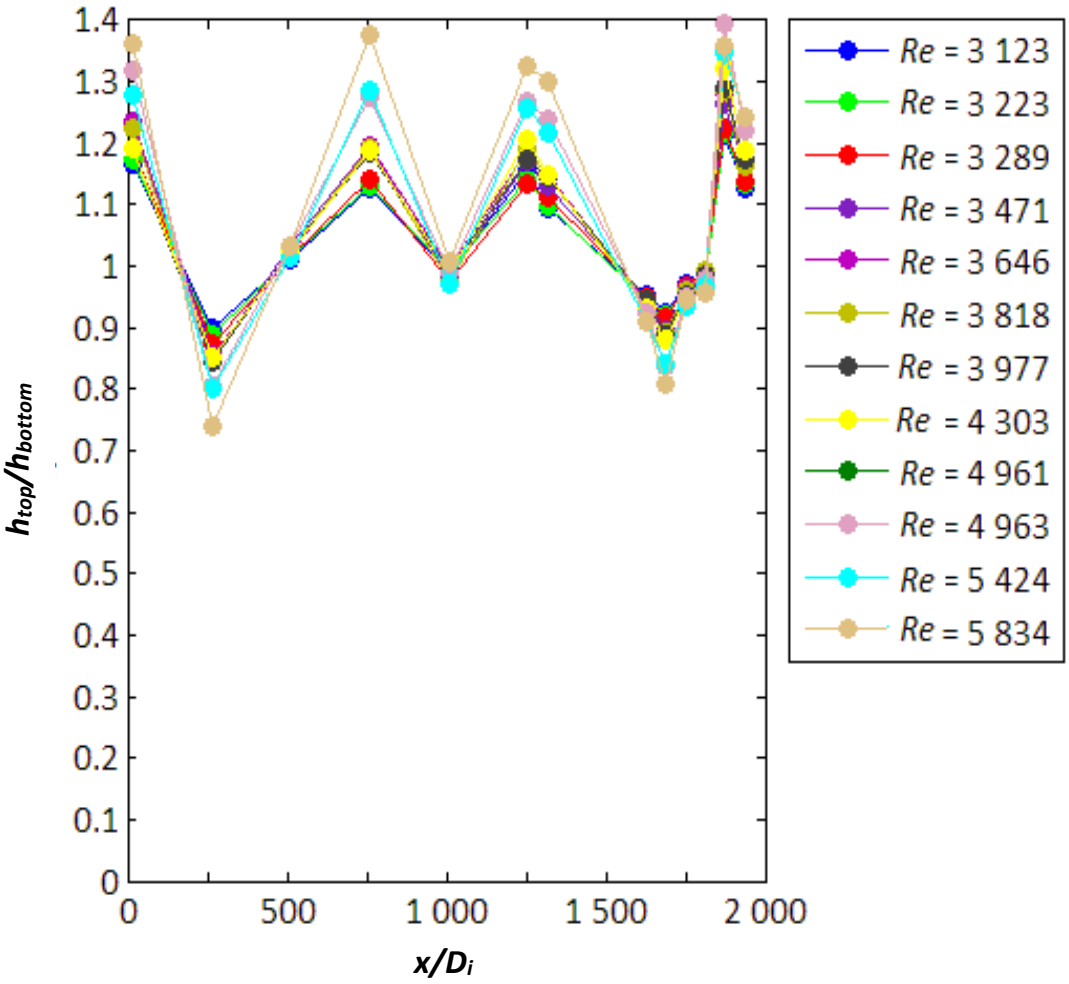

Fig. 5-8 - Ratio of heat transfer coefficients over the length of the test section for Reynolds numbers between 3 123 and 5 834 in the turbulent flow regime with a heat flux of 3.23 kW/m²

5.5 Heat transfer

5.5.1 Nusselt number

The calculated Nusselt number as a function of Reynolds number for the study is shown in Fig. 5-9. This is for fully developed flow. Theoretically, fully developed flow is expected to occur within 3.8 m of the test section inlet for a Reynolds number of 2 300. As a result, the average Nusselt number for thermocouple stations E – Q is reflected. Thermocouple stations R and S were neglected as discussed in 5.2.

The results are reflected in all three flow regimes with a bulk Reynolds number range from 1 081 to 10 974 for thermocouple stations E-Q. The Nusselt number increases from 4.15 in the laminar flow regime to 76 in the fully turbulent flow regime. Transition from laminar flow to turbulent flow is sharp from a Reynolds number of 2 457 to 2 812.

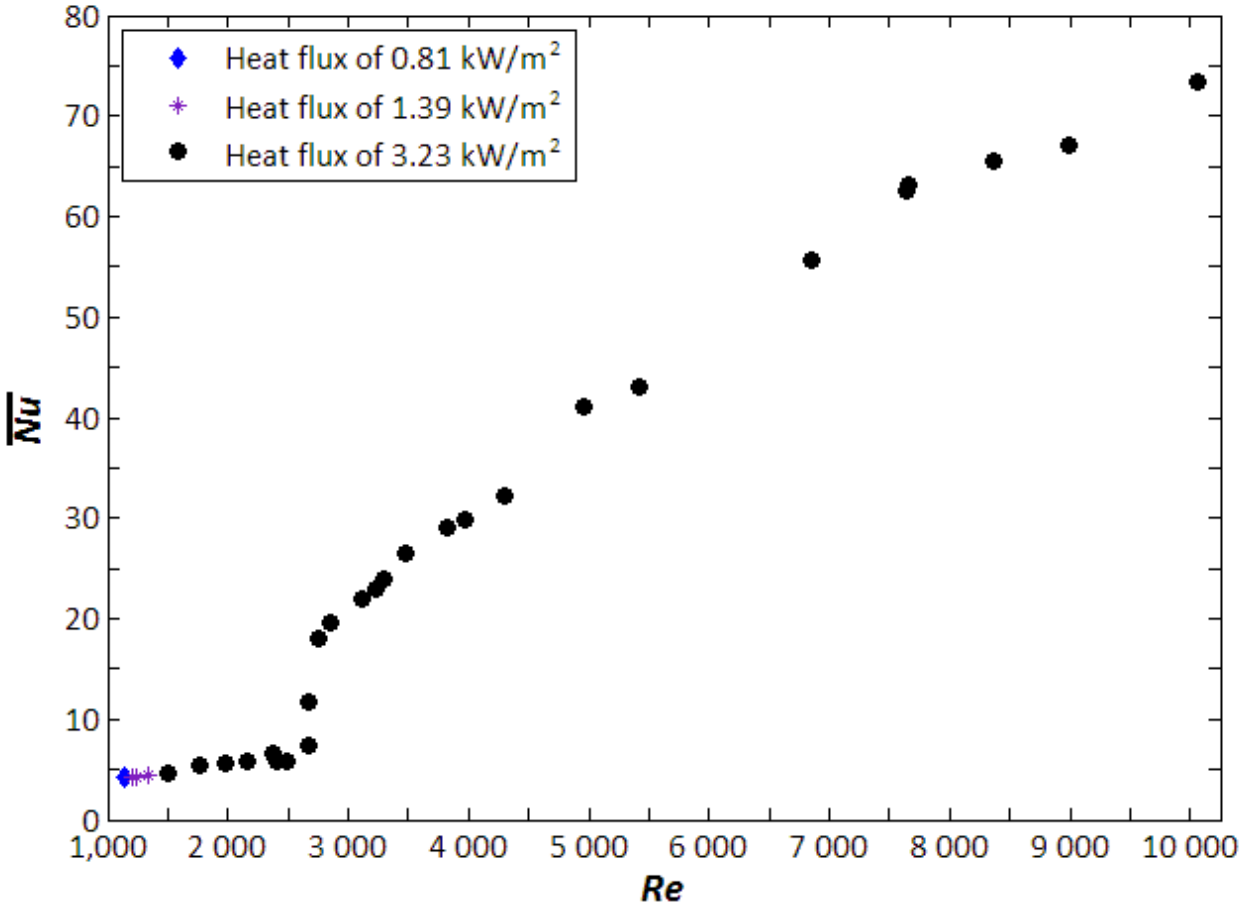

Fig. 5-9 - Nusselt number results for fully developed flow for a bulk Reynolds number range from 1 081 to 10 974 for a heat flux of between 0.81 kW/m² and 3.23 kW/m²

An exploded view of the transitional regime is shown in Fig. 5-10. The sharp transition from laminar flow to turbulent flow is seen clearly, taking place between a Reynolds number of 2 484 and 2 849.

The measured results are compared to the transitional correlation of Ghajar and Tam [14]. While results show a transition range of between 2 484 and 2 812, the transition range is slightly longer for that of Ghajar and Tam, from 2 156 to 3 123. An average error of 26% is seen when comparing the measured Nusselt numbers and the predicted Nusselt numbers between Reynolds numbers of 2 156 and 3 123 with a maximum error of 49%.

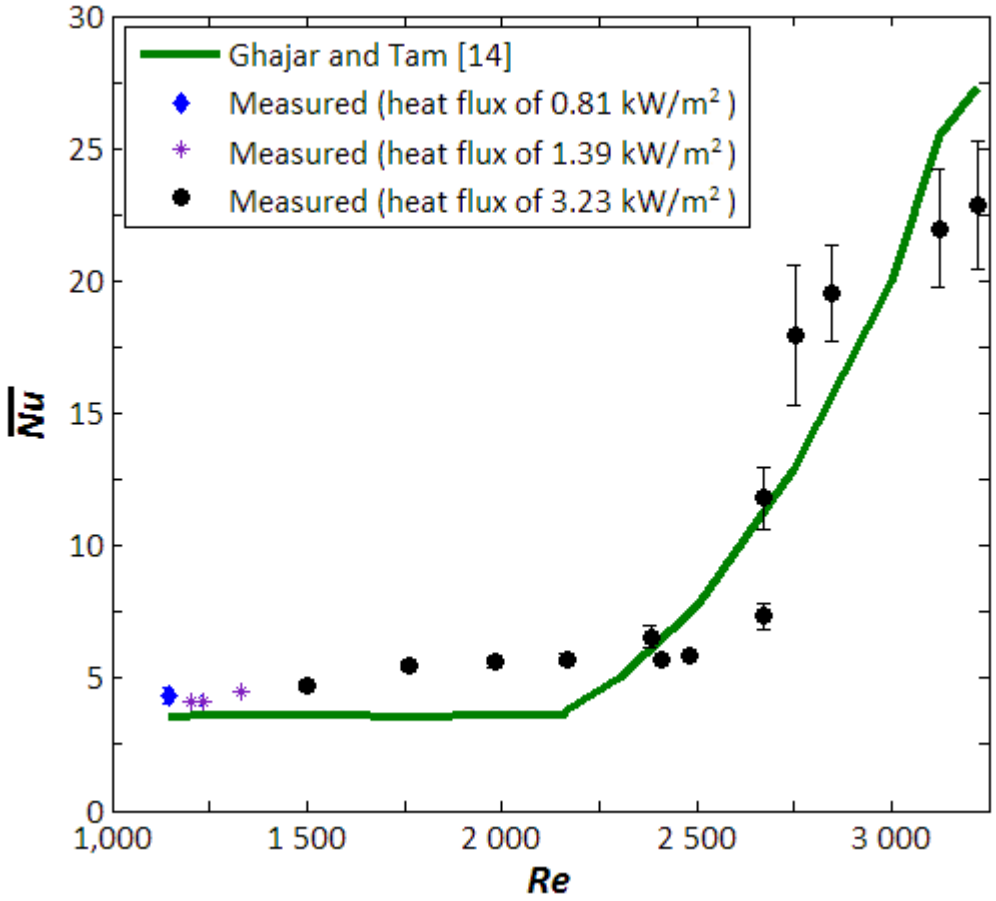

Fig. 5-10 - Exploded view of the transitional flow regime

The correlations of Ghajar and Tam [14] show a more gradual transition as compared to the measured results. The reason for the discrepancy may be attributed to the difference in parameters when comparing the predicted results. The correlation of Ghajar and Tam is bounded by a x/D_i range of between 3 and 192. The measured results are bounded between 17 and 1 935.

5.5.2 Colburn j_H-factor

The effect of varying property variations in the Prandtl numbers on Nusselt number is eliminated by expressing the results in terms of the Colburn j_H-factor. The measured heat transfer results, as shown in Fig. 5-9, are plotted in the form of the Colburn j_H-factor and compared to the predicted theoretical results in Fig. 5-11.

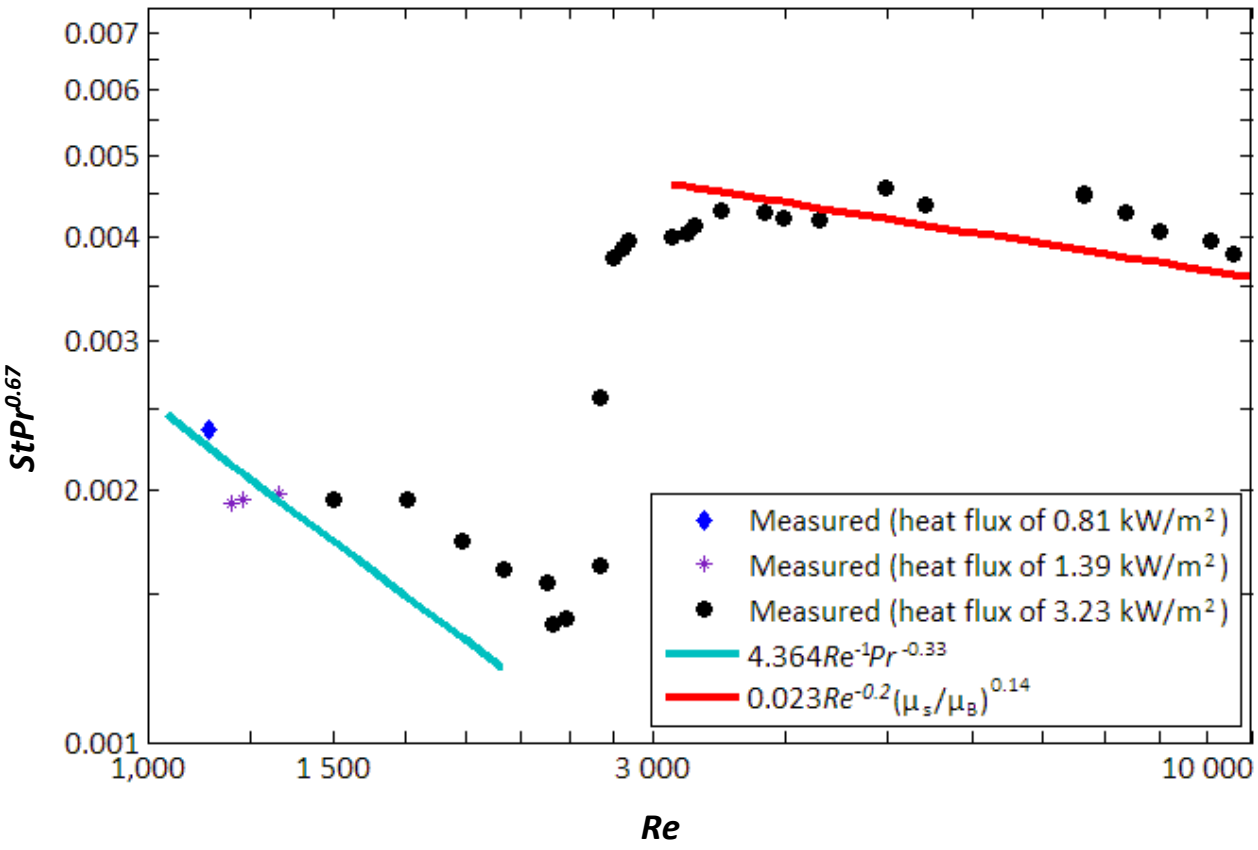

Fig. 5-11 – Measured heat transfer in the different flow regimes expressed as Colburn j_H-factors as a function of the Reynolds number

In the low Reynolds number range, where the heat flux on the test section was limited to less than 1.41 kW/m^2 (1 081 < Re < 1 498) there is very good agreement with literature, where an average error of 7.8% is calculated. This is indicative that forced convection was the dominant mode of heat transfer. This is within the uncertainty of the measurements of 18%.

As the heat flux was increased to 3.26 kW/m^2 (1 761 < Re < 2 411) the error between the measured results and the predicted results increases as well, to an average of 16%. It seems from Fig. 5-11 that mixed convection was present. However, the uncertainty of the measurement for the Colburn j_H-factor for laminar flow is in excess of 18%. As a result, this observation is not conclusive. In the turbulent flow regime there is very good agreement with literature where an average error of 8.5% is calculated with a predicted uncertainty of 33.%.

Transition between the laminar flow regime and the turbulent flow regime is very sharp (1 081 < Re < 2 849), though there is an indication of a low-Re-end as described by Everts [44] between Reynolds numbers of 2 849 and 3 818 where the turning point is very gradual.

It is concluded that forced convection and mixed convection was achieved during this study. This is shown conclusively in Fig. 5-11. There is graphical evidence of mixed convection in the upper region of the laminar flow regime, however the calculated error is still within the uncertainty of the results.

5.6 Friction factor

The diabatic friction factor results for all of the Nusselt number results report in Fig. 5-9 is shown in Fig. 5-12.

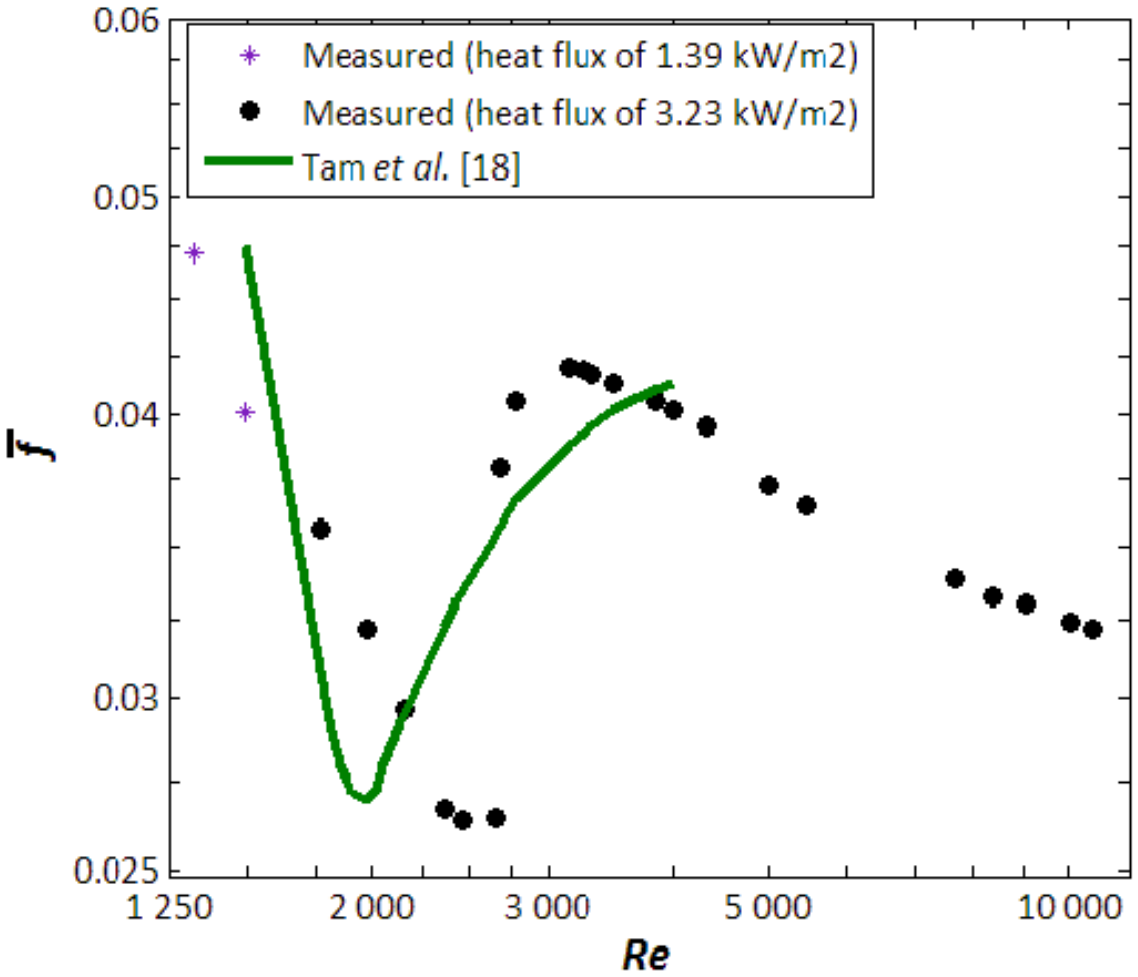

Fig. 5-12 - Diabatic friction factor results for a bulk Reynolds number range from 1 081 to 10 974

The measured results show that transition occurs between the Reynolds numbers of 2 457 and 2 812. The gradient of the transition is sharp and coincides almost perfectly with the transition range described by the measured Nusselt number in Fig. 5-9. This is an expected result as pressure and friction are directly related to each other.

The friction factor as described by Tam *et al.* [18] shows a softer transition, where the range of transition is seen between the Reynolds numbers of 2 050 and 3 615. This range coincides with the transition range described by the predicted Nusselt number of Ghajar and Tam [14] in Fig. 5-9.

It is concluded that the difference when comparing the measured heat and pressure drop results in the transitional with that of Ghajar and Tam [14] and Tam *et al.* [18] is attributed to the variance in the working parameters of the correlations of Ghajar and Tam [14] and Tam *et al.* [18].

5.7 Flow regime maps

Three different flow regime maps were described in section 2.3.5, namely the map of Metais and Eckert [32], Petukhov and Polyakov [54] and Ghajar and Tam [16]. In all three instances, the maps consider Reynolds number as a function of the Rayleigh number where the Rayleigh number describes the dominant mode of heat transfer.

In the instance where the Rayleigh number is low where the Reynolds number is below 10 000, forced convection is the dominant mode of heat transfer. As the Rayleigh number increases, mixed convection is predicted. Only the map of Ghajar and Tam [16] is considered as the other maps are not valid for this study.

Consider the map of Ghajar and Tam [16] with the measured Rayleigh number results is shown in Fig. 5-13. The map is redacted from a Rayleigh number of 5 000 000 to reflect results up to Rayleigh numbers of 10 000.

The measured laminar regime results, where a heat flux of 1.39 kW/m^2 was applied to the test section, fall into the forced convection category. This is well within the forced convection boundary of the map for laminar flow as the Rayleigh number boundary for forced convection is in excess of 290 000.

Where a higher heat flux of 3.23 kW/m^2 is applied to the tube, the measured results move into the transition band for the map. However, as shown in section 5.5.1, the lower limit of transition occurred at a Reynolds number of 2 484, therefore all of the laminar flow results fall within the forced convection region of the map.

This is contrary to the Nusselt number results shown in section 5.5.1 where only half of the laminar regime measurements fall are considered to be in forced convection.

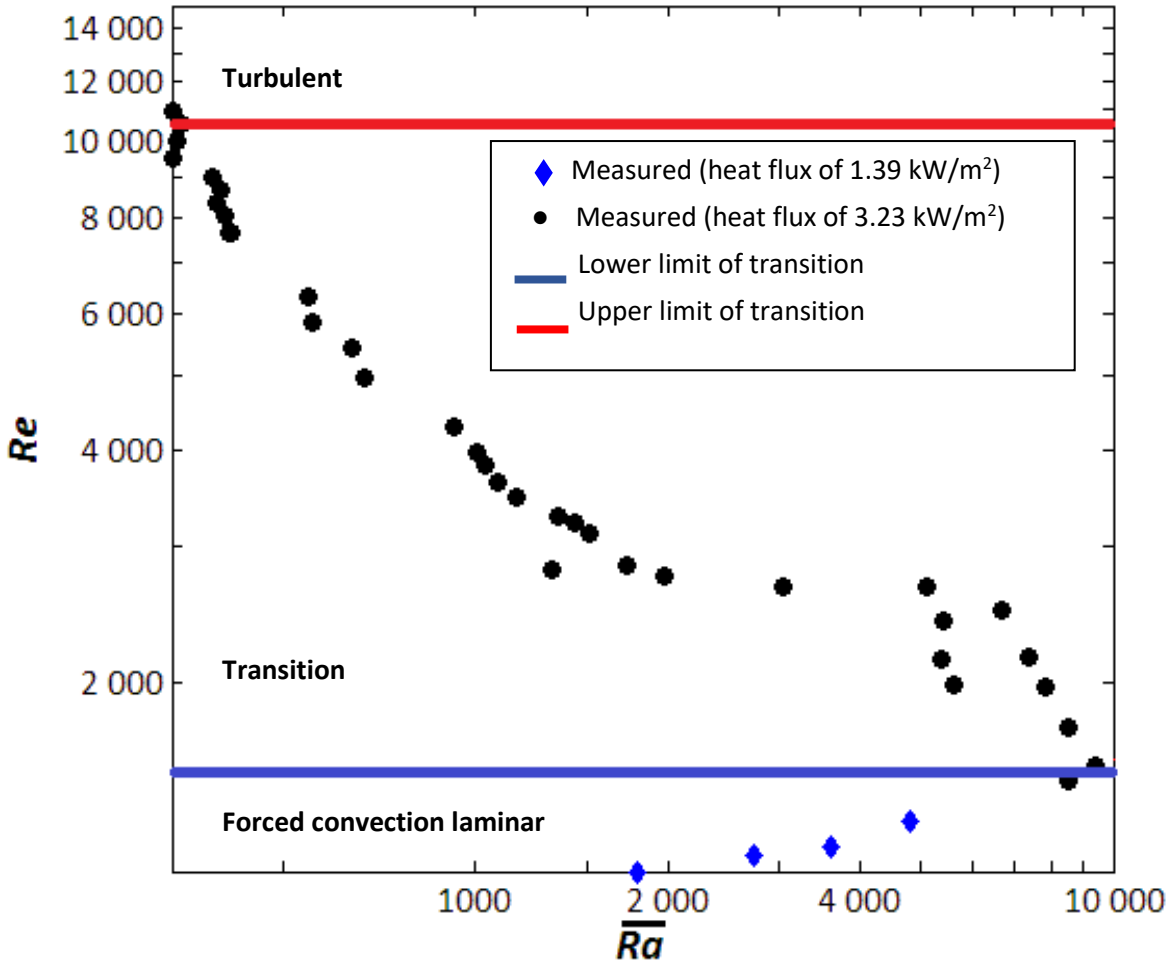

Fig. 5-13 - Measured Rayleigh number results plotted on the flow regime map of Ghajar and Tam [16]

5.8 Conclusion

The results of 42 data sets was presented in this chapter. Each data set consisted of 6 200 measurements which were averaged and reduced to meaningful results that was consequently compared where possible to available literature.

The temperature profile for the extremes of the data sets was presented. It was proven the theoretical calculation for entrance lengths is conservative and can be used with confidence when assessing the entrance length of tubes. The heat transfer coefficient profiles were reviewed and it became clear that there were upstream disturbances in the boundary layer profile in the last two thermocouple station on the test section (stations R and S). Due to these disturbances, the results from these thermocouple stations were neglected.

Temperature profiles per thermocouple station was reviewed. This was conducted as theory dictates that where there is forced convection, the wall temperature at the thermocouple station remains constant. This was proven to be the case for the laminar, transitional and turbulent flow regime. A maximum standard deviation of 0.21°C was seen for the data sets which is within the accuracy of the temperature measurements.

Ghajar and Tam [14] and Tam and Ghajar [10] have published literature regarding the ratio of the heat transfer coefficients. They have concluded that for forced convection the ratio of the heat transfer coefficient at the top of the tube to the heat transfer coefficient at the bottom of the tube (h_{top}/h_{bottom}) should be close to unity (between 0.8 and 1.2). This was reviewed for laminar flow, transitional flow and low turbulent flow.

In laminar flow, the ratio of h_{top}/h_{bottom} conformed to literature, where the range of the ratio varied between 0.87 and 1.16. This was indicative of forced convection in the laminar flow regime. When considering transitional flow, the ratio remained similar to laminar flow, where it varied between 0.83 and 1.17. There was some discrepancy in the low turbulent flow regime where forced convection is always expected. A ratio of 0.758 and 1.395 was seen. It was concluded that this deviation was due to the high uncertainty of the heat transfer coefficients in the turbulent flow regime.

Heat transfer results and pressure drops was presented in detail. In most instances, the heat transfer and pressure drop results had a very good agreement with literature. In the laminar flow regime, forced convection results were achieved, where the measured Nusselt number compared well to the classical forced convection Nusselt number of 4.364. This was for low heat flux conditions where a heat flux of less than 1.41 kW/m^2 was applied to the test section. In instances where high heat fluxes were applied, the laminar Nusselt number error increased.

Heat transfer transition between laminar flow and turbulent flow was seen between Reynolds numbers of 2 484 and 2 849. Transition showed a very sharp gradient with extreme changes in gradient on each end of the flow regime.

The effect of mixed convection was further investigated by reviewing the Colburn j_H-factor. In this instance, some of the laminar flow regime results coincided with literature, namely where the measured Nusselt number was approximately 4.364. In the instance where the Nusselt number exceeded 5, the j_H-factor indicated that mixed convection was present. However, the uncertainty of the j_H-factor results was in excess of the error between the predicted results and the measured results.

In the turbulent flow regime, the j_H-factor compared well with the predicted results, where the error was well below the uncertainty of the measurements.

The corresponding friction factors were presented as well. Very good agreement in both the laminar flow regime and turbulent flow regime was seen. The friction factor transition was seen to occur between Reynolds numbers of 2 452 and 2 812. Once again, transition showed a very sharp gradient with extreme changes in gradient on each end of the flow regime. This is in line with the predicted behaviour of heat and pressure which are directly proportional to one another.

The heat transfer results were compared in the form of Rayleigh numbers to the Reynolds numbers on the flow regime map of Ghajar and Tam [16]. The map has been developed for

Rayleigh numbers in the tens of thousands, where significant heat flux is applied to the test section. In the case of this study, the heat flux was limited to 3.23 kW/m^2 due to experimental limitations. As a result, the measured Rayleigh number range was between 330 and 9 411. When plotting the results all results fell well within the forced convection regimes. This is in line with most of the measured results.

An analysis of the combined results reflects that forced convection in the laminar flow regime was achieved. There are conflicting observations regarding the dominant mode of heat transfer. While the measured Nusselt number in the high end of the laminar flow regime exceeded 4.364, the temperature profile and the heat transfer coefficient ratio per thermocouple station reflected that that forced convection was the dominant mode of heat transfer. The calculated error in the Colburn j_H-factor was within the uncertainty of the measurement. The results from the flow regime map show that forced convection of the dominant mode of heat transfer.

6 Summary, conclusions and recommendations

6.1 Summary

The characterisation of convective heat transfer and pressure drop in smooth tubes in the laminar and turbulent flow regimes has been extensively researched. However, little work was completed in the transitional flow regime. The purpose of this study was to determine the heat transfer and pressure drop characteristics specifically in the forced convection flow regime in transitional flow. The characteristics were determined by forcing fluid to flow through a smooth circular horizontal tube. The test section was heated at a constant heat flux. A calming section with a square edge inlet was upstream of the test section. Temperatures at the tube inlet, outlet and outer surface of the test section were measured. Two pressure taps were also installed on the test section and was connected to a pressure transducer for pressure drop measurements. Experiments were conducted mainly on the last part of the test section where fully developed flow occurred.

6.2 Conclusions

The measured heat transfer was validated using both the average and local Nusselt numbers. An error of 21% when seen when considering the classical Nusselt number of 4.364. This was indicative that some secondary flow was present during validation testing. Turbulent flow heat transfer results showed excellent agreement with predicted results, where an average error of 5.8% was seen when comparing the measured results with those predicted by Gnielinski.

It was proven the theoretical calculation for entrance lengths is conservative and can be used with confidence when assessing the entrance length of tubes. Temperature profiles per thermocouple station was reviewed and forced convection was indicated as the temperatures per thermocouple station were equal. A review of the ratio of the heat transfer coefficients was conducted. In laminar flow, the ratio of h_{top}/h_{bottom} conformed to literature, where the range of the ratio varied between 0.87 and 1.16. This was indicative of forced convection in the laminar flow regime. When considering transitional flow, the ratio remained similar to laminar flow, where it varied between 0.83 and 1.17. There was some discrepancy in the low turbulent flow regime where forced convection is always expected. A ratio of 0.758 and 1.395 was seen. It was concluded that this deviation was due to the high uncertainty of the heat transfer coefficients in the turbulent flow regime.

Heat transfer results and pressure drops were presented. The heat transfer and pressure drop results had a very good agreement with published literature. Heat transfer transition between laminar flow and turbulent flow was seen between Reynolds numbers of 2 484 and 2 849. Transition showed a very sharp gradient with extreme changes in gradient on each end of the flow regime.

The corresponding friction factors were presented as well. Very good agreement in both the laminar flow regime and turbulent flow regime was seen. The friction factor transition was seen to occur between Reynolds numbers of 2 452 and 2 812. Once again, transition showed a very sharp gradient with extreme changes in gradient on each end of the flow regime. This is in line with the predicted behaviour of heat and pressure which are directly proportional to one another.

In literature, Ghajar concluded that the transitional heat transfer range was wider than the transitional friction factor range for all inlet geometries, Meyer had conflicting results that stated that the ranges were approximately the same. This study conferred with the conclusions of Meyer.

The effect of mixed convection was further investigated by reviewing the Colburn j_H-factor. In this instance, the uncertainty of the measurements exceeded the calculated error in both the laminar flow regime and the turbulent flow regime. As a result, it was concluded that both forced and mixed convection results were obtained.

Flow regime maps were assessed. Their applicability to this study is inconclusive due to the limitations of the heat flux applied to the test section. In all instances, the maps have been developed for Rayleigh numbers in the tens of thousands, where significant heat flux is applied to the test section. In the case of this study, the heat flux was limited to 3.26 kW/m^2 due to experimental limitations. As a result, the measured Rayleigh number range was between 330 and 9 411.

There are conflicting observations regarding the dominant mode of heat transfer in the laminar flow regime. At the low end of the laminar flow regime, the Nusselt number was approximately 4.364 which a classical indication of forced convection. However, at the high end of the laminar flow regime, where the Nusselt number exceeded 4.364 which is indicative of mixed convection, the temperature profile and the heat transfer coefficient ratio per thermocouple station reflected that that forced convection was the dominant mode of heat transfer.

6.3 Recommendations

The following recommendations are made for future studies for fully developed flow in the transitional flow regime in smooth horizontal pipes:

- Increase the heat flux applied to the test section.
- Investigate the upstream effects of the mixing well on the fully developed boundary layer in the test section.
- Use a finer resolution in mass flow rate in the transitional flow regime. A resolution of 0.5 l/hr was used for this study.

- Determine the effects of different inlet geometries on the heat transfer and friction transition range.
- Install additional pressure taps along the length of the tube.
- Develop a new flow regime map for the combined work of Meyer and his co-workers.

7 References

[1] N.A.o.E.o.t.N. Academies, NAE Grand Challenges for Engineering, in, NAE.

[2] R.H. Perry, D.W. Green, Perry's Chemical Engineers Handbook, 7th ed., McGraw-Hill, 1997.

[3] W. Gu, X. Chen, K. Liu, B. Zhang, Q. Chen, C.W. Hui, Retrofitting of the Heat Exchanger Network with Steam Generation in a Crude Oil Distillation Unit, Chemical Engineering and Technology, 38(2) (2015) 203-214.

[4] H. Wagner, The management of heat flow in deep mines, Mining Report, 149(2) (2013) 88-100.

[5] A.M. Hussein, R.A. Bakar, K. Kadirgama, K.V. Sharma, Heat transfer enhancement using nanofluids in an automotive cooling system, International Communications in Heat and Mass Transfer, 53 (2014) 195-202.

[6] P. Agarwal, Adhirathsik, V. Shanthi, Application of heat exchangers in bioprocess industry: A review, International Journal of Pharmacy and Pharmaceutical Sciences, 6(1) (2014) 24-28.

[7] N. Alvarez, G. Daufin, G. Gésan-Guiziou, Recommendations for rationalizing cleaning-in-place in the dairy industry: Case study of an ultra-high temperature heat exchanger, Journal of Dairy Sciences, (93) (2010) 14.

[8] A. Bar-Cohen, C.A. Holloway, Thermal Science and Engineering - From Macro to Nano in 200 Years, in: Proceedings of the 15th International Heat Transfer Conference, IHTC-15, Kyoto, Japan, 2014.

[9] J.P. Meyer, J.A. Olivier, Heat transfer and pressure drop characteristics of smooth horizontal tubes in the transitional flow regime, Heat Transfer Engineering, 35(14-15) (2014) 1246-1253.

[10] L.M. Tam, A.J. Ghajar, Transitional Heat Transfer in Plain Horizontal Tubes, Heat Transfer Engineering, 27(5) (2006) 23-38.

[11] J.P. Meyer, Heat Transfer in Tubes in the Transitional Flow Regime, in: 15th International Heat Transfer Conference, Kyoto, Japan, 2014.

[12] J.P. Meyer, J.A. Olivier, Transitional flow inside enhanced tubes for fully developed and developing flow with different types of inlet disturbances: Part II–heat transfer, International Journal of Heat and Mass Transfer, 54(7–8) (2011) 1598-1607.

[13] J.A. Olivier, J.P. Meyer, Single-Phase Heat Transfer and Pressure Drop of the Cooling of Water inside Smooth Tubes for Transitional Flow with Different Inlet Geometries (RP-1280), HVAC&R Research, 16(4) (2010) 471-496.

[14] A.J. Ghajar, L.-M. Tam, Heat transfer measurements and correlations in the transition region for a circular tube with three different inlet configurations, Experimental Thermal and Fluid Science, 8(1) (1994) 79-90.

[15] A.J. Ghajar, K.F. Madon, Pressure drop measurements in the transition region for a circular tube with three different inlet configurations, Experimental Thermal and Fluid Science, 5(1) (1992) 129-135.

[16] A.J. Ghajar, L.M. Tam, Flow regime map for a horizontal pipe with uniform wall heat flux and three inlet configurations, Experimental Thermal and Fluid Science, 10(3) (1995) 287-297.

[17] A.J. Ghajar, C.C. Tang, W.L. Cook, Experimental investigation of friction factor in the transition region for water flow in minitubes and microtubes, Heat Transfer Engineering, 31(8) (2010) 646-657.

[18] H.K. Tam, L.M. Tam, A.J. Ghajar, Effect of inlet geometries and heating on the entrance and fully-developed friction factors in the laminar and transition regions of a horizontal tube, Experimental Thermal and Fluid Science, 44 (2012) 680-696.

[19] H.K. Tam, L.M. Tam, A.J. Ghajar, C. Sun, H.Y. Leung, Experimental investigaton of the single-phase friction factor and heat transfer inside the horizontal internally micro-fin tubes in the transition region, in: ASME-JSME-KSME 2011 Joint Fluids Engineering Conference, AJK 2011, 2011, pp. 2963-2970.

[20] L.M. Tam, H.K. Tam, A.J. Ghajar, Simultaneous heat transfer and pressure drop measurements for a horizontal micro-tube, in: ASME/JSME 2011 8th Thermal Engineering Joint Conference, AJTEC 2011, 2011.

[21] L.-M. Tam, A.J. Ghajar, The unusual behavior of local heat transfer coefficient in a circular tube with a bell-mouth inlet, Experimental Thermal and Fluid Science, 16(3) (1998) 187-194.
[22] L.-M. Tam, A.J. Ghajar, Effect of inlet geometry and heating on the fully developed friction factor in the transition region of a horizontal tube, Experimental Thermal and Fluid Science, 15(1) (1997) 52-64.
[23] J. Dirker, J.P. Meyer, D.V. Garach, Inlet flow effects in micro-channels in the laminar and transitional regimes on single-phase heat transfer coefficients and friction factors, International Journal of Heat and Mass Transfer, 77 (2014) 612-626.
[24] M. Everts, S.R. Ayres, F.A.M. Houwer, C.P. Vanderwagen, N.M. Kotze, J.P. Meyer, The Influence of Surface Roughness on Heat Transfer in the Transitional Flow Regime, in: 15th International Heat Transfer Conference IHTC-15, Kyoto, Japan, 2014, pp. 12.
[25] M. Everts, J.P. Meyer, Heat Transfer Characteristics of Developing Flow in the Transistional Flow Regime of a Solar Receiver Tube in: South African Solar Energy Conference SASEC2015, Kruger National Park, South Africa, 2015, pp. 6.
[26] J.P. Meyer, T.J. McKrell, K. Grote, The influence of multi-walled carbon nanotubes on single-phase heat transfer and pressure drop characteristics in the transitional flow regime of smooth tubes, International Journal of Heat and Mass Transfer, 58(1-2) (2013) 597-609.
[27] D.D. Ndenguma, J. Dirker, J.P. Meyer, Heat Transfer and PRessure Drop Characteristics of a Horizontal Annular Passage in the Transitional Flow Regime in, University of Pretoria, South Africa, 2015, pp. 6.
[28] J.A. Olivier, Single-phase heat transfer and pressure drop of water cooled at a constant wall temperature inside horizontal circular smooth and enhanced tubes with different inlet configurations in the transitional flow regime, University of Pretoria, South Africa, 2009.
[29] J.P. Meyer, J.A. Olivier, Transitional flow inside enhanced tubes for fully developed and developing flow with different types of inlet disturbances: Part I – Adiabatic pressure drops, International Journal of Heat and Mass Transfer, 54(7–8) (2011) 1587-1597.
[30] P. Wang, P. McCluskey, A. Bar-Cohen, Hybrid solid-and liquid-cooling solution for isothermalization of insulated gate bipolar transistor power electronic devices, IEEE Transactions on Components, Packaging and Manufacturing Technology, 3(4) (2013) 601-611.
[31] C.Y. Yang, T.Y. Lin, Heat transfer characteristics of water flow in microtubes, Experimental Thermal and Fluid Science, 32(2) (2007) 432-439.
[32] B. Metais, E.R.G. Eckert, Forced, Mixed and Free Convection Regimes, Journal of Heat Transfer, 86(2) (1964) 2.
[33] Y.A. Cengel, A.J. Ghajar, Internal Forced Convection, in: Fundamentals of Heat and Mass Transfer, McGrawHill, New York, 2011, pp. 465-518.
[34] Y.A. Cengel, R.H. Turner, J.M. Cimbala, Fundamentals of Thermal-Fluid Sciences, 3rd ed., McGraw Hill, New York, 2008.
[35] Y.A. Cengel, A.J. Ghajar, Heat and Mass Transfer Fundamentals and Applications, 4th ed., McGrawHill, New York, 2011.
[36] S. Garvey, Forced convection heat transfer in straight tubes Part 2: laminar and transitional flow, ESDU, 2001.
[37] F.M. White, Viscous Fluid Flow, 2nd ed., McGraw-Hill, Singapore, 1991.
[38] F.M. White, Fluid Mechanics, 4th ed., McGraw-Hill, New York, 1999.
[39] L.F. Moody, N. Princeton, Friction Factors for Pipe Flow, Transactions of the A.S.M.E, (1944).
[40] X. Fang, Y. Xu, Z. Zhou, New correlations of single-phase friction factor for turbulent pipe flow and evaluation of existing single-phase friction factor correlations, Nucl Eng Des, 241(3) (2011) 897-902.
[41] R.W. Allen, E.R.G. Eckert, Friction and Heat-Transfer Measurements to Turbulent Pipe Flow of Water (Pr=7 and 8) at Uniform Wall Heat Flux, Journal of Heat Transfer, 86 (1964) 10.
[42] G.L. Morini, M. Lorenzini, S. Salvigni, G.P. Celata, Experimental analysis of microconvective heat transfer in the laminar and transitional regions, Experimental Heat Transfer, 23(1) (2010) 73-93.

[43] G.P. Celata, M. Cumo, V. Marconi, S.J. McPhail, G. Zummo, Microtube liquid single-phase heat transfer in laminar flow, International Journal of Heat and Mass Transfer, 49(19-20) (2006) 3538-3546.
[44] M. Everts, Heat Transfer and Pressure Drop of Developing Flow in Smooth Tubes in the Transitional Flow Regime, Research, University of Pretoria, Pretoria, 2014.
[45] S.M. Morcos, A.E. Bergles, Experimental Investigation of Combine Force and Free Laminar Convection in Horizontal Tubes, Journal of Heat Transfer, 97(2) (1975) 8.
[46] V. Gnielinski, On heat transfer in tubes, International Journal of Heat and Mass Transfer, 63(0) (2013) 134-140.
[47] J.L.M. Poiseuille, Recherches expérimentelles sur le mouvement des liquids dans le tubes de trés petits diamétres, Comptes Rendu, 11 (1840) 7.
[48] A.P. Colburn, A Method of Correlating Forced Convection Heat Transfer Data and a Comparison with Fluid Friction, Transactions of the American Institute of Chemical Engineers, 26 (1933) 33.
[49] F.W. Dittus, L.M.K. Boelter, Heat transfer in automobile radiators of the tubular type, International Communications in Heat and Mass Transfer, 12(1) (1985) 3-22.
[50] E.N. Sieder, G.E. Tate, Heat Transfer and Pressure Drop of Liquids in Tubes, Industrial and Engineering Chemistry 28 (1936) 6.
[51] V. Gnielinski, New equations for heat and mass transfer in turbulent pipe and channel flow, International Chemical Engineering, 16(2) (1976) 9.
[52] H. Blasius, R. Baumann, Das Aehnlichkeitsgesetz bei Reibungsvorgängen in Flüssigkeiten. Versuche über die Elastizität und Festigkeit von Bambus, Akazien-, Eschen- und Hikoryholz / Baumann, Springer, Berlin, 1913.
[53] B.S. Petukhov, Heat Transfer and Friction in Turbulent Pipe Flow with Variable Physical Properties, (1970).
[54] B. Petukhov, A. Polyakov, Flow and heat transfer in horizontal tubes under combined effect of forced and free convection, Heat Transfer NC 3.7 (1970) 11.
[55] G. Maranzana, I. Perry, D. Maillet, Mini- and micro-channels: influence of axial conduction in the walls, International Journal of Heat and Mass Transfer, 47(17–18) (2004) 3993-4004.
[56] E.S. Szalai, F.J. Muzzio, Fundamental Approach to the Design and Optimization of Static Mixers, American Institute of Chemical Engineers. AIChE Journal, 49(11) (2003) 2687-2699.
[57] Z.D. Husain, Theorectical uncertainty of orifice flow measurement, in: Danie Measurement and Control White papers, Emerson Process Management, Houston, 2010.
[58] R.K. Singh, S.N. Singh, V. Seshadri, Performace evaluation of orifice plate assemblies under non-standard conditions using CFD, Indian Journal of Engineering and Material Sciences, 17 (2010) 10.
[59] B.J. McKeon, A.J. Smits, Static pressure correction in high Reynolds number fully developed turbulent pipe flow, Measurement Science and Technology, 13(10) (2002) 1608-1614.
[60] C.O. Popiel, J. Wojtkowiak, Simple formulas for thermophysical properties of liquid water for heat transfer calculations [from O°C to 150°C, Heat Transfer Engineering, 19(3) (1998) 87-101.

Appendix A Tube surface roughness experiments

A.1 Introduction

The purpose of this appendix is to quantify the internal surface roughness of the tube that was described as the test section in Chapter 3. The specimen geometrical properties of the tube are given where after results are given from two different surface roughness measurement techniques (surface roughness measurements tester and profilometer measurements). The results of the two techniques are compared and contextualized with friction factor information from literature.

A.2 Tube properties

The tube which was used to take the surface roughness measurements was made of the same type that was used for the test section. It was a hard drawn copper tube with an average internal diameter, D_i, of 4.04 mm and an outer diameter, D_o, of 5.04 mm. This tube type was sourced from Maksal, a local copper tube manufacturing company. An appropriately sized tube cutter was used to cut the tube. Special care was taken to remove the burs on the tube ends so that this would not influence the inner diameter measurements.

The internal diameter was determined by averaging various measurements taken at the tube inlet and outlet using a transfer gauge and micrometer. The consistency of the inner and outer diameter was verified by taking measurements of other tubes from the same manufacturing batch of tubes.

Maksal normally produce tubes at a maximum length of 5.5 m, however, for the purposes of this study, a special order was manufactured to a length of 9.5 m. A total of five tubes were obtained from this batch. Shorter tube lengths of 20 mm, which were cut from another tube in the same batch, was used for the surface roughness measurement experiments.

A.3 Surface roughness measurements

Two methods were used to determine the surface roughness measurements. The first was done with a surface roughness tester and the seconds with a profilometer. Each method is discussed separately, where after the results are compared.

a. Surface roughness tester technique

Surface roughness measurements were conducted by an independent laboratory (SGS MetLab in Boksburg, South Africa). The tubes were prepared by the laboratory by sectioning the tubes axially and mounting the half sections of tube in a plastic specimen block to ensure that the tube section was level.

A surface roughness tester with a standard inductive pickup, consisting of a diamond stylus with a diameter of 10 µm and a tip angle of $90°$ was used to take the measurements. Testing was done in accordance with the ASME Y14.36M-1996 and EN 4287 standards [A1], and the expected inaccuracies of the results were ±10%.

A total of six repeatable results were reported by the laboratory [A1]. The average internal roughness, ε, of the results was measured as 0.0987 µm and the resulting relative surface roughness ε/D_i, of the tube was therefore obtained as 2.5×10^{-5}.

b. Profilometer

Measurements were taken at the Physics Department at the University of Pretoria with a profilometer. Four samples of the tube were prepared by sectioning pieces of the tube along its axis. These tube sections were then each levelled and secured on the test stage of the profilometer where a diamond-tipped stylus with a diameter of 12.5 µm measured the surface roughness to an inaccuracy of ±5 nm [A2]. The test was conducted four times per sample to ensure repeatability was obtained.

The average internal surface roughness (ε) was measured to be 0.0461 µm and from this measurement the tube relative surface roughness, ε/D_i, was obtained as 1.16×10^{-5}. As the surface roughness could be measured to an inaccuracy of ±5 nm, the inaccuracy of this measurement was a maximum of approximately 10%.

A.4 Comparison of results

According to the surface roughness testing method, the tube relative surface roughness was obtained as $\varepsilon/D_i = 2.5 \times 10^{-5}$, while as an $\varepsilon/D_i = 1.16 \times 10^{-5}$ was obtained with the profilometer. The inaccuracies of both methods are ±10%. However, the two surface roughness measurements were not within ± 10 % of each other which was expected. The result differed with approximately 50-100%, depending on which measurement is the most accurate.

What is consistent is that both measurement techniques gave relative surface roughness measurement values in the order of 10^{-5}. Furthermore, it is also important to emphasise that the operators of the equipment of both laboratories considered the surface measurements as extremely challenging as the “smoothness” exceeded the limits of previous work conducted.

A.5 Friction factor information from literature

In Table 1, the friction factors for a smooth tube ($\varepsilon/D_i = 0$), as a function of Reynolds numbers, is compared to the friction factors obtained of the two methods that were used to measure the tube relative surface roughness. The friction factors were calculated with the Colebrook equation (Eq. A-1) [A3], which gives the friction factor as a function of Reynolds number and relative surface roughness.

$$\frac{1}{\sqrt{f}} = -2log_{10}\left(\frac{\varepsilon/d_i}{3.7} + \frac{2.51}{Re\sqrt{f}}\right) \quad \text{(A-1)}$$

The equation is valid for both smooth and rough tubes. The comparison was made for Reynolds numbers of 2 300 to 10 000. Comparisons were also made at the maximum expected Reynolds numbers of 10 000 and beyond, up to a Reynolds number of 50 000.

The results showed that at a Reynolds number of 2 300, the friction factor of a smooth tube according to the Colebrook equation is 0.04849. Using the same equation, the friction factors from the surface roughness tester and profilometer measurements are both 0.04850. The friction factors are therefore within 0.02%. If the same type of comparison is made at a Reynolds number of 50 000, the friction factor for the smooth tube is 0.02071 and the friction factors obtained from the surface roughness tester and profilomter are 0.02077 and 0.02074 respectively. The maximum error in this case is 0.3%.

It is therefore concluded that the friction factors that was obtained from the two surface measurement techniques both confirmed that the relative surface roughness values are so small that their friction factors are similar to that of a smooth tube.

Table A.1 - Comparison of friction factor results

Reynolds number	**Friction factor with smooth tube, $\varepsilon/D = 0$**	**Friction factor with surface roughness tester, $\varepsilon/D = 2.5 \times 10^{-5}$**	**Friction factor with profilometer, $\varepsilon/D = 1.16 \times 10^{-5}$**
2 300	0.04849	0.04850	0.04850
8 000	0.03287	0.03289	0.03288
10 000	0.03089	0.03091	0.03090
50 000	0.02071	0.02077	0.02074

A.6 Summary and conclusion

The surface roughness of the tube that was used for the experimental set-up was measured with two different methods and in two different laboratories. The one measurement method was with a surface roughness tester and the other with a profilometer. The two measurements were compared and the results did not compare well. However both testing methods verified that the relative surface roughness is in the order of 10^{-5}.

Using the two relative surface roughness values, the friction factors were obtained from literature within the range of expected Reynolds numbers for this study. Both values confirmed that the friction factors were similar to that of a smooth tube. It can therefore be assumed that for the purposes of this study, that the test section is a smooth tube.

A.7 References

[A1] I. Greenhorn, Copper Tubing, in: N. Kotze (Ed.), 2014.
[A2] Tencor, Tencor Alphastep 200 Automatic Step Profiler, in, Tencor, pp. User Manual.
[A3] Y.A. Cengel, A.J. Ghajar, Heat and Mass Transfer Fundamentals and Applications, 4th ed., McGrawHill, New York, 2011.

Appendix B Thermocouple calibration

B.1 Introduction

The thermocouples were calibrated to improve the accuracy of the measurements. The purpose of this appendix is to discuss the calibration technique used.

B.2 Calibration procedure

Each thermocouple used on the experimental set-up was constructed by cutting the OMEGA T- type thermocouple wire to length and soldering the exposed point on the one end together. The thermocouple wire has an accuracy of ±0.5°C when used in this state, which can be improved to as much as 0.1°C if calibrated.

In the past [B1], calibration factors were derived by placing these thermocouples in a temperature controlled thermal bath with a calibrated PT100 probe. The temperature of the bath would be varied and an overall calibration factor for each thermocouple would be derived. The thermocouples would then be attached to the tube using heat.

During this study, it was found that the properties of the thermocouples changed once the thermocouples were attached to the tube. This was expected as the heat application at the thermocouple junction to the test section changes the thermal properties of the thermocouple tip. However, the magnitude of the change in the accuracy of the thermocouple was expected to be negligible and a ±0.1°C accuracy was still expected. This was not the case and accuracy bands of ±0.5°C was observed during trial isothermal test runs.

In order to improve the accuracy of the thermocouples and their associated calibration factors, a new in-situ calibration procedure was derived. This involved placing Ultra Precise Immersion RTD PT100 probes ($^{1}/_{10}$ DIN) on the inlet and outlet of the test section. The PT100 probes were calibrated in the thermal bath to an accuracy of 0.1°C using a LAUDA ECO RE 1225 thermal bath and a secondary PT100 probe that was calibrated and validated by an independent testing facility.

The test section was connected to a temperature controlled geyser and water from the geyser was passed through the test section. The temperature of the geyser was varied between 19°C and 54°C. Once a steady state condition where both the inlet and outlet PT100 probe read within 0.05°C of each other, a measurement was taken and the average of the PT100 probes was recorded.

The thermocouple measurement consisted of 100 data points which was averaged to a single value per thermocouple, per temperature interval. A MATLAB POLYFIT function was then applied to the data which compares the average thermocouple measurement to the recorded PT100 value by forcing the thermocouple data to match the linear PT100 value. The calibrated thermocouple value, T_{cal} was calculated using Eq. B-1.

$$T_{cal} = T_{raw} \times c_1 + c_2 \quad \text{(B-1)}$$

where T_{raw} is the uncalibrated temperature and c_1 and c_2 is the calibration factors.

B.3 Calibration factors

The thermocouple calibration factors can be found in Table B.1.

Table B.1 - Thermocouple calibration data

	c_1	c_2		c_1	c_2		c_1	c_2
A1	1.00227	-0.48956	G2	1.01013	-0.98057	M3	1.0103	-0.72494
A2	1.00314	-0.66926	G3	1.00724	-0.95704	N1	1.01197	-1.07027
A3	1.00332	-0.52659	H1	1.00929	-1.16164	N2	1.0142	-1.29934
B1	1.00401	-0.55048	H2	1.00784	-1.25416	N3	1.01145	-1.06538
B2	1.00428	-0.5933	H3	0.341547	480.98	O1	1.0114	-1.08519
B3	1.00166	-0.51922	I1	18.3289	-4579.71	O2	1.0101	-1.06979
C1	1.00622	-0.58539	I2	1.01057	-0.85154	O3	1.01108	-1.27454
C2	1.0071	-1.03099	I3	1.00825	-0.73655	P1	1.0146	-1.37917
C3	1.00461	-0.94046	J1	1.01263	-0.85147	P2	1.01337	-1.18823
D1	1.00673	-1.12385	J2	1.00748	-0.80981	P3	1.01425	-1.46371
D2	1.00513	-1.10583	J3	1.00795	-0.90349	Q1	1.01829	-1.36678
D3	1.00644	-0.98673	K1	1.02141	-1.12859	Q2	1.01249	-1.24341
E1	1.00891	-1.0192	K2	1.01062	-0.80913	Q3	1.01418	-1.55998
E2	1.00498	-0.65327	K3	1.01321	-0.98489	R1	1.02002	-1.4641
E3	1.0059	-1.1142	L1	1.01111	-0.72611	R2	1.01515	-1.63979
F1	1.00851	-0.71822	L2	1.00859	-0.66177	R3	1.01439	-1.61136
F2	1.00551	-0.95095	L3	1.0076	-0.46449	S1	1.01001	-0.49048
F3	1.0087	-1.03476	M1	1.01323	-0.86451	S2	1.01257	-0.84263
G1	1.00915	-1.14444	M2	1.00885	-0.60857	S3	1.05728	-2.33279

B.4 Calibration results

An example of the uncalibrated temperature profile and calibrated temperature profile for thermocouple F1 can be seen in Fig. B.1.

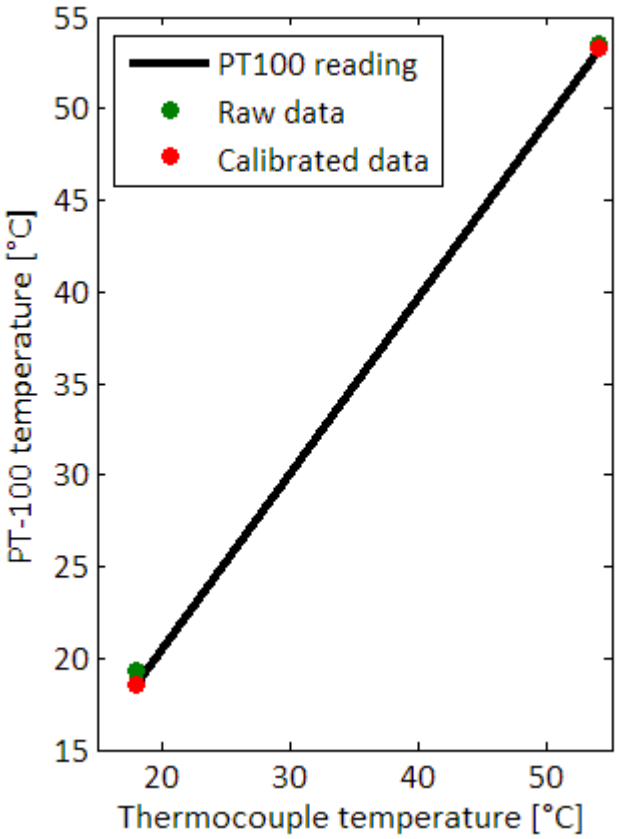

Fig. B.1 - Graphical representation of the data in its raw form and calibrated form

It is clear that the linear calibration factor forces the raw, uncalibrated data to match the PT100 results.

After calibration was completed, the accuracy of the calibration factors was tested by running fluid at varying constant temperatures through the test section. Three different isothermal results can be seen in Fig. B.2, Fig. B.3 and Fig. B.4 for PT100 readings of 25.08°C, 36.95°C and 46.02°C respectively. All thermocouple measurements along the test section can been seen in these figures.

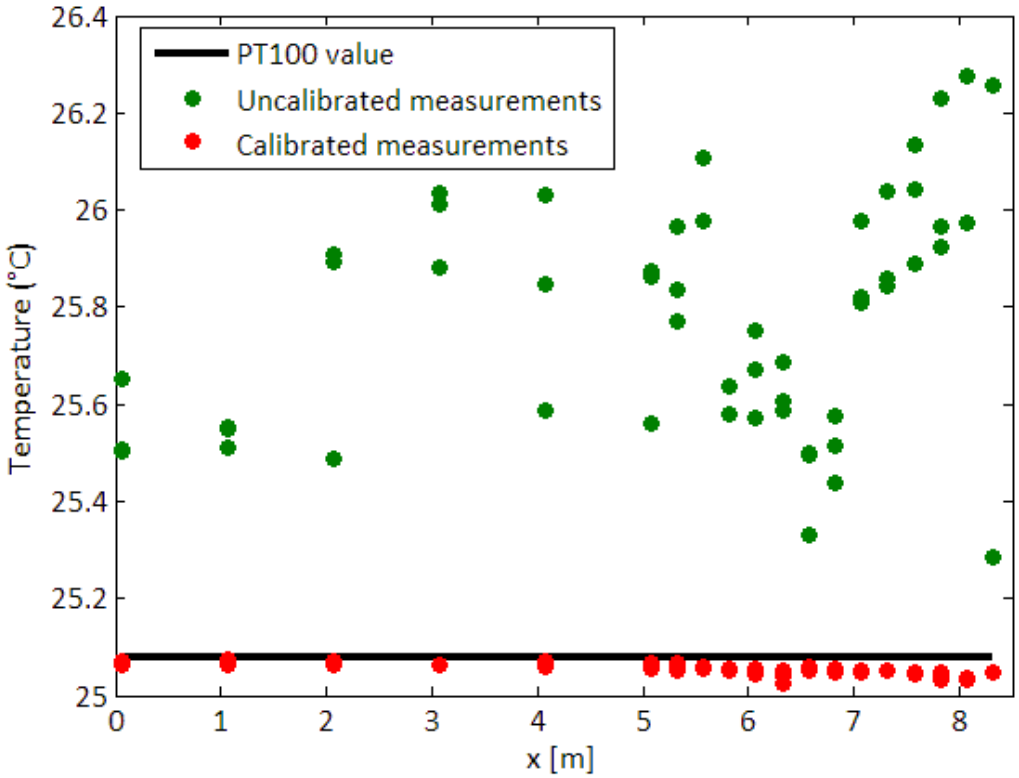

Fig. B.2 - Graphical representation of the calibrated and uncalibrated temperature measurements along the length of the test section for a PT100 reading of 25.08°C

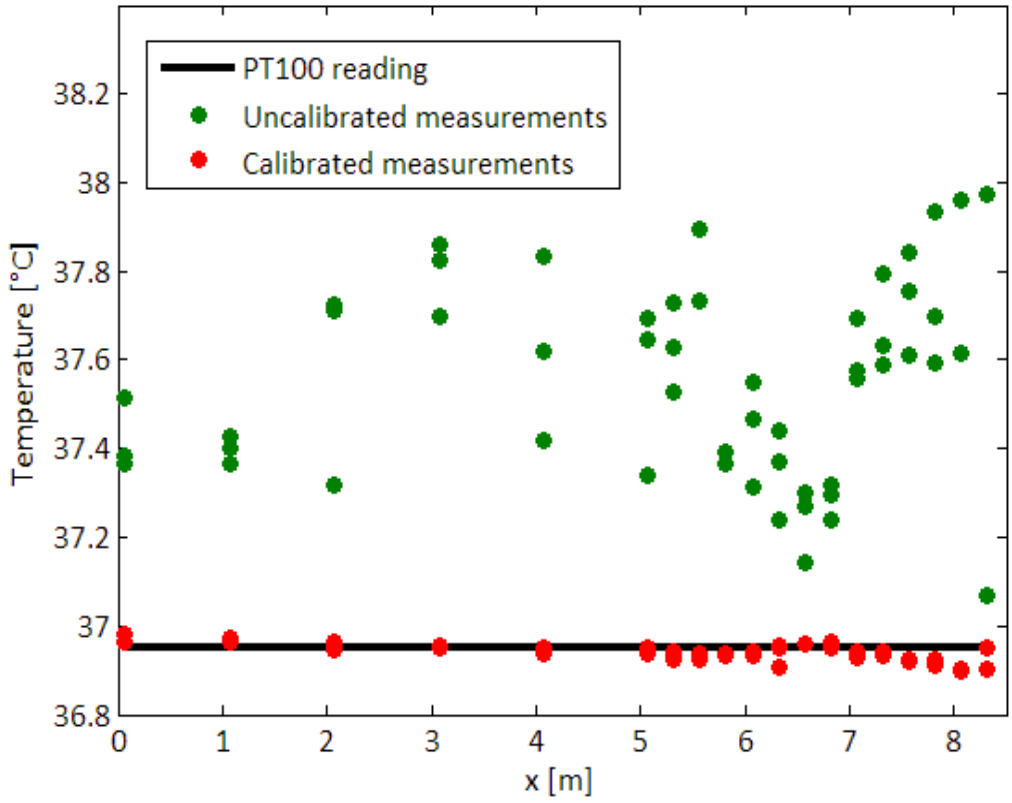

Fig. B.3 - Graphical representation of the calibrated and uncalibrated temperature measurements along the length of the test section for a PT100 reading of 36.95°C

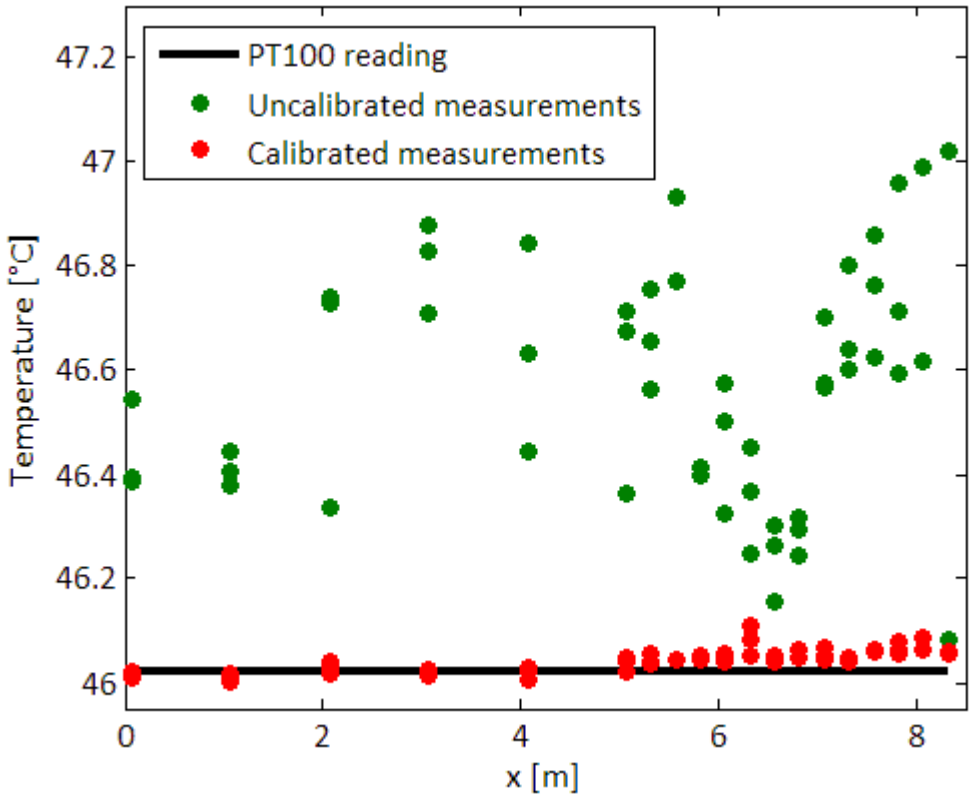

Fig. B.4 - Graphical representation of the calibrated and uncalibrated temperature measurements along the length of the test section for a PT100 reading of 46.02°C

In all instances, the uncalibrated measurements have a wide scatter of at least 1°C. Once the calibration factors have been applied, the accuracy band of the thermocouples is drastically reduced to less than 0.1°C and in all instances, the calibrated thermocouple results are within 0.1°C of the PT100 probe reading.

B.5 Conclusion

The thermocouple calibration procedure used during the study has been described. The procedure was modified to maximise the accuracy of the thermocouples. Raw data was compared to laboratory validated instruments and calibration factors have been derived. These calibration factors have been applied to uncalibrated measurements and the calibrated results have been compared to PT100 temperature readings. The calibrated measurements show very good agreement with the PT100 readings and remain within 0.1°C of the PT100 reading during varying isothermal conditions.

B.6 References

[B1] J.A. Olivier, Single-phase heat transfer and pressure drop of water cooled at a constant wall temperature inside horizontal circular smooth and enhanced tubes with different inlet configurations in the transitional flow regime, University of Pretoria, South Africa, 2009.

Appendix C Pressure transducer calibration

C.1 Introduction

The purpose of this appendix is to discuss pressure transducer calibration. It describes the pressure transducer, the calibration procedure and results of the pressure transducer calibration.

C.2 Pressure transducer

Two Validyne multiple range differential pressure transducers was used during the study. These transducers are specifically designed to allow for interchangeability of different size pressure diaphragms. Consequently, the transducer can measure differential pressures as low as 0.55 kPa or as high as 22 000 kPa, dependent on the diaphragm been used.

It is therefore very important that the transducer/diaphragm assembly is calibrated before any measurements can be taken. The accuracy of the transducer/assembly is a function of the full-scale pressure of the diaphragm, where the accuracy is ±0.25% of the full-scale value associated to the diaphragm.

Two transducers were used, namely a -32 or 14 kPa diaphragm and a -38 or 55 kPa diaphragm. The size of the diaphragms was specifically selected to allow for maximum accuracy over the full range of tests used during the study.

C.3 Calibration procedure

Before calibration could be started, the diaphragm was inserted into transducer in accordance with the manufacturer requirements. The body bolts were then torqued to prevent any leaks on the body and prevent incorrect measurements.

Each pressure diaphragm was calibrated using a static water column and a digital manometer. The manometer, with an accuracy of 10 Pa, the water column and the transducer were all exposed to the same pressure due to the configuration of the hydraulic tubing. It is important to note that all tubing as well as the transducer was bled to ensure that any trapped air within the system was released. The transducer was also wired to the data acquisition unit to capture all current measurements. This is shown schematically in Fig. C.1.

The zero and span for the transducer/diaphragm assembly was set. Once this action was concluded, water was introduced into the positive column in small volumes and the values measured by the transducer was logged. The manometer reading was also recorded at these intervals. The water was drained from the column in small volumes as well, thus measurements were logged for an increasing pressure and decreasing pressure situation.

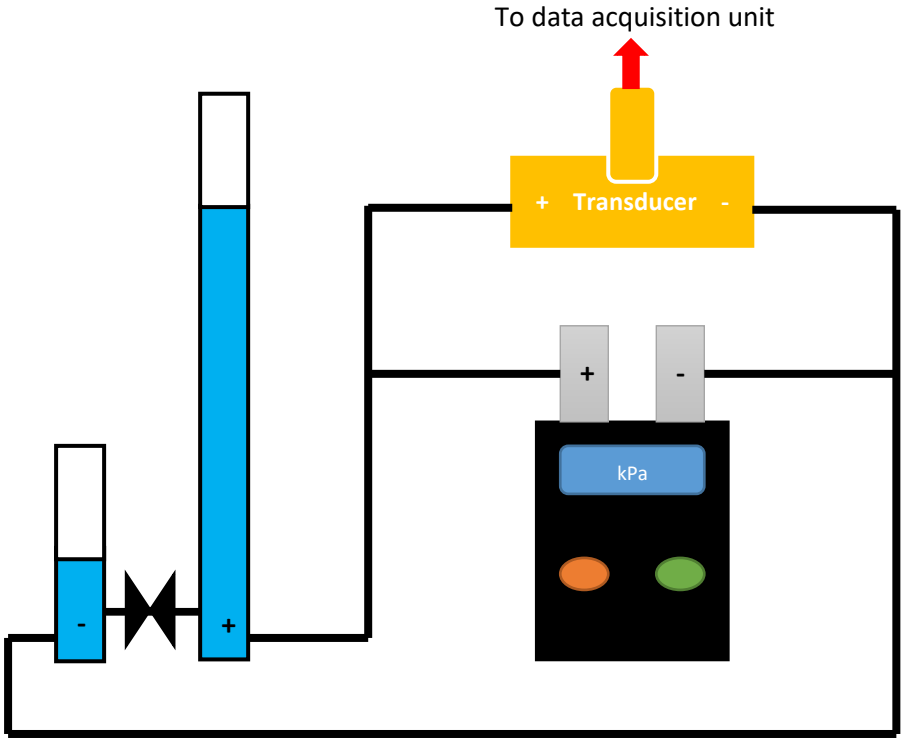

Fig. C.1 - Schematic representation of pressure calibration

C.4 Calibration factor and results

A total of 100 data points per pressure interval was logged. This was averaged to a single value for each pressure interval. A MATLAB POLYFIT function was then applied to the data which compared the average pressure measurement to the recorded manometer value by forcing the pressure data to match the linear manometer value. The calibrated factor, P_{cal} was calculated using Eq. C-1.

$$P_{cal} = P_{raw} \times c_1 + P_{raw} \times c_2 + P_{raw} \times c_3 + c_4 \quad \text{(C-1)}$$

where P_{raw} is the uncalibrated pressure current measurement and c_1, c_2, c_3 and c_4 are the calibration factors which convert the current measurement into a pressure measurement.

The calibrated transducer data as compared to the manometer reading is shown in Fig. C.2 and Fig. C.3 for the 14 kPa and 55 kPa diaphragms respectively. It is clear in both figures that the calibrated results match the manometer readings.

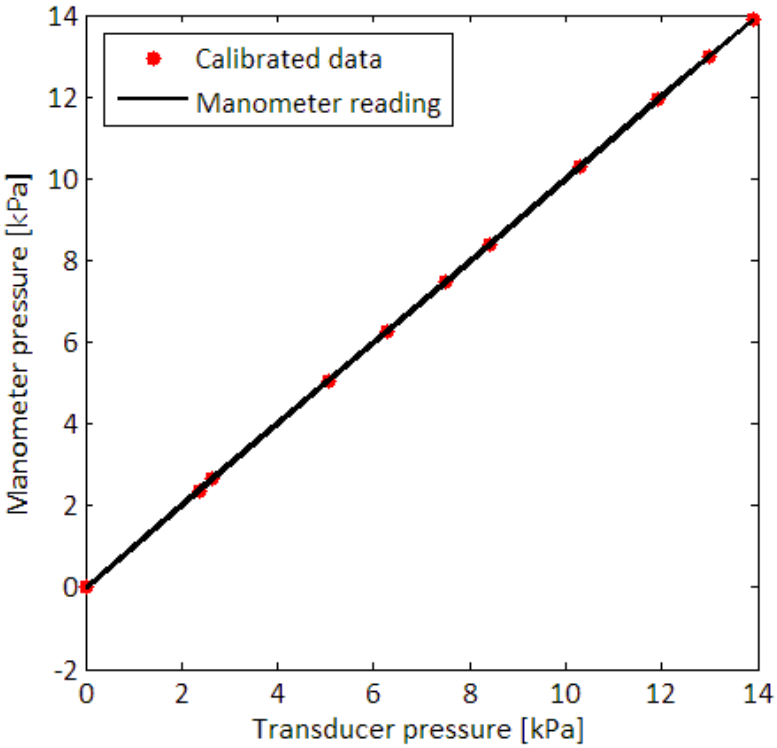

Fig. C.2 - Calibration points and manometer readings for the 14 kPa diaphragm

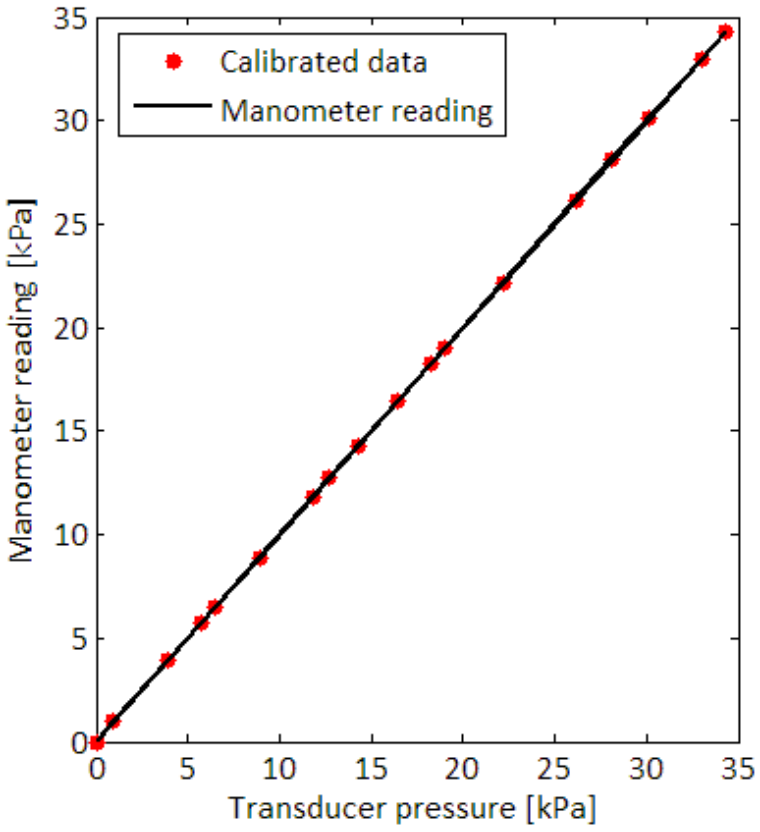

Fig. C.2 - Calibration points and manometer readings for the 55 kPa diaphragm

The calibration factors for both diaphragms can be found in Table C.1.

Table C.1 - Calibration factors for the pressure diaphragms

	c_1	c_2	c_3	c_4
14 kPa diaphragm	103380	-2932.7	894.673	-3.54951
55 kPa diaphragm	1.14E+06	-24073.9	3558.91	-13.9

C.5 Daily offset

Due to the nature of the environment, there is constant fluctuation in the ambient pressure. As a result, it was necessary to take a "zero" pressure measurement, namely where the test section was filled with water and all air had been bled out of the system. This was done on a daily basis and the "zero" measurement, which was a current measurement, was recorded. These current measurements were then offset against the test measurements before the calibration factor was applied.

C.6 Conclusion

The pressure transducer calibration procedure was described in this appendix. A manometer with an accuracy of 10 Pa was used to calibrate the pressure transducer/diaphragm assembly. This resulted in a linear curve fit whereby the relationship between the pressure measurements and the current measurements is clearly defined.

Appendix D Uncertainty analysis

D.1 Introduction

The purpose of this appendix is to describe the uncertainty analysis that was used to determine the accuracy of the final results. Each instrument has a predefined accuracy. However, when multiple measurements are combined determine results such as heat transfer coefficients or friction factors, the sum total of these inaccuracies can lead to high uncertainties. The uncertainty analysis was conducted for these parameters as well as some non-dimensional parameters that are relevant to this study such as the Reynolds number, Nusselt number and Colburn j_H-factor.

D.2 Analysis method

In general, two specific components are analysed when considering the uncertainty of a measurement, name a random error or the precision (P) and the fixed error or the bias (B) [D1]. The precision error refers to the variation that is present during testing. These errors are always present and are mainly due to electrical noise and changes during the testing process. The bias error is defined as a predetermined offset that is defined and repeatable.

The uncertainty for a single point measurements, δx_i, is defined in Eq. D-1:

$$\delta x_i = \sqrt{B_i^2 + P_i^2} \tag{D-1}$$

where x_i is the single observation variable.

Consider that an equation R may be a function of several variables or observation points, where [D1]:

$$R = R(x_1, x_2, x_3, \dots, x_n) \tag{D-2}$$

If the uncertainties of the single point variables is known, the uncertainty in the equation can be determined by [D1]:

$$\delta R = \frac{\partial R}{\partial x_i} \delta x_i \tag{D-3}$$

where the partial derivative of R, δR is called the sensitivity coefficient and defines the effect that the uncertainty of a single measurement has on the overall uncertainty of a result.

In the instance where several independent variables are to be considered, the uncertainty of R is determined by employing the root sum squared method as shown in Eq. D-4 [D1]:

$$\delta R = \sqrt{\left(\frac{\partial R}{\partial x_1}\right)^2 \delta x_1 + \left(\frac{\partial R}{\partial x_2}\right)^2 \delta x_2 + \left(\frac{\partial R}{\partial x_3}\right)^2 \delta x_3 + \cdots + \left(\frac{\partial R}{\partial x_n}\right)^2 \delta x_n} \quad \text{(D-4)}$$

D.3 Water properties

The water properties are calculated using the equation described by Popeil and Wojtkowiak [D2]. During the course of their study, they determined the specific uncertainties associated to their equations. These are given in Table D.1.

Table D.1 - Calibration factors for the pressure diaphragms

	$\boldsymbol{\rho}$ $[\boldsymbol{kg/m^3}]$	$\boldsymbol{\beta}$ $[-]$	$\boldsymbol{C_p}$ $[\boldsymbol{J/kg \cdot K}]$	$\boldsymbol{k}$ $[\boldsymbol{W/m \cdot K}]$	$\boldsymbol{\mu}$ $[\boldsymbol{kg/m \cdot s}]$	$\boldsymbol{Pr}$ $[-]$
Uncertainty	0.004%	0.5%	0.04%	2%	1%	2.3%

D.4 Instruments

D.4.1 PT100 probe

The prescribed manufacturer accuracy or bias of the PT100 probe is 0.055°C. The precision error of the data acquisition unit used during the calibration process is 0.06°C. Using Eq. D-1, the uncertainty of the PT100 was calculated to be 0.0814°C.

D.4.2 Thermocouples

Each thermocouple was calibrated using in-situ calibration methods as discussed in Appendix B. As the PT100 probe was used as the point of reference for the calibration calculations, its uncertainty of 0.0814°C is defined as the bias for each thermocouple.

The precision of each thermocouple varies based on the conditions under which the measurements were obtained. The standard deviation (confidence interval of 95%) of the measurements was taken and used as the precision error.

Using Eq. D-1, the uncertainty of the thermocouple measurements varied between 0.081°C and 0.083°C.

D.4.3 Pressure transducers

Both pressure transducers were calibrated as discussed in Appendix C. The bias of the transducer/diaphragm assembly is 0.25% of the full-scale value of the diaphragm. The precision error of the manometer is 10 Pa. Using Eq. D-1, the uncertainty of the 14 kPa

transducer/diaphragm was calculated to be 36.4 Pa. Similarly, the uncertainty of the 55 kPa transducer/diaphragm was calculated to be 137.9 Pa.

The pressure measurements precision error was based on the standard deviation of the pressure measurements. Using Eq. D-1, the uncertainty of the 14 kPa transducer/diaphragm measurements varied between 36.1 Pa and 36.8Pa. Similarly, the uncertainty of the 55 kPa transducer/diaphragm measurements varied between 137.6 Pa and 138.2 Pa.

D.4.4 Flow meters

Due to the wide range of flow rates used for the duration of the study, two Coriolis flow meters were used. The smaller of the two flow meters was specified to operate in a range from 5 l/hr up to 108 l/hr. The bias of the flow meters is 0.05% of the full-scale value of the flow meter, therefore an accuracy of 0.054 l/hr was used. The larger flow meter had an operation range of 54 l/hr up to 2 180 l/hr with an accuracy of 1.09 l/hr.

D.4.5 Power supply

One power supply was used during the study for heating purposes. The accuracy of the PS 8000 2U is 0.2% of the nominal rated voltage and current values of 360 V and 15 A respectively.

The accuracies of the power supply were fixed at 0.72 V and 0.03 A.

D.4.6 Length measurements

A measuring tape with an accuracy of 2 mm was used to take length measurements.

D.4.7 Internal diameter of the test section

The internal diameter was determined by averaging various measurements taken at the tube inlet and outlet using a transfer gauge and micrometer. The accuracy of the instrument is 20 µm.

D.4.8 Outer diameter of the test section

The outer diameter was measured using a calliper. The accuracy of the instrument was 20 µm.

D.5 Analysis

D.5.1 Average temperatures

Each thermocouple station consisted of three thermocouples. An average surface temperature, $\overline{T_s}$, for each thermocouple station was determined by Eq. D-5:

$$\overline{T_s} = \frac{T_{top} + T_{left/right} + T_{bottom}}{3} \tag{D-5}$$

The uncertainty for this average temperature was calculated using Eq. D-6:

$$\delta\overline{T_s} = \sqrt{\left(\frac{\delta T_{top}}{3}\right)^2 + \left(\frac{\delta T_{left/right}}{3}\right)^2 + \left(\frac{\delta T_{bottom}}{3}\right)^2} \tag{D-6}$$

D.5.2 Cross-sectional area of test section

The cross-sectional area of the test section tube was calculated as:

$$A_c = \frac{\pi}{4} D_i^2 \tag{D-7}$$

The associated uncertainty is:

$$\delta A_c = \sqrt{\left(\frac{\partial A_c}{\partial D_i}\delta D_i\right)^2}$$

$$\delta A_c = \frac{\pi D_i}{2}\delta D_i$$

$$\delta A_c = 1.27 \times 10^{-7} m^2 \tag{D-8}$$

D.5.3 Heat transfer area

The heat area of the tube is calculated as:

$$A_s = \pi D_i L_{heated} \tag{D-9}$$

The uncertainty associated to the heat transfer area is shown in Eq. D-10:

$$\delta A_s = \sqrt{\left(\frac{\partial A_s}{\partial D_i}\delta D_i\right)^2 + \left(\frac{\partial A_s}{\partial L_{heated}}\delta L_{heated}\right)^2}$$

$$\delta A_s = \sqrt{(\pi L_{heated}\delta D_i)^2 + (\pi D_i \delta L_{heated})^2}$$

$$\delta A_s = \sqrt{(\pi \times 8.314 \times 0.00002)^2 + (\pi \times 0.00404 \times 0.002)^2}$$

$$\delta A_s = 0.000523\ mm \quad \text{(D-10)}$$

D.5.4 Electrical power input

The Electrical power input into the system was calculated as follows:

$$E_p = V \times I \quad \text{(D-11)}$$

The uncertainty of Eq. D-11 is shown in Eq. D-12:

$$\delta E_p = \sqrt{\left(\frac{\partial E_p}{\partial V}\delta V\right)^2 + \left(\frac{\partial E_p}{\partial I}\delta I\right)^2}$$

$$\delta E_p = \sqrt{(I\delta V)^2 + (V\delta I)^2}$$

$$\delta E_p = \sqrt{(0.72I)^2 + (0.03V)^2} \quad \text{(D-12)}$$

D.5.5 Heat input into the water

The heat input into the water is defined as:

$$\dot{Q}_{water} = \dot{m}C_p(T_e - T_i) \quad \text{(D-13)}$$

The associated uncertainty of Eq. D-13 is shown in Eq. D-16:

$$\delta\dot{Q}_{water} = \sqrt{\left(\frac{\partial \dot{Q}_{water}}{\partial \dot{m}}\delta\dot{m}\right)^2 + \left(\frac{\partial \dot{Q}_{water}}{\partial C_p}\delta C_p\right)^2 + \left(\frac{\partial \dot{Q}_{water}}{\partial T_e}\delta T_e\right)^2 + \left(\frac{\partial \dot{Q}_{water}}{\partial T_i}\delta T_i\right)^2}$$

$$\delta\dot{Q}_{water} = \sqrt{\left(C_p(T_e - T_i)\delta\dot{m}\right)^2 + \left(\dot{m}(T_e - T_i)\delta C_p\right)^2} \quad \text{(D-14)}$$

D.5.6 Heat flux

Eq. D-15 describes how heat flux was calculated:

$$\dot{q} = \frac{\dot{Q}_{water}}{A_s} \tag{D-15}$$

The uncertainty of the heat flux was determined by:

$$\delta\dot{q} = \sqrt{\left(\frac{\partial\dot{q}}{\partial\dot{Q}_{water}}\delta\dot{Q}_{water}\right)^2 + \left(\frac{\partial\dot{q}}{\partial A_s}\delta A_s\right)^2}$$

$$\delta\dot{q} = \sqrt{\left(\frac{1}{A_s}\delta\dot{Q}_{water}\right)^2 + \left(-\frac{\dot{Q}_{water}}{A_s^2}\delta A_s\right)^2} \tag{D-16}$$

D.5.7 Heat transfer coefficient

The heat transfer coefficient was determined by:

$$h = \frac{\dot{q}}{T_s - T_m} \tag{D-17}$$

Eq. D-18 describes the uncertainty of the heat transfer coefficient:

$$\delta h = \sqrt{\left(\frac{\partial h}{\partial\dot{q}}\delta\dot{q}\right)^2 + \left(\frac{\partial h}{\partial T_s}\delta T_s\right)^2 + \left(\frac{\partial h}{\partial T_m}\delta T_m\right)^2}$$

$$\delta h = \sqrt{\left(\frac{1}{T_s - T_m}\delta\dot{q}\right)^2 + \left(-\frac{\dot{q}}{(T_s - T_m)^2}\delta T_s\right)^2 + \left(\frac{\dot{q}}{(T_s - T_m)^2}\delta T_m\right)^2} \tag{D-18}$$

D.5.8 Friction factor

The friction factor was calculated by:

$$f = \frac{\pi^2 \Delta P D_i^5 \rho}{8\dot{m}^2 L_{PD}} \tag{D-19}$$

The uncertainty of the friction factor is shown in Eq. D-20:

$$\delta f = \sqrt{\left(\frac{\partial f}{\partial \Delta P}\delta \Delta P\right)^2 + \left(\frac{\partial f}{\partial D_i}\delta D_i\right)^2 + \left(\frac{\partial f}{\partial \rho}\delta \rho\right)^2 + \left(\frac{\partial f}{\partial \dot{m}}\delta \dot{m}\right)^2 + \left(\frac{\partial f}{\partial L_{PD}}\delta L_{PD}\right)^2}$$

$$\delta f = \sqrt{\begin{matrix}\left(\frac{\pi^2 D_i^5 \rho}{8\dot{m}^2 L_{PD}}\delta \Delta P\right)^2 + \left(\frac{5\pi^2 D_i^4 \rho}{8\dot{m}^2 L_{PD}}\delta D_i\right)^2 + \left(\frac{\pi^2 D_i^5}{8\dot{m}^2 L_{PD}}\delta \rho\right)^2 + \left(-\frac{\pi^2 D_i^5}{\dot{m}^3 L_{PD}}\delta \dot{m}\right)^2 \\ + \left(-\frac{\pi^2 D_i^5}{8\dot{m}^2 {L_{PD}}^2}\delta L_{PD}\right)^2\end{matrix}} \quad \text{(D-20)}$$

D.5.9 Reynolds number

The Reynolds number was determined by:

$$Re = \frac{\dot{m} D_i}{\mu A_c} \quad \text{(D-21)}$$

Using Eq. D-21, the uncertainty of the Reynolds number can be described as shown in Eq. D-22:

$$\delta Re = \sqrt{\left(\frac{\partial Re}{\partial \dot{m}}\delta \dot{m}\right)^2 + \left(\frac{\partial Re}{\partial D_i}\delta D_i\right)^2 + \left(\frac{\partial Re}{\partial \mu}\delta \mu\right)^2 + \left(\frac{\partial Re}{\partial A_c}\delta A_c\right)^2}$$

$$\delta Re = \sqrt{\left(\frac{D_i}{\mu A_c}\delta \dot{m}\right)^2 + \left(\frac{\dot{m}}{\mu A_c}\delta D_i\right)^2 + \left(-\frac{\dot{m} D_i}{\mu^2 A_c}\delta \mu\right)^2 + \left(-\frac{\dot{m} D_i}{\mu A_c^2}\delta A_c\right)^2} \quad \text{(D-22)}$$

D.5.10 Nusselt number

The Nusselt number was determined by:

$$Nu = \frac{h D_i}{k} \quad \text{(D-23)}$$

Eq. D-24 describes the uncertainty of the Nusselt number:

$$\delta Nu = \sqrt{\left(\frac{\partial Nu}{\partial h}\delta h\right)^2 + \left(\frac{\partial Nu}{\partial D_i}\delta D_i\right)^2 + \left(\frac{\partial Nu}{\partial k}\delta k\right)^2}$$

$$\delta Nu = \sqrt{\left(\frac{D_i}{k}\delta h\right)^2 + \left(\frac{h}{k}\delta D_i\right)^2 + \left(-\frac{h D_i}{k^2}\delta k\right)^2} \quad \text{(D-24)}$$

D.5.11 Colburn j-factor

Eq. D-25 describes the calculation of the Colburn j_H-factor:

$$j_H = \frac{Nu}{RePr^{1/3}} \tag{D-25}$$

The uncertainty of the Colburn j_H-factor was determined by:

$$\delta j_H = \sqrt{\left(\frac{\partial j_H}{\partial Nu}\delta Nu\right)^2 + \left(\frac{\partial j_H}{\partial Re}\delta Re\right)^2 + \left(\frac{\partial j_H}{\partial Pr}\delta Pr\right)^2}$$

$$\delta j_H = \sqrt{\left(\frac{1}{RePr^{1/3}}\delta Nu\right)^2 + \left(-\frac{Nu}{Re^2Pr^{1/3}}\delta Re\right)^2 + \left(-\frac{Nu}{3RePr^{4/3}}\delta Pr\right)^2} \tag{D-26}$$

D.6 Summary

The mass flow rate of the water through the test section as well as the electrical heat input into the system had distinct impact on the uncertainty of the results. The associated uncertainties at low Reynolds numbers (± 1 000) and low heat input (100 W) is shown in Table D.2. Please note that local results are shown for thermocouple station F which is located closest to the centre of the test section.

Table D.2 - Uncertainties of the equations used to determine the results of this study at low Reynolds numbers and low electrical heat input. Local results are described at thermocouple station F.

Result	Uncertainty
$\overline{T_{s,F}}$	0.19%
E_p	2.3%
$\dot{Q}_{water}$	1.69%
$\dot{q}$	1.75%
h_F	6.85%
f	6.53%
$\overline{Re}$	1.56%
Re_F	1.56%
$\overline{Nu}$	7.55%
Nu_F	6.85%
$\bar{J}_H$	17.86%
$j_{H,F}$	16.51%

All uncertainties shown in Table D.2 are below 10% besides the Colburn j_H-factor which is at 17%. This is expected as the while the heat flux is very low, the mass flow rate is also very low. As a result, the temperature difference between the tube surface and the centre of the tube is bigger than the measurement accuracy of the thermocouples.

The converse is true for very high mass flow rates. The temperature difference between the tube surface and the centre of the tube is very small and encroaches on the measurement accuracy of the thermocouples. As a result, the heat transfer coefficient and Nusselt number uncertainties are high. The associated uncertainties at high Reynolds numbers (± 10 000) and a higher heat input (342 W) is shown in Table D.3. Please note that local results are shown for thermocouple station F which is located closest to the centre of the test section.

Table D.3 - Uncertainties of the equations used to determine the results of this study at high Reynolds numbers and high electrical heat input. Local results are described at thermocouple station F

Result	Uncertainty
$\overline{T_{s,F}}$	0.21%
E_p	1.24%
$\dot{Q}_{water}$	4.29%
$\dot{q}$	4.32%
h_F	39.38%
f	4.94%
$\overline{Re}$	1.81%
Re_F	1.81%
$\overline{Nu}$	29.91%
Nu_F	39.38%
$\bar{J}_H$	33.2%
$j_{H,F}$	34.58%

D.7 Conclusion

The uncertainty analysis for this study has been discussed in this appendix. The theory behind uncertainty, the method followed and sample results have been given. The effect of high mass flow rates on the heat transfer coefficients and Nusselt numbers is attributed to the negligible temperature difference between the tube surface and the centre of the tube.

D.8 Reference

[D1] P.F. Dunn, Measurement and Data Analysis for Engineering and Science, 2 ed., 2010.